Interactions at Metal-GaAs(100) Interfaces

A thesis for the degree of Ph.D.

Presented to Dublin City University

by

Liam Roberts, B.Sc.
School of Physical Sciences
Dublin City University

Research Supervisor

Dr. Greg Hughes

May 1993

CONTENTS

Declaration (iii)

Acknowledgements (iv)

Abstract (vi)

Chapter 1 General Introduction 1
References 4

Chapter 2 Interactions at Metal-Semiconductor Interfaces 5
2.1 Introduction 5
2.2 The Semiconductor Surface and the Structure of GaAs(100) 5
2.3 Schottky Barrier Formation 7
2.4 Sulphur Passivation of III-V Semiconductors 11
References 19

Chapter 3 Experimental Techniques 22
3.1 Introduction 22
3.2 Electrical Studies 22
3.2.1 I-V and C-V Measurements 22
3.2.2 I-V Characteristics 23
3.2.3 C-V Measurements 25
3.2.4 Deep Level Transient Spectroscopy 27
3.2.4.1 Conventional DLTS and the Detection of Bulk Traps 27
3.2.4.2 Detection of Interface States 32
3.3 Surface Science Studies 33
3.3.1 Photoemission 33
3.3.1.1 Binding Energy Measurement 37
3.3.1.2 Reference Level 37
3.3.1.3 Chemical Shifts 38
3.3.1.4 Surface Sensitivity 39
3.3.1.5 Photoionisation Cross-section 41
3.3.1.6 Synchrotron Radiation 42
3.3.2 Low Energy Electron Diffraction 42
3.3.3 Auger Electron Spectroscopy 43
References 45

Chapter 4 Experimental Methods 46
4.1 Introduction 46
4.2 Electrical Studies 46
4.2.1 UHV System 1 47
4.2.2 Sample Preparation and Transfer 47
4.2.3 Sulphur Passivation 49
4.2.4 Metal Evaporation 51
4.2.5 DLTS Sample Mounting 54
4.2.6 I-V and C-V Measurement 54
4.2.7 Deep Level Transient Spectroscopy 57
4.3 Surface Science Studies 60
4.3.1 UHV System 2 and Related Techniques 60
4.3.1.1 Electron Energy Analyser 64

4.3.1.2 LEED System 66
4.3.1.3 Monochromator 66
4.3.2 Sample Preparation and Manipulation 67
4.3.3 Sulphur Passivation 69
References 71

Chapter 5 An Investigation of Metal-GaAs(100) Interfaces by Deep Level Transient Spectroscopy 72
5.1 Introduction 72
5.2 Metals on Unoxidised GaAs(100) 74
5.2.1 I-V Measurements 74
5.2.2 C-V Measurements 77
5.2.3 DLTS Studies 77
5.3 Metals on H_2O_2 Oxidised GaAs(100) 84
5.3.1 I-V Measurements 84
5.3.2 C-V Measurements 87
5.3.3 DLTS Studies 89
5.4 Discussion 89
5.5 Summary 95
References 96

Chapter 6 Sulphur Passivation of the GaAs(100) Surface 98
6.1 Introduction 98
6.2 H_2S Passivation 100
6.3 Molecular Sulphur Passivation 102
6.4 Discussion 110
6.5 Summary 119
References 120

Chapter 7 Photoemission Studies of the Deposition of Titanium on Oxidised GaAs(100) Surfaces 122
7.1 Introduction 122
7.2 Ti Deposition on Chemically Etched and Oxidised GaAs(100) 124
7.3 Ti Deposition on As- Decapped and Oxidised GaAs(100) 126
7.4 Discussion 130
7.5 Summary 134
References 135

Chapter 8 Conclusions and Future Work 137
8.1 Summary and Conclusions 137
8.2 Suggestions for Future Work 138

APPENDIX A List of refereed publications pertaining to this work

Declaration

I hereby certify that this material, which I now submit for assessment on the programme of study leading to the award of Doctor of Philosophy is entirely my own work and has not been taken from the work of others save and to the extent that such work has been cited and acknowledged within the text of my work.

Signed: Liam Roberts Date: 10/6/93

Candidate

Acknowledgements

I would like to express my sincere thanks to my supervisor, Dr. Greg Hughes, for his guidance, encouragement and extreme patience throughout the course of this work. I would also like to thank Optronics Ireland for funding parts of this research project. To Dr. Paul Bailey, I must acknowledge his help during my time at Daresbury laboratory. I am indebted to all the Physics postgraduates, both past and present (and some who are not really there at all). I would like to thank the lecturers, technical staff and of course, Marion and Jackie. I would also like to express my sincere gratitude to my parents for their continued support and encouragement. Finally, I would like to thank Antoinette for always being there.

I dedicate this to Antoinette

Abstract

Liam Roberts

Interactions at Metal-GaAs(100) Interfaces

The interaction of reactive and unreactive metals with clean, oxidised and sulphur passivated GaAs(100) surfaces has been investigated using a range of experimental techniques. The deposition of both gold and iron on chemically cleaned and oxidised GaAs(100) surfaces has revealed a correlation between the magnitude of the ideality parameter determined by current-voltage measurements and the presence of interface states as detected by the deep level transient spectroscopy (DLTS) technique. Schottky barrier diodes exhibiting near-ideal behaviour were fabricated by deposition of both gold and iron on GaAs surfaces immediately after chemical etch in H_2SO_4:H_2O_2:H_2O (5:1:1). No interface states were detected on these diodes. However, metals deposited on oxidised surfaces gave rise to highly non-ideal IV characteristics. In addition, DLTS studies revealed the presence of interface states, caused by defects induced during the oxidation of the GaAs surfaces prior to metal deposition. The passivating effects of sulphur in the forms of hydrogen sulphide. H_2S and molecular sulphur, S_2 on the GaAs surface have also been investigated. In particular, the adsorption of molecular sulphur on the As decapped GaAs surface has been studied using surface sensitive synchrotron radiation. Clean GaAs(100) surfaces with different As to Ga surface atom ratios were prepared by the thermal decapping of a protective As overlayer deposited on MBE grown GaAs. Studies have shown that the uptake of sulphur by the As and Ga surface atoms depends strongly on the As to Ga ratio of the clean decapped surface. Such sulphur treatments result in the adsorption of a monolayer of sulphur which is bonded to both the Ga and As surface atoms. As a complement to sulphur passivation, which has the effect of slowing down and/or preventing oxidation of GaAs surfaces, the reduction and removal of oxides by the deposition of ultrathin layers of titanium has been investigated. By exposing clean GaAs surfaces to air at atmosphere, a monolayer of oxides was grown. The subsequent deposition of titanium resulted in the complete removal of the As and Ga oxides and the formation of an extremely abrupt Ti-TiO_x-GaAs ($x \sim 1$) interface.

Chapter 1 General Introduction

The precise way in which a metal interacts with a semiconductor surface to form a potential barrier has been the subject of much debate over the last several decades. While a number of models have been put forward[1-8], no one theory is capable of explaining the clearly complicated behaviour of such Schottky barriers in terms of both their chemical and physical properties and their electrical characteristics. Furthermore, it has now become widely accepted that there is no simple relationship between Schottky barrier behaviour and the intrinsic properties of the metal or semiconductor surface. Indeed, experimental studies over the last 15 years have revealed that interface-specific states produced by the interaction between metal and semiconductor dominate the interface electronic properties[8]. It is thus clear that there is an ongoing need to study Schottky barrier behaviour, not only for its fundamental scientific interest, but moreover for its technological importance, since electrical contacts to semiconductors necessitate metal-semiconductor junctions, whether they result in low barriers (ohmic contacts), or high barriers (rectifying contacts).

Silicon based semiconductor components and devices have become the norm in terms of device applications. Much of the success is due to the nature of the surface - it consists only of silicon atoms. As well as this, the native oxide SiO_2, which forms on silicon, is a stable oxide, and can be used as an insulator in many device applications. However, as the demand for devices which consume less power and operate at higher speeds continues, a lot research work has been directed towards other types of semiconductor, in particular the III-V compound semiconductors GaAs and InP. Indeed, these materials have only made a place for themselves in recent years, not by supplanting silicon, but by complementing it in new applications such as photonics and high speed FET technologies.

The formation of metal contacts to GaAs is, like silicon, not fully understood. What makes the problem more difficult is the fact that GaAs is a compound semiconductor and so interactions the metal and both Ga and As atoms have to be considered. Another problem is that the stable oxides of GaAs: Ga_2O_3, As_2O_3, As_2O_5 and $GaAsO_4$[9] react with the GaAs substrate to form Ga_2O_3 and elemental As, so irrespective of what oxide is grown on the GaAs surface, As and Ga_2O_3 will always

be present. All of these effects give rise to potential barriers whose rectifying properties are dependent, not exclusively on the metal or semiconductor, but on defect or interface states due to the interaction between the metal and the clean or oxidised semiconductor surface.

The aim of the work presented in this thesis was to study in detail Schottky barrier formation and behaviour as a function of semiconductor surface preparation, in an attempt to control the electronic properties at the metal-semiconductor interface. Initial work focused on the electrical characterisation of chemically etched GaAs(100) surfaces using current-voltage (I-V), capacitance-voltage (C-V) and Deep Level Transient Spectroscopy (DLTS) techniques. An attempt was made to correlate the degree of rectification as determined by the I-V characteristics with the presence of interface states as detected by DLTS for ideal[10] and non-ideal Schottky barrier diodes.

The observation that oxidised GaAs surfaces gave rise to a high density of interface states, coupled with the fact that oxidation of GaAs in air is a natural process, encouraged the need to attempt to passivate the GaAs surface. The group VI element, sulphur has been found to both electronically and chemically passivate the GaAs surface. Two methods of sulphur passivation were employed in these experiments. Chemically etched GaAs(100) surfaces were treated with hydrogen sulphide gas, H_2S, prior to metal deposition. Electrical studies were carried out on these samples to determine the effectiveness of the passivation treatment. The subsequent development of a UHV compatible electrochemical sulphur cell provided a highly controllable means of sulphur treatment in the form of molecular sulphur, S_2. The surface chemistry resulting from the interaction of S_2 with the clean GaAs(100) was investigated using surface sensitive synchrotron radiation. Clean GaAs(100) surfaces were obtained by the thermal decapping of a protective arsenic overlayer deposited on a molecular-beam-epitaxy (MBE) grown GaAs epilayer. A particular advantage of controlled thermal decapping is that it offers the ability to predetermine the clean surface composition, a facility not afforded by other methods used to obtain a clean surface, such as cleaving or ion-bombardment and annealing.

As an alternative to sulphur passivation, the interaction of titanium with oxidised GaAs surfaces was investigated using surface sensitive synchrotron radiation. Two

types of surface were studied; unintentionally oxidised chemically etched GaAs and As decapped surfaces which were briefly exposed to air. For both surface preparations, complete reduction of the oxides was observed upon Ti deposition.

The layout of this thesis is as follows. In Chapter 2, the development of the different theories put forward to describe Schottky barrier behaviour is presented. An extensive overview of the passivation studies using sulphur based compounds is also given in this chapter. The basis of the experimental techniques used in this work are described in Chapter 3. In Chapter 4, the different experimental systems and methods used to obtain the results presented in Chapters 5,6 and 7 are described. Finally, some general conclusions pertaining to the overall results, as well as suggestions for future work, are presented in Chapter 8.

References

[1] Schottky W., Naturwiss **26** (1938) 843.

[2] Bardeen J., Phys. Rev. **71** (1947) 717.

[3] Heine V., Phys. Rev. **138** (1965) A1689.

[4] Spicer W.E., Lindau I., Skeath P.R., Su C.Y. and Chye P.W. Phys. Rev. Lett. **44** (1980) 420.

[5] Williams R.H., J. Vac. Sci. Technol. **18** (1981) 929.

[6] Freeouf J. and Woodall J.M., Appl. Phys. Lett. **39** (1981) 727.

[7] Spicer W.E., Liliental-Weber Z., Newman N., Kendelwicz T., Cao R., McCants C., Mahowald P., Miyano K. and Lindau I., J. Vac. Sci Technol. B **6** (1988) 1245.

[8] Brillson L.J., Surf. Sci. Reports **2** (1982) 123 and references therein.

[9] Thurmond C.D., Schwartz G.P., Kammlot G.W. and Schwartz B., J. Electrochem. Soc. **127** (1980) 1366.

[10] Rhoderick E.H. and Williams R.H., Metal-Semiconductor Contacts, 2nd Edition, Oxford Science Publications (1988) 39.

Chapter 2 Interactions at Metal-Semiconductor Interfaces

2.1 Introduction

The practical applications of the rectifying properties of metal-semiconductor interfaces have advanced so quickly in the last twenty years that it is difficult to appreciate that the fundamental understanding of these properties is still rather limited. One of the main reasons for this is that interactions between metals and semiconductor surfaces are very complex and rarely atomically abrupt. There is therefore an ongoing need to study the phenomena associated with Schottky barrier formation in an attempt to control the electronic properties. This chapter describes the development of some of the most popular theories that have been put forward in attempt to explain the electronic behaviour at the metal-semiconductor interface. These theories are presented in Section 2.3, following a description of the semiconductor surface and the structure of GaAs(100), presented in Section 2.2. In Section 2.4, the extensive amount of work that has already been carried out in an attempt to modify the surface properties of GaAs by various sulphur treatments.

2.2 The Semiconductor Surface and the Structure of GaAs(100)

The regular periodic structure of atoms in the bulk of a crystalline solid terminates abruptly at the surface, and leads to an alteration of the surface structural environment which is different to that in the bulk. Because of the absence of neighbouring atoms, the surface can become "relaxed"[1], whereby the spacial arrangement and spacing of the surface atoms differs from that in the bulk, while the symmetry in a plane parallel to the surface remains the same. Alternatively, the surface atoms may be "reconstructed"[2]. In this case, the symmetry in the plane of the surface differs from that in the bulk. Relaxation and reconstruction effects can extend over several atomic layers into the crystal. The depth over which this occurs is known as the selvedge region. Another important distinction between the bulk and surface is associated with the chemical nature of the surface. If a clean semiconductor surface is exposed to air at atmosphere, atoms such as carbon and oxygen are adsorbed, generally leading to a disordered surface. Only by placing in a UHV environment can a clean surface be retained long enough to perform routine study.

Interactions at GaAs surfaces formed the basis of the studies presented in this thesis. GaAs, in common with other III-V compound semiconductors, displays a zinc-blende crystal structure. These tetrahedrally co-ordinated zinc-blende semiconductors are structurally equivalent to the elemental semiconductors but with two different constituent atoms placed alternatively throughout the crystal lattice. The (100) surface is a polar surface i.e. alternating planes parallel to the surface contain atoms of one kind only. In the unrelaxed surface, shown in Figure 2.1, these atoms are equally spaced and every atom has two bonds to the layer above and below. A number of stable surface reconstructions has been shown to exist for GaAs(100), depending on the amount of As in the topmost layer[3].

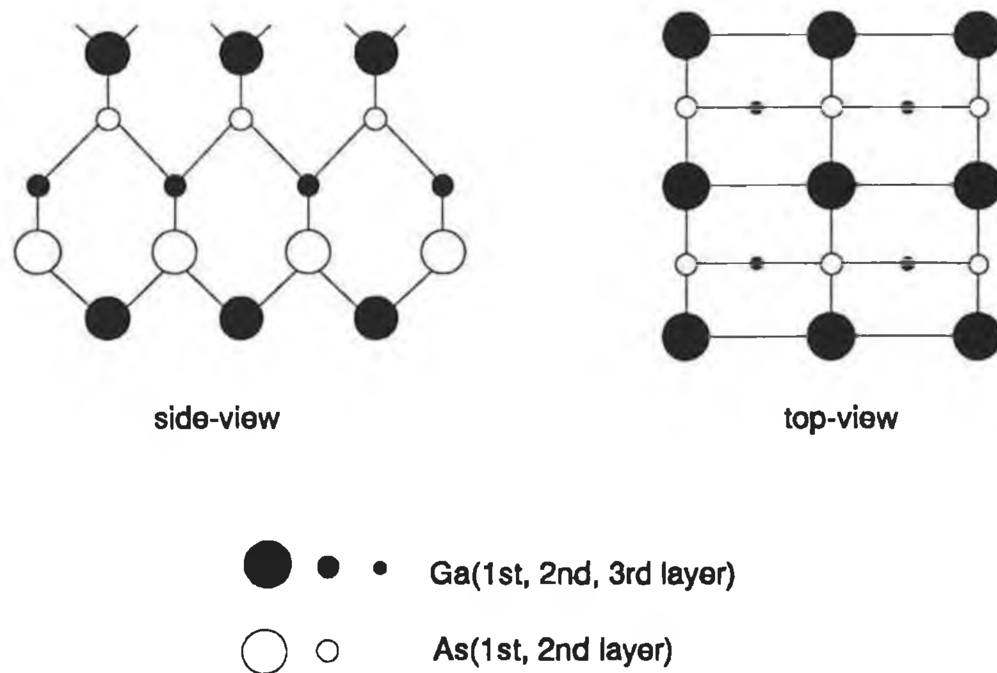

Figure 2.1. Side view and top view of the unrelaxed GaAs(100) surface.

The discontinuity of the semiconductor bulk structure gives rise to energy states known as intrinsic surface states whose energies can differ from the allowed energies in the bulk. These states may influence the interface electronic behaviour. The wave functions corresponding to intrinsic states are localised at the semiconductor-vacuum interface and decay, both into the bulk of the crystal and into the vacuum outside the crystal. A variety of influences such as crystal orientation, surface reconstruction and crystal preparation can have an effect on the energetic position and density of intrinsic states. For example, it has been shown that the (110) cleavage surfaces of

most III-V semiconductors have no intrinsic states within the bandgap[1,4,5].

States induced by impurities on the semiconductor surface are referred to as extrinsic surface states. Like intrinsic states, the energy associated with extrinsic states may overlap the bulk bandgap of the semiconductor. Adsorbed gases or metals can interact with the surface atoms to produce new extrinsic sources of trapped charge which are foreign to the clean surface. These states may also have an effect on the electronic behaviour at the interface.

2.3 Schottky Barrier Formation

The rectifying nature of metal-semiconductor contacts has been reported as far back as 1874. However, no plausible explanation was given until 1938, when Schottky[4] suggested that the rectification properties are derived from the difference in the work function ϕ_m and the electron affinity χ_{SC} of the free surfaces of the metal and semiconductor, respectively. This results in a potential barrier or Schottky barrier being set up at the interface between the two materials, the barrier height of which is given by:

$$\phi_B = \phi_m - \chi_{SC} \tag{2.1}$$

Figure 2.2(a) shows the formation of a Schottky barrier between an n-type semiconductor and a metal, where $\phi_m > \chi_{SC}$. Upon contact, electrons flow from the semiconductor to the metal until the two Fermi-levels coincide. Because the density of conduction electrons is many orders of magnitude less than the density in a metal, electrons must come from the bulk to enable the equalization of the Fermi-levels. This gives rise to an upward bending of the semiconductor bands which extends into a region depleted of electrons. Figure 2.2(b) depicts a p-type Schottky contact. In this case rectification occurs when $\chi_{SC} > \phi_m$.

The linear dependence of the barrier height on the metal work function predicted by the Schottky model was unfortunately found to be too simple in that it did not describe a number of experimental findings. In particular, it was found that the barrier height for many metals in contact with silicon were practically independent of the metal work function. This led Bardeen[5] to propose a model in 1947 in which surface states, located energetically in the forbidden bandgap, played a central role

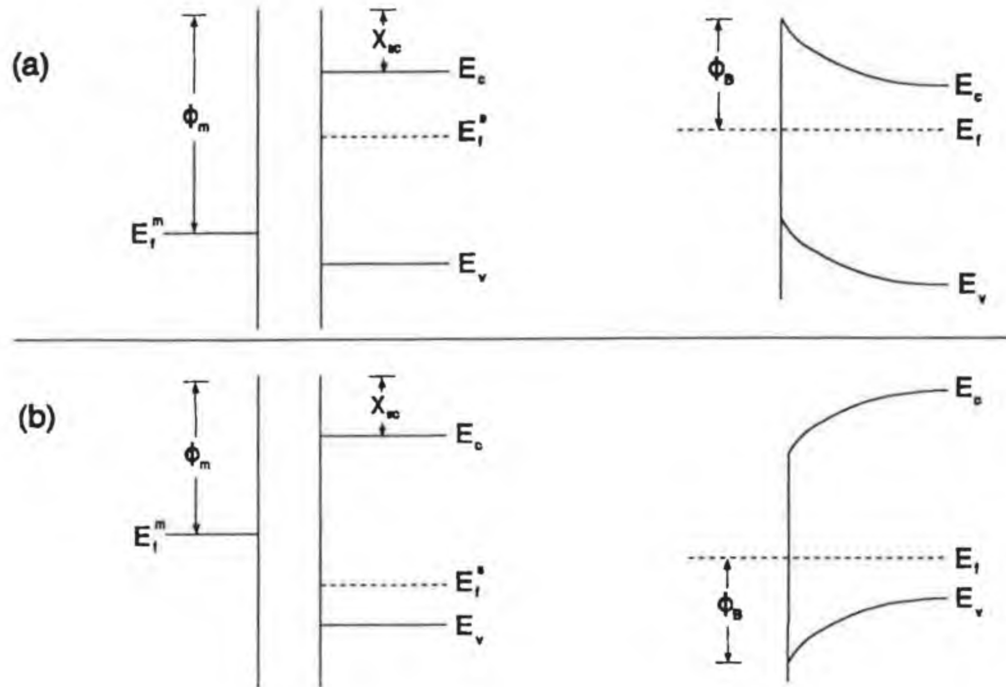

Figure 2.2. Schottky barrier formation on (a) n-type and (b) p-type semiconductors.

in the determination of the barrier height. Bardeen recognised that a relatively low density of surfaces states, of the order of 0.1% of surface atoms, on the free semiconductor surface would be sufficient to effectively "pin" the Fermi-level at the surface, as illustrated in Figure 2.3(a). Thus, when the semiconductor is brought into contact with a metal, as shown in 2.3(b), charge can flow from the metal into these surface states and set up a microscopic interface dipole, Δ in order to compensate for the difference between the metal and semiconductor work functions. The interface states effectively screen the interior of the semiconductor from the metal and the rectification properties are then effectively independent of the metal work function. For a surface state density less than that for the Bardeen limit to be reached, the barrier height is dependent on both the metal work function and the surface state density. The main feature of the Bardeen model i.e. the influence of these surface states on the pinning of the Fermi-level, has remained the principal factor of most interface theories up to the present.

In 1965, Heine[6] commented on the properties of interface states at metal-semiconductor junctions. He argued that localised surface states could not exist at

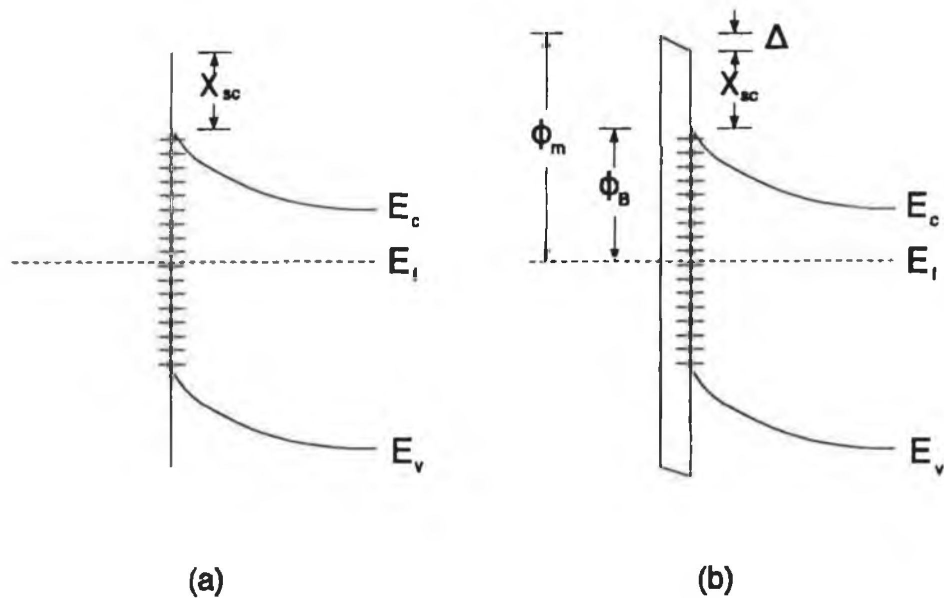

Figure 2.3. (a) Surface states on the free surface of the semiconductor. (b) Formation of a Schottky barrier with such a surface.

such junctions because of a coupling to a continuum of free-electron-like wavefunctions in the metal. However, he pointed out that Bardeen's interface states could be interpreted as the tails of the metal wavefunctions which decay into the semiconductor. These metal induced gap states (MIGS) could have the similar effect of pinning the Fermi-level. In the same year, Cowley and Sze[7] derived a linear relationship between the barrier height and the metal work function according to the equation:

$$\phi_B = \gamma\phi_m + C \tag{2.2}$$

where γ is a weighting factor which depends on the surface state density and the thickness of the interfacial layer and C is a constant. In deriving this relationship they assumed that (i) the metal-semiconductor junction has an interfacial layer of the order of atomic dimensions and (ii) the density of surface states is a only a property of the semiconductor and is independent of the metal work function. By considering the cases where $\gamma \rightarrow 0$ and $\gamma \rightarrow 1$, they were able to account for the Bardeen and Schottky models, respectively.

A fundamental assumption of all the theories discussed thus far was that the interface between the metal and semiconductor is abrupt. In the case of the Bardeen-Heine models, it was further assumed that the interface states at the metal-semiconductor junction are intrinsic to the semiconductor and not modified by the contact metal. From the 1970s onwards, the increasing availability of a range of surface sensitive techniques, which could probe the interface on a microscopic scale, gave way to new and varied perceptions of Schottky barrier formation. Effects such as chemical bonding, atomic interdiffusion and the creation of defects, which lead to non-abrupt metal-semiconductor interfaces, have been considered. In addition, a variety of investigations[1,8-10] established that the (110) cleavage faces of most III-V semiconductors undergo relaxation, which has the effect of forcing the intrinsic surface states out of the forbidden bandgap. Thus, assuming that no structural rearrangement of the relaxed surfaces occurred during metal deposition, intrinsic states were not considered to be responsible for the observed Fermi-level pinning in the bandgap of these semiconductors. Investigations also carried out on the early stages of metal deposition on clean surfaces have revealed that Fermi-level pinning can occur for coverages which are less than one monolayer[11]. Furthermore, it has been found that, provided the metal reacts with the semiconductor, the final Fermi-level pinning position is relatively independent of the particular metal[12-14]. These various results formed the basis of a defect model which was independently put forward by Spicer *et al*[13,14] and Williams[15] between 1979-1981. The model suggested that during metal deposition, defects are created in the semiconductor lattice. These defects can result in the generation of new electronic levels in the semiconductor bandgap which could control the final Fermi-level position at the interface. It was suggested that interface state densities of 10^{12}-10^{13} cm^{-2} are sufficient to effectively pin the Fermi-level. Experimental evidence for Fermi-level pinning by defect levels has been put forward by a number of researchers. Skeath *et al*[16] observed that deposition of various metals on n- and p-type GaAs(110) led to pinning positions at $\approx$0.8 eV and $\approx$0.55 eV, respectively. Lindau and co-workers[17] carried out studies of both metal and oxygen adsorption on the III-V semiconductors InP, GaSb and GaAs. They found that the Fermi-level pinning position is independent of the precise nature of the adatom, suggesting that induced defect levels are responsible. Theoretical calculations on the energies of a range of possible defect levels have been carried out by a number of researchers. Daw and Smith[18,19] predicted pinning energies based on

simple cation or anion vacancies, derived by tight binding methods. Allen and Dow[20] obtained similar results for pinning energies by assuming antisite defects rather than simple vacancies. In 1981 Weber *et al*[21], who carried out studies of defects in GaAs(110), suggested the As_{Ga} antisite defect (an As atom on a Ga site) is responsible for the observed Fermi-level pinning positions. They calculated two energy levels for the As_{Ga} antisite 0.75 eV and 0.52 eV above the valence band maximum. These levels are similar to the pinning positions of 0.75 eV and 0.5 eV for metals and oxygen on GaAs(110) which Spicer *et al* had deduced for their defect model in 1979-80. The results of Weber *et al* led Spicer's group to propose an advanced unified defect model[22] in 1988 in which they associated the observed pinning levels with the As_{Ga} antisite. Based on the AUDM, an As/Ga increase enhances the ratio of As_{Ga}/Ga_{As} antisites in the GaAs near the interface and this is expected to move the Fermi-level toward the conduction band minimum; whereas, a decrease should move it toward the valence band maximum.

In summary, the history of attempts to explain Schottky barrier behaviour has been very complex. A number of theories have been developed that can at least partially describe the interactions which occur at metal-semiconductor interfaces. Most theories, however are limited to particular systems. It is thus evident that no one theory has yet been developed that can wholly describe Schottky barrier behaviour. Therefore, more study is necessary to clarify experimental results which still remain unexplained.

2.4 Sulphur Passivation of III-V Semiconductors

The reduction of the high density of states on the GaAs surface, as well as on other III-V semiconductors surfaces, has limited the potential growth of applications of these semiconductors. As discussed in the last section, there have been significant widespread efforts to understand and thereby control the mechanism of Fermi-level pinning at adsorbate-semiconductor interfaces. Recent reports that sulphur treatment of GaAs surfaces is both effective at reducing the surface state density and partially unpinning the surface Fermi-level have thus, not surprisingly, attracted considerable attention. Sulphur is a versatile element with regard to GaAs and it forms many stable binary compounds with both Ga and As. Indeed, there have been several reports[23-25] of the ability of the chalcogenides to lower the surface state density of

states in GaAs, due to the strong chemical affinity between sulphur and GaAs.

The beneficial passivating effects of sulphur treatment were first described by Sandroff and co-workers[26] in 1987. They used a solution of sodium sulphide, $Na_2S.9H_2O$, to passivate GaAs(100) surfaces and found a 60-fold increase in photoluminescence (PL) intensity over that of untreated surfaces. Yablonovitch *et al*[27] and Nottenburg *et al*[28] found that improvements in the surface recombination velocity of $Na_2S.9H_2O$-treated GaAs approach that of nearly ideal AlGaAs/GaAs. A disadvantage of this means of passivation was that exposure to air at room temperature caused rapid degradation of the passivated surface characteristics. As an alternative approach, Spindt and co-workers[29] passivated GaAs(100) surfaces with ammonium sulphide, $(NH_4)_2S$. They suggested that the $(NH_4)_2S$ treatment effectively removed the GaAs surface oxides and terminated the surface with a thin layer of sulphur, possibly a monolayer, thereby leaving the near-surface GaAs undamaged and relatively free of defects. This contrasts with the disruptive nature of Ga and As oxides, which as Spicer *et al*[13] suggested, are responsible for the formation of defects on the GaAs surface. Indeed, in another work, Spindt and Spicer[30] suggested that the reduction of excess As atoms and therefore the number of double donor As antisite defects by sulphur treatment, coupled with an increase in observed band bending, was consistent with the predictions of the defect model[13] discussed earlier. Carpenter *et al*[31] investigated Schottky barriers formed on $(NH_4)_2S$ treated n- and p-type GaAs and observed an order of magnitude reduction in the surface state density at the ammonium sulphide treated metal-GaAs interface relative to an untreated surface. Carpenter *et al*[32] also found that the effects of ammonium sulphide treatment were more durable and dependable than those of sodium sulphide passivated GaAs surfaces. Cowans and co-workers[33] studied the effect of $(NH_4)_2S$-treated GaAs(100) surfaces using XPS. They found that the treatment produces a slightly Ga enrichment on the surface and leaves approximately 0.6 of a monolayer of sulphide. Upon exposure to air, the surface becomes oxidised. However the sulphide is not lost but remains near the oxide-GaAs interface.

The treatment of GaAs with hydrogen sulphide gas, H_2S has been investigated by several groups. Ranke *et al*[34] used AES and XPS to investigate the interaction of H_2S with different crystal faces of GaAs at different temperatures. Both MBE and

sputter annealed surfaces were used in the study. The sulphur uptake was found to depend on both crystal orientation and temperature. In addition, the sputtered surfaces had a higher density of defects and thus adsorbed more sulphur. The kinetics of adsorption were thought to have a strong dependence on the microscopic structure of the adsorbing surface. At high temperatures (280-450 °C), the sulphur adsorption mainly changed the Ga *3d* core-level peak while the As *3d* core-level peak was affected at lower temperatures. Kawanishi and co-workers[35] performed a study of H_2S-treated GaAs(100) surfaces using AES and RHEED. They showed that oxygen uptake on such surfaces is much less than that on untreated surfaces and attributed this observation to the fact that the passivation effect prevents oxygen from intruding deep into the bulk GaAs. Tiedje *et al*[36] chemically prepared GaAs surfaces and then capped them with elemental As which was later removed by heating in vacuum to a temperature hot enough to remove the oxides. Sulphur was adsorbed on these surfaces at room temperature from activated H_2S. This resulted in more sulphur bonding to Ga than to As. Heating the surface removed the As-sulphides while the Ga-sulphide bonds remained. In another work, Tiedje and co-workers[37] reported that, in comparison with the inorganic sulphide solutions, $Na_2S.9H_2O$ and $(NH_4)_2S$, a much higher fraction of sulphur bonding was found from photoemission studies of H_2S exposed GaAs surfaces. Their studies also indicate that the H_2S treated surface seems to be a better defined surface than those produced by either Na_2S or $(NH_4)_2S$ chemical treatments.

In an attempt to identify the bonding nature of sulphur on GaAs, Shin, Geib and Wilmsen performed AES and XPS analyses of GaAs treated with $Na_2S.9H_2O$, $(NH_4)_2S$ and H_2S. Geib *et al*[38] observed that for H_2S exposed GaAs surfaces, three distinct S-GaAs bonding states appear: As-S bonding peaks in the As *3d* spectra exhibit core-level shifts of 1.0 and 1.6 eV, Ga-S bonding causes a core-level shift of 0.6 eV. These chemical shifts are similar to those for $Na_2S.9H_2O$ and $(NH_4)_2S$ reported by Sandroff *et al*[26-28] and Spindt *et al*[29-30]. From Auger studies, Geib and co-workers estimated that H_2S treatment results in 1 monolayer of sulphur bonded to the GaAs surface whereas less than monolayer coverages were achieved with sodium sulphide and ammonium sulphide. This led to the suggestion that H_2S dissolved in the inorganic solutions may play a role in the passivation of GaAs surfaces.

Shin *et al*[39] carried out an XPS study of S-GaAs, also using the forms of sulphur discussed above. They found that, in the absence of an external source of excitation, such as heat, light, electron stimulation or of the presence on surface defects, sulphur only physisorbs on the surface. With an excitation and/or surface defects, the sulphur chemisorbs on the surface and causes chemically shift core-level peaks to appear in the XPS spectra. Monolayer order sulphur coverages were measured from Auger spectra under these conditions. To account for these observations, and for the variety of chemical shifts reported in the literature, Shin and co-workers proposed a model in which there is a kinetic barrier to the formation of strong S-GaAs bonds and that this barrier can only be overcome by the application of an excitation source. In another work, Shin *et al*[40] performed a study of sulphur uptake on GaAs surfaces of varying As/Ga surface composition. By using different chemical etches followed by heating in vacuum, surface As/Ga ratios of between 0.6 and 6.0 were obtained. From their results they established that sulphur bonds to whichever atoms are on the surface. The amount of bonding to As and Ga depends on their surface composition and is independent of how the surface composition is obtained or of the source of sulphur, although more sulphur is found to bond to the GaAs surface with H_2S. They also found that heating the GaAs surface in a atmosphere of H_2S caused the removal of elemental As at a lower temperature than heating in vacuum.

Recently, there has been considerable investigation, by Japanese research groups in particular, into sulphur treatment of III-V semiconductors using ammonium polysulphide, $(NH_4)_2S_x$. Nannichi and co-workers[41-43] have demonstrated that the surface treatment of GaAs(100) with a $(NH_4)_2S_x$ solution, which contains more sulphur than a $(NH_4)_2S$ solution, is even more effective at removing the GaAs surface oxides due to its enhanced etching nature. This has led to significant improvements in metal-insulator-semiconductor, (MIS) capacitance-voltage (C-V) characteristics and a remarkable dependence of Schottky barrier height on the work function of the contact metal. According to a close experimental analysis of the surface[44,45], the $(NH_4)_2S_x$ treatment first removes the surface oxide on the GaAs. A monatomic layer of sulphur is then adsorbed on the surface, together with an accumulated amorphous sulphur layer which desorbs relatively easily in vacuum. Oigawa *et al*[46] extended this passivation treatment to the (100) surfaces of a number of other III-V compounds such as GaP, InP and (Al,Ga)As. Schottky barrier diodes were fabricated by

evaporating In, Al and Au metals onto chemically etched and $(NH_4)_2S_X$-treated semiconductor surfaces. Schottky barrier heights were derived from C-V measurements. They showed that, whereas Schottky barrier heights of as-etched surfaces remain unchanged, there is a universal dependence of barrier height on metal work function for all sulphur-treated surfaces. These results are shown graphically in Figure 2.4. In order to shed more light on the passivating mechanism of the $(NH_4)_2S_x$ treatment, Sugahara and co-workers[47] investigated the chemistry and band bending of $(NH_4)_2S_x$-treated GaAs(100) surfaces using synchrotron radiation photoemission spectroscopy. Ga-S, As-S and S-S bonds are found to exist on such as-treated surfaces. However, after annealing at 360 °C for 10 mins, the Ga-S bonds become dominant and a 0.3 eV surface Fermi-level towards the CBM is observed. Their results imply that firstly, sulphur atoms easily form As-S bonds, although As-S bonds are thermodynamically less stable and secondly, sulphur treatment leads to partial unpinning of the surface Fermi-level. They suggested that the Ga-S bonds play a key role in the passivation of GaAs surfaces. Following Sugahara *et al*'s work and in an attempt to elucidate the mechanism of sulphur passivation of the GaAs(100) surface by $(NH_4)_2S_x$ treatment, Ohno and Shiraishi[48] carried out a theoretical study of the structural and electronic properties of both Ga- and As-terminated GaAs(100)-(1x1) surfaces adsorbed with a sulphur monolayer. By using the first-principles pseudopotential method, they determined the optimal adsorption geometry for S atoms on both Ga- and As-terminated surfaces to be the bridge bond configuration, i.e. each S atom is bonded to two Ga (As) atoms on the Ga- (As-) terminated surface. This enabled the surface electronic structure to be evaluated. For the Ga-terminated surface, the adsorption of a sulphur monolayer is seen to reduce the surface state density within the energy gap. However, such a reduction does not occur on the As-terminated GaAs surface, due to the presence of an As-S antibonding state which lies within the forbidden energy gap.

A major problem which affects the long-term stability of GaAs surfaces passivated by the sulphur containing compounds discussed thus far, is the inherent thermodynamic instability of the gallium and arsenic sulphides with respect to the corresponding oxides[49]. Recently, Lee *et al*[50] reported that treatment with a new source of sulphur, phosphorus pentasulphide (P_2S_5), resulted in a passivated GaAs(100) surface which exhibited a five-fold increase in PL intensity as compared

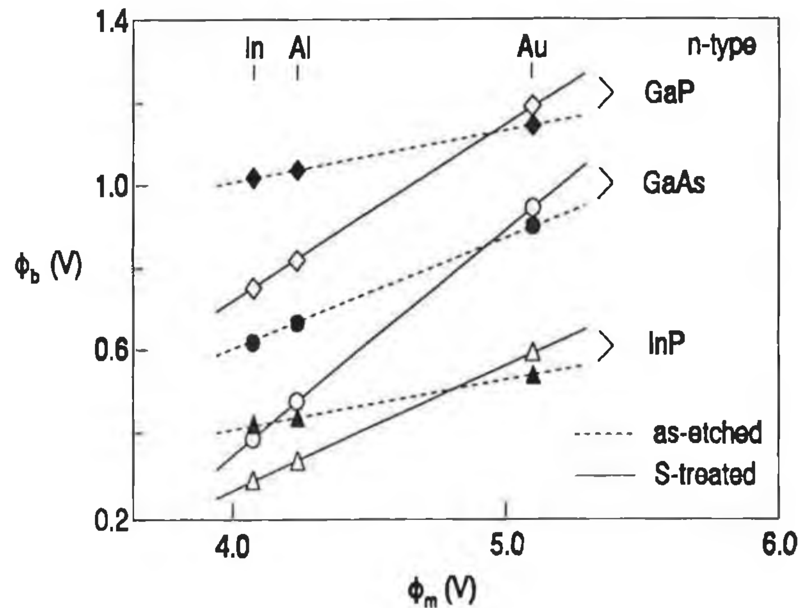

Figure 2.4. Dependence of Schottky barrier height on the work function of metals deposited on (100) surfaces of GaP, GaAs and InP. (After reference 46).

with surfaces which had been passivated with either sodium or ammonium sulphides. Furthermore, the PL intensity remained constant over 10 days exposure to light and laboratory air. They suggested that the addition of phosphorus compounds to the passivation treatment offered a distinct advantage through the enhanced thermodynamic stability of phosphorus oxide over gallium oxide. This would indicate that the gallium atoms could not reduce the surface phosphorus oxide, thus inhibiting the reaction sequence in which gallium reduces the arsenic oxides thereby leading to arsenic segregation. Hwang and Li[51] used a $P_2S_5/(NH_4)_2S$ solution to passivate a GaAs(100) epitaxial layer after which Au or Al was deposited to form Schottky contacts. I-V and C-V measurements of these contacts indicated that the Fermi-level of the GaAs surfaces was partially unpinned. These authors also noted significantly lower leakage currents for surfaces treated with this solution, in contrast to other sulphide treatments. Wang and co-workers[52] performed an extensive study of GaAs(100) surfaces treated with a variety of sulphur containing compounds. By using an aqueous solution of $P_2S_5/(NH_4)_2S$, both with and without additions of free sulphur, they compared their results with those obtained for surfaces treated with sodium, ammonium and hydrogen sulphides, as well as solid sulphur. An increase in PL intensity of up to 23 times the signal for the freshly etched surface was

observed for surfaces passivated with $P_2S_5/(NH_4)_2S/S_x$. This treatment also yielded the surface with the slowest PL intensity degradation rate on exposure to air. Their XPS studies of P_2S_5-treated surfaces indicate that the phosphorus is not bonded to the Ga or As atoms but is involved only in P-S and P-O bonding configurations. This would substantiate the proposal put forward by Moriarty and co-workers[53] that phosphorus plays a key role in stabilising the passivated surface against oxidation. These authors performed a scanning tunnelling microscopy (STM) study of GaAs(100) surfaces which were treated in aqueous solutions of $(NH_4)_2S_x$, $P_2S_5/(NH_4)_2S$ and $P_2S_5/(NH_4)_2S_x$. By monitoring the ambient oxidation rate of the passivated surfaces through a "relative surface roughness" parameter they found that $P_2S_5/(NH_4)_2S_x$-treated surfaces exhibited the most resistance to oxidation. Both of the above groups have reported that the degree of phosphorus pentasulphide passivation across the surface varies considerably; Wang *et al* observed a 40% variation in PL intensity from different areas whereas Moriarty and co-workers measured surface roughnesses for isolated areas on a sample which varied as much as five times that of the surface as a whole.

It is generally considered that chemical treatments using dry processes are superior to wet processing in terms of producing uniform and contamination-free surfaces. The use of a conventional K-cell as means of solid sulphur deposition has however met with some difficulties. This is due mainly to the high vapour pressure of sulphur and hence the difficulty in controlling the sulphur flux. An innovative method of producing an controllable atomic/molecular sulphur flux, involving the electrochemical decomposition of silver sulphide, Ag_2S, was first reported by Wagner[54] in 1956 and subsequently by Heegeman *et al*[55] in 1975. It has recently been used as an effective means of passivating GaAs surfaces. Mokler and Watson[56] carried out a comparative study of passivation of GaAs(100) surfaces by H_2S and molecular sulphur, S_2, generated by an electrochemical sulphur cell. From LEED and AES studies of the passivated surfaces, they reported that while H_2S-treatment resulted in single monolayer coverages, S_2 was found to adsorb sufficently to form multilayers up to 5 monolayers thick. This result contrasts with that of Sugahara and co-workers[57] who observed monolayer order coverages on GaAs(100) surfaces which had been exposed to sulphur from an electrochemical cell. Sugahara *et al* studied the bonding nature of S-treated GaAs(100) surfaces using photoemission from

synchrotron radiaition. They determined that Ga-S and As-S bonds are formed after S deposition at room temperature but that Ga-S bonds become dominant following annealing at 360 °C for 10 min in vacuum. Similar results were obtained for $(NH_4)_2S_x$-treated surfaces.

In summary, The treatment of GaAs with sulphur containing compounds has been shown to provide an effective means of passivating the surface. It is widely reported that sulphur treatments result in a reduction of the surface state density as well as partially unpinning the surface Fermi-level.

References

[1] Van Laar J. and Scheer J.J. Surf. Sci. **8** (1967) 342.

[2] Haneman D., Phys. Rev. **121** (1961) 1093.

[3] Drathen P., Ranke W. and Jacobi K., Surf. Sci. **77** (1978) L162.

[4] Schottky W., Naturwiss **26** (1938) 843.

[5] Bardeen J., Phys. Rev. **71** (1947) 717.

[6] Heine V., Phys. Rev. **138** (1965) A1689.

[7] Cowley A.M. and Sze S.M., J. Appl. Phys. **36** (1965) 3212.

[8] Kurtin S., McGill T.C. and Mead C.A., Phys. Rev. Lett. **22** (1970) 1433.

[9] Williwms R.H., Varma R.R. and McKinley A. J. Phys. C. **10** (1977) 4545.

[10] Van Laar J., Huijser A. and Van Rooy J.L., J. Vac. Sci. Technol. **14** (1977) 894.

[11] Skeath P., Lindau I., Chye P.W., Su C.Y. and Spicer W.E., J. Vac. Sci. Technol. **16** (1979) 1143.

[12] Williams R.H., Varma R.R. and Montgomery V., J. Vac. Sci. Technol. **16** (1979) 1418.

[13] Spicer W.E., Chye P.W., Skeath P.R., Su C.Y. and Lindau I., J. Vac. Sci. Technol. **16** (1979) 1427.

[14] Spicer W.E., Lindau I., Skeath P.R., Su C.Y. and Chye P.W. Phys. Rev. Lett. **44** (1980) 420.

[15] Williams R.H., J. Vac. Sci. Technol. **18** (1981) 929.

[16] Skeath P.R., Su C.Y., Hino I., Lindau I. and Spicer W.E., Appl. Phys. Lett. **39** (1981) 349.

[17] Lindau I., Chye P.W., Garner C.M., Pianetta P., Su C.Y. and Spicer W.E., J. Vac. Sci. Technol. **15** (1978) 1332.

[18] Daw M.S. and Smith D.L., J. Vac. Sci. Technol. **17** (1980) 1028.

[19] Daw M.S. and Smith D.L. Appl. Phys. Lett. **8** (1980) 690.

[20] Allen R.E. and Dow J.D., J. Vac. Sci. Technol. **19** (1981) 383.

[21] Weber E.R., Ennen H., Kaufmann V., Windscheif J., Schneider J. and Wosinski T. J. Appl. Phys. **53** (1982) 6140.

[22] Spicer W.E., Liliental-Weber Z., Newman N., Kendelwicz T., Cao R., McCants C., Mahowald P., Miyano K. and Lindau I., J. Vac. Sci Technol. B **6** (1988) 1245.

[23] Nelson R.J., Williams J.S., Leamy H.J., Miller B.I. Casey Jr. H.C., Parkinson B.A. and Heller A., Appl. Phys. Lett. **38** (1980) 76.

[24] Massies J., Chalpart J., Laviron M. and Linh N.T., Appl. Phys. Lett. **38** (1981) 693.

[25] Horowitz G., Allongue P. and Cachet H., J. Electrochem. Soc. **131** (1984) 2563.

[26] Sandroff C.J., Nottenburg R.N., Bischoff J.C. and Bhat R., Appl. Phys Lett. **52** (1987) 33.

[27] Yablonovitch E., Sandroff C.J., Bhat R. and Gmitter T., Appl. Phys. Lett. **51** (1987) 439.

[28] Nottenburg R.N., Sandroff C.J., Humphrey D.A., Hollenbeck and Bhat R., Appl. Phys. Lett. **52** (1988) 218.

[29] Spindt C.J., Liu D., Miyano K., Meissner P.L., Chiang T.T., Kendelwicz T., Lindau I. and Spicer W.E., Appl. Phys. Lett. **55** (1989) 861.

[30] Spindt C.J. and Spicer W.E., Appl. Phys. Lett. **55** (1989) 1653.

[31] Carpenter M.S., Melloch M.R., Lundstrom M.S. amd Tobin S.P., Appl. Phys. Lett. **52** (1988) 2157.

[32] Carpenter M.S., Melloch M.R. and Dungan T.E., Appl. Phys. Lett. **53** (1988) 66.

[33] Cowans B.A., Dardas Z., Delgass W.N., Carpenter M.S. and Melloch M.R., Appl. Phys. Lett. **54** (1989) 365.

[34] Ranke W., Finster J. and Kuhr H.J., Surf. Sci. **187** (1987) 112.

[35] Kawanishi H., Sugimoto Y. and Akita K., J. Appl. Phys. **70** (1991) 805.

[36] Tiedje T., Wong P.C. and Mitchell K.A.R., Solid State Commun. **70** (1989) 355.

[37] Tiedje T., Colbow K.M., Rogers D., Fu Z. and Eberhardt W., J. Vac Sci. Technol. B **7** (1989) 837.

[38] Geib K.M., Shin J. and Wilmsen C.W., J. Vac. Sci Technol. B **8** (1990) 838.

[39] Shin J., Geib K.M., Wilmsen C.W. and Lilliental-Weber Z., J. Vac. Sci. Technol. A (1990) 1894.

[40] Shin J., Geib K.M. and Wilmsen C.W., J. Vac. Sci. Technol. B **9** (1991) 2337.

[41] Nannichi Y., Fan J-. F., Oigawa H. and Koma A., Jpn. J. Appl. Phys. **27** (1988) L2367.

[42] Fan J-.F., Oigawa H. and Nannichi Y., Jpn. J. Appl. Phys. **27** (1988) L2125.

[43] Fan J-.F., Kurata K. and Nannichi Y., Jpn, J. Apl. Phys. **28** (1989) L2255.

[44] Oigawa H., Fan J.-F., Nannichi Y., Ando K., Saiki K. and Koma A., Jpn J. Appl. Phys. **28** (1989) L340.

[45] Sugahara H., Oshima M., Oigawa H., Shigekawa H. and Nannichi Y., "Extended Abstracts of the 21st Conference on Solid State Devices and Materials", (Tokyo, 1989) 547.

[46] Oigawa H., Fan J-.F., Nannichi Y., Sugahara H. and Oishima M. **30** (1991) L322.

[47] Sugahara H., Oshima M., Oigawa H., Shigekawa H. and Nannichi Y., J. Appl. Phys. **69** (1991) 4349.

[48] Ohno T. and Shiraishi K., Phys. Rev. B. **42** (1990) 11194.

[49] Kubaschewski O. and Alcock A.B., Metallurgical Thermochemistry, 5th ed. (Pergamon, New York 1979).

[50] Lee H.H., Racicot R.J. and Lee S.H., Appl. Phys. Lett. **54** (1989) 724.

[51] Hwang K.C. and Li S.S., J. Appl. Phys. **67** (1990) 2162.

[52] Wang Y., Darici Y. and Holloway P.H., J. Appl. Phys. **71** (1992) 2746.

[53] Moriarty P., Murphy B. and Hughes G., J. Vac. Sci. Technol. A, accepted for publication (1993).

[54] Wagner C., J. Chem. Phys. **21** (1953) 1819.

[55] Heegeman W., Meister K.H., Bechtold E. and Hayek K., Surf. Sci. **49** (1975) 161.

[56] Mokler S.M. and Watson R., J. Vac. Sci. Technol. A **9** (1991) 1374.

[57] Sugahara H., Oshima M., Klauser R., Oigawa H. and Nannichi Y., Surf. Sci. **242** (1991) 335.

Chapter 3 Experimental Techniques

3.1 Introduction

The purpose of this chapter is to describe in detail the theoretical bases and underlying principles of the techniques used to obtain the experimental results presented in this thesis. For the sake of clarity, the techniques are divided under two main headings, electrical studies and surface science studies. Electrical studies, consisting of current-voltage (I-V) and capacitance-voltage (C-V) measurements, carried out on metal-GaAs(100) Schottky barrier diodes, were used to characterise the current transport properties and the degree of rectification of these devices. In particular, the role of interface states as a function of semiconductor surface preparation, was studied in detail using Deep Level Transient Spectroscopy (DLTS). As a complement to electrical characterisation, surface science studies were undertaken to assess mainly the chemical composition and quality of the clean GaAs(100) surface both before and during the adsorption of different adatoms. Low Energy Electron Diffraction (LEED) gave information regarding the surface structure while Auger Electron Spectroscopy (AES) was used to determine the concentration of different elemental species in the surface layers of the semiconductor. Soft X-Ray Photoemission (SXPS) using a synchrotron radiation source provided detailed information regarding the chemical nature and bonding configuration of the topmost atomic layers of the semiconductor surface.

3.2 Electrical Studies

3.2.1 I-V and C-V Measurements

As discussed in chapter 2, section 2.3, when a metal comes in contact with an n-type semiconductor, electrons flow from the semiconductor to the metal until the two Fermi levels equalise and thus a potential barrier is formed. The height of this potential barrier i.e. $\phi_B = \phi_M - \chi_S$ characterises the rectifying properties of the Schottky barrier. Two of the most basic, but extremely useful methods of determining the barrier height are those of measuring either the current through, or the capacitance of the Schottky diode as a function of bias voltage. The general theory behind these measurements is now discussed.

3.2.2 I-V Characteristics

Schottky barrier diodes are majority carrier devices. Thus for an n-type Schottky barrier contact, it is mostly electrons that constitute current flow. There are four basic mechanisms in which electrons can be transported across Schottky barrier junctions under forward bias. These mechanisms are shown schematically in fig. 3.1. The inverse processes occur for the case of reversed bias.

The four processes are:

1) transport of electrons from the semiconductor over the potential barrier to the metal;

2) quantum mechanical tunnelling of electrons through the barrier;

3) recombination of electrons in the depletion region;

4) hole injection from the metal to the semiconductor.

The processes 2) and 4) are only applicable for high and low doped semiconductors respectively. Diffusion of electrons through the barrier is important for low mobility semiconductors.

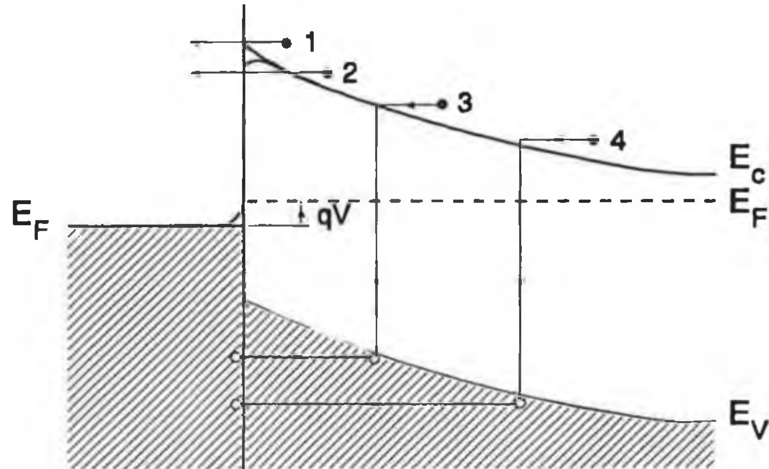

Figure 3.1. Current transport mechanisms. (After reference 1.)

The Schottky barrier diodes in these experiments were fabricated from moderately doped (N_D-N_A = $5x10^{16}$ cm^{-3}) GaAs. Thus the principal mechanisms of current

transport are those of thermionic emission and recombination. The current for such a diode is given by:

$$I = I_s \exp\left(\frac{qV}{nkT}\right) \tag{3.1}$$

where I_s is the saturation current and:

$$I_s = SA^{**}T^2 \exp\left(-\frac{q(\phi_B^{IV} - \Delta\phi)}{kT}\right)$$

where S is the diode area, A^{**} is Richardson's constant, T is the absolute temperature and n is the ideality factor. $\Delta\phi$ is a correction term due to the image force lowering of the barrier. Richardson's constant takes account of the ratio of the semiconductor effective mass to the free electron mass. For GaAs(100), A^{**} is $8.6 \times 10^4 Am^{-2}K^{-2}$. The ideality factor is an important parameter, as it is effectively a measure of how well a diode obeys the thermionic emission theory. A value of n equal to 1 indicates an "ideal" diode.

If equation 3.1 is plotted for forward bias voltages, an extrapolation of the linear region of this graph to cross the y-axis gives a value for the saturation current I_s, from which the barrier height ϕ_B^{IV} can be determined, i.e.

$$\phi_B^{IV} = \ln\left(\frac{I_s}{SA^{**}T^2}\right)\frac{kT}{q} \tag{3.2}$$

A more exact form of equation 3.2 enables the plot to extend through V=0 for reverse bias, thus permitting more accurate determination of the barrier height and ideality factor. In this case, the I-V characteristic is written as:

$$I = I_s \exp\left(\frac{qV}{nkT}\right)\left[1 - \exp\left(-\frac{qV}{kT}\right)\right] \tag{3.3}$$

This effect is shown diagrammatically in Figure 3.2.

In theory, for pure thermionic emission, the ideality factor n should be exactly 1. In practice, however, deviations from n=1 are not unlikely and for the semiconductors

used in these experiments, are more pronounced in Schottky barriers at low forward bias and at low temperatures. These deviations are mainly due to recombination of electrons in the depletion region. Thus, to take account of recombination current, equation 3.3 may be rewritten as:

$$I = I_{te} + I_{rc} = \left[I_s \exp\left(\frac{qV}{nkT}\right) + I_r \exp\left(\frac{qV}{2kT}\right)\right]\left[1 - \exp\left(-\frac{qV}{kT}\right)\right] \tag{3.4}$$

where I_{te} is the thermionic emission current and I_{rc} is the current due to recombination in the depletion region as discussed in section 3.2.2. Note that the assumption of a value of n=2 in the recombination term is a gross simplification. Nevertheless, the addition of a recombination term may be necessary for "non-ideal" diodes as failure to do so can lead to erroneous values for ϕ_B. This problem has been discussed in a paper by McLean *et al*[2].

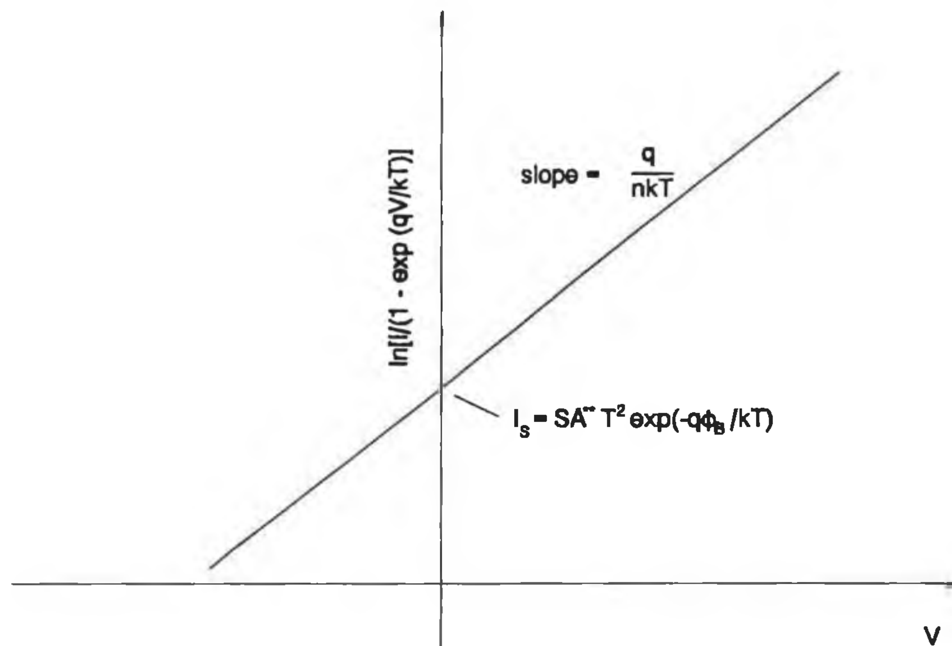

Figure 3.2. Current versus applied voltage for Schottky barrier diode.

3.2.3 C-V Measurements

When a small ac voltage is superimposed on a reverse dc bias V_r across a Schottky diode, charges of opposite sign are induced on both the metal and semiconductor, at either side of the depletion region. As the reverse bias is increased, electrons in the

conduction band recede further from the metal and increase the width of the depletion region. Similarly, if there is a significant number of holes immediately adjacent to the metal, the hole concentration will decrease because the hole quasi-Fermi level[1] coincides with the Fermi level in the metal. This change in charge gives rise to a capacitance and the diode effectively behaves as a variable capacitor. Assuming the diode is ideal and the donor concentration is uniform in the semiconductor, the differential capacitance under reverse bias is given by:

$$\frac{\delta Q_d}{\delta V} = C = S(qN_d\varepsilon_s/2)^{1/2}\left(\phi_B - V_n + V_r - \frac{kT}{q}\right)^{-1/2} \tag{3.5}$$

where S is the diode area, N_d is the effective donor concentration, ε_s is the permittivity of the semiconductor (for GaAs $\varepsilon_s = 12\varepsilon_o$). $V_n = kT/q\ln(N_c/N_d)$ is the depth of the Fermi level below the conduction band. (For the material used V_n has an approximate value of 0.06 eV.) Rewriting equation 3.5 we have:

$$\frac{1}{C^2} = \left(\frac{2}{S^2qN_d\varepsilon_s}\right)\left[\phi_B^{CV} - V_n + V_r - \frac{kT}{q}\right] \tag{3.6}$$

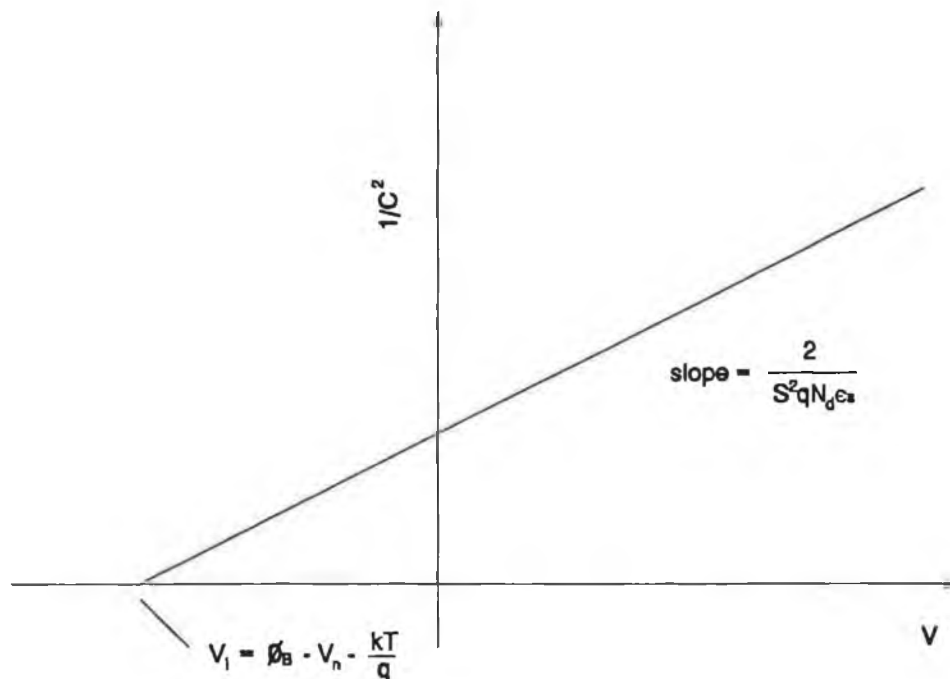

Figure 3.3. $1/C^2$ versus V plot for a Schottky barrier diode.

Assuming ϕ_B is independent of V_r, a plot of $1/C^2$ vs V_r should yield a straight line with an intercept V_I on the x-axis given by:

$$V_I = \phi_B^{CV} - V_n - \frac{kT}{q} \tag{3.7a}$$

The intercept V_I is also related to the diffusion potential V_d by:

$$V_I = V_d - \frac{kT}{q} \tag{3.7b}$$

The barrier height ϕ_B is given by:

$$\phi_B^{CV} = V_d + V_n \tag{3.8}$$

The slope of the graph can be used to the determine the donor concentration, as shown in Figure 3.3.

3.2.4 Deep Level Transient Spectroscopy

Deep Level Transient Spectroscopy (DLTS) has become a powerful tool for the characterisation of both deep levels and interface states in Schottky barrier diodes. It can be used to provide complementary information on the electronic nature of the metal-semiconductor interface. The transient technique used in these experiments was first introduced by Lang in 1974[3] and is based on the measurement of the capacitance transient associated with the temperature dependent emission of electrons which occupy deep levels within the semiconductor depletion region.

3.2.4.1 Conventional DLTS and the Detection of Bulk Traps

The capacitance DLTS technique employed in these experiments is most widely used for the characterisation of majority traps in semiconductors. The technique is described as follows. Figure 3.4(a) shows the depletion region of a Schottky barrier diode (n-type) at thermal equilibrium or zero voltage. Note the position of the Fermi level at energy E_F and that of E_T, which indicates a deep level of activation energy E_T below the conduction band extending into the bulk. Under zero bias conditions, the space-charge layer has a depletion width W_o, and the occupancy of the deep level is determined by the thermal equilibrium Fermi energy E_F. Under the condition of reverse bias of voltage V_r, as shown in Figure 3.4(b), a depletion region of width $W_r > W_o$ exists in which the steady state occupation of deep levels is determined by

the quasi-Fermi level ξ. If a zero bias pulse V=0 is applied to the Schottky barrier diode, the quasi-Fermi level moves to a position closer to the conduction band and the depletion region width decreases to $W = W_0$. This condition, illustrated in Figure 3.4(c), results in occupancy of the deep level in a region immediately below the Fermi level. Provided the duration of the zero bias pulse is longer than the characteristic filling time, or capture rate, of the deep level, complete occupancy of the deep level within this region results. A return to the reverse bias condition, Figure 3.4(d), results in the emission of electrons to the conduction band from the region of the deep level above the quasi-Fermi level. Unlike the movement of free electrons, the response time of electrons emitted from deep levels is relatively slow, and more importantly, very temperature sensitive. The principle of capacitance DLTS is based on the fact that as these thermal electrons are emitted from the deep levels, they leave behind a net positive charge, thereby increasing the space charge density within the depletion region, and hence the width of the depletion region itself.

As W is related to the applied bias by the depletion approximation[1]:

$$W = \left(\frac{2\varepsilon_s S V}{q(N_d - N_T)} \right)^{1/2} \tag{3.9}$$

where N_T is the trap concentration and V is the applied voltage. The total increase in capacitance is therefore:

$$C = \frac{\varepsilon_s S}{W} = \left(\frac{\varepsilon_s q (N_d - N_T) S}{2V} \right) \tag{3.10}$$

The actual kinetics of electron emission can be described by the equation:

$$\frac{dn_T}{dt} = -e_n n_T \quad \left. \begin{array}{ll} n_T = N_T & at\ t=0 \\ n_T = 0 & at\ t=\infty \end{array} \right. \tag{3.11}$$

e_n is the probability per unit time for emission and is defined by the equation:

$$e_n = \sigma_n N v_n \exp\left(-\frac{E_C - E_T}{kT} \right) \tag{3.12}$$

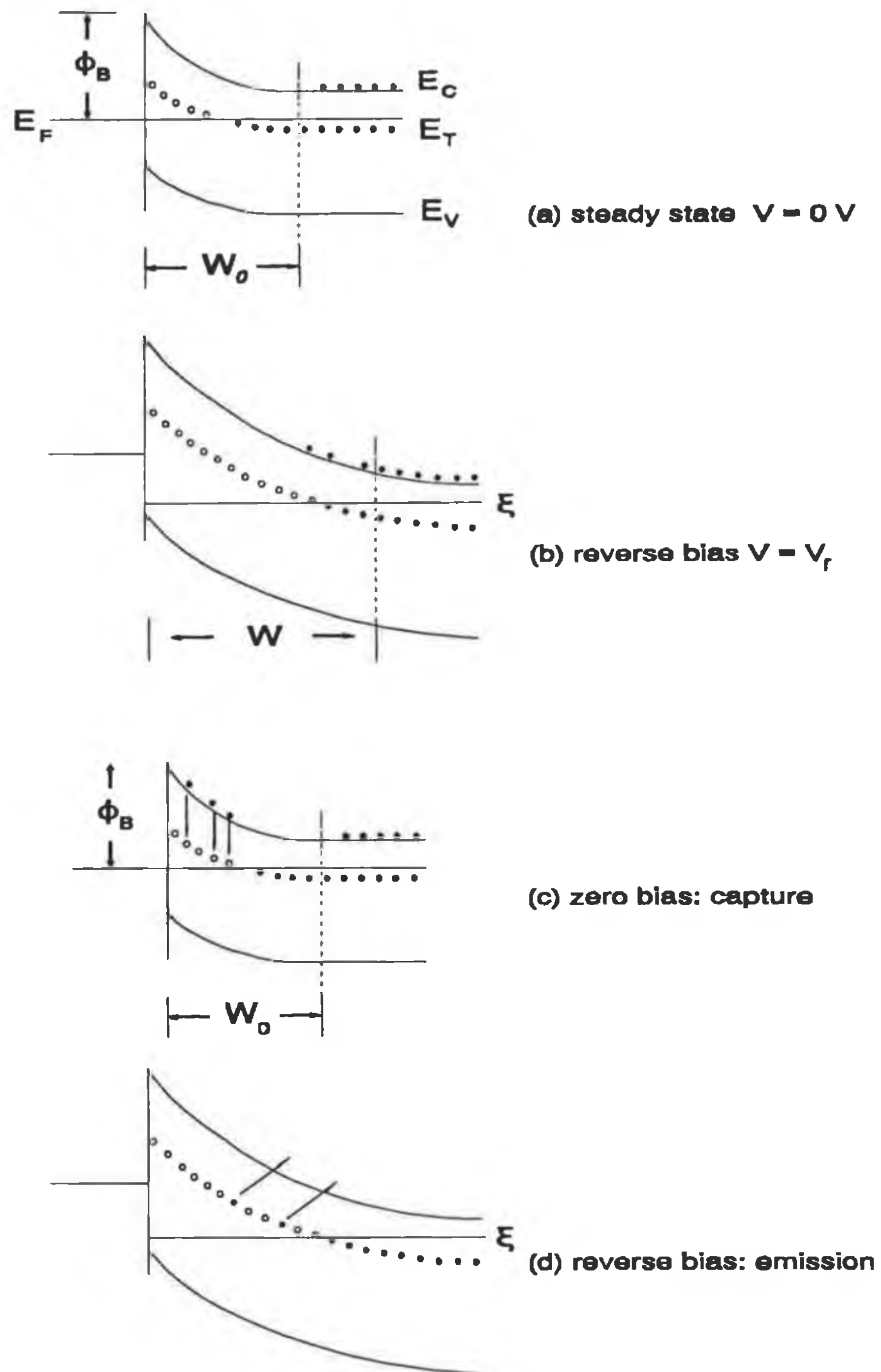

Figure 3.4. Energy band diagrams for different bias conditions. (a) Zero bias (equilibrium condition). (b) Reverse bias. (c) Zero bias. (d) Reverse bias reestablished.

where σ_n is the capture cross section for trapped electrons, v_n is the mean thermal velocity of electrons and N is the free electron concentration. The product v_nN has a temperature dependency i.e. $v_nN=BT^2$ with $B=2.21\times10^{20}$ $K^{-2}cm^{-2}s^{-1}$ for GaAs[4]. Rewriting equation 3.11 we have:

$$n_T(t) = N_T\exp(-e_n t) \tag{3.13}$$

Thus, the electron concentration decays as e_n^{-1} and the positive space charge and hence the capacitance builds up with a time dependence $\tau = 1-\exp(-e_n t)$. Figure 3.5 shows the bias pulse sequence and corresponding capacitance transient.

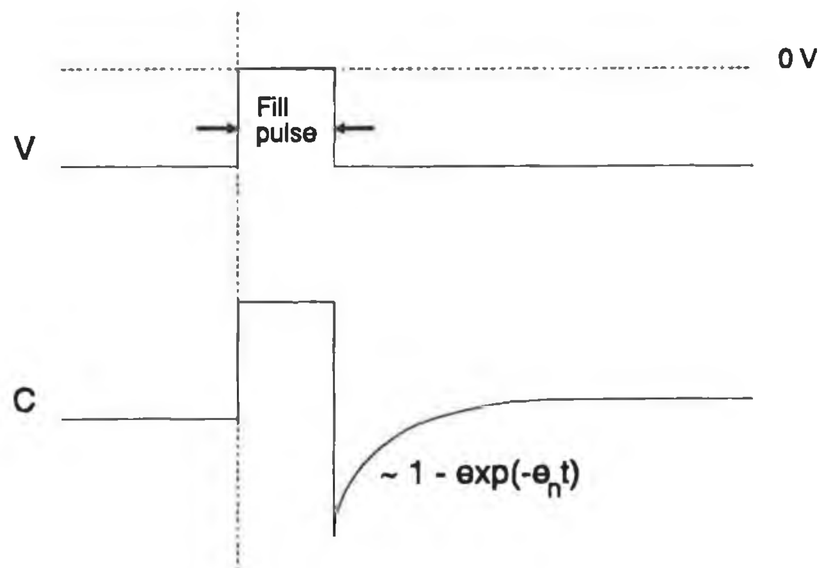

Figure 3.5. Bias pulse sequence and corresponding capacitance change.

If a series of voltage pulses is applied to the Schottky barrier diode during a temperature ramp, a capacitance transient results whose profile is governed by the emission of electrons from deep levels. For a particular deep level, these temperature varying transients pass through a peak when the electron emission rate is maximum. By the application of an "emission rate window", a DLTS signal can be obtained. This concept is illustrated in Figure 3.6 and shows a series of capacitance transients for a discrete trap level at various temperatures. According to equation 3.12, the emission rate is small for low temperatures and becomes more rapid as the temperature is increased. Repetitive transient signals are fed to a boxcar averager with gates which sample at times t_1 and t_2 as shown in the figure. The signal from the differential output of the of the boxcar averager is simply the capacitance

difference $\Delta C = C(t_1) - C(t_2)$. This is the DLTS signal. It goes through a maximum at that temperature for which the trap emission rate equals the "emission rate window" $e_n=e_0$ set by the DLTS system. The rate window e_0 is related to the sampling times t_1 and t_2 according to the equation:

$$e_0 = \frac{\ln(t_2/t_1)}{(t_2 - t_1)} \tag{3.14}$$

Plotting the DLTS signal over a range of temperatures yields a DLTS spectrum, as illustrated in Figure 3.6.

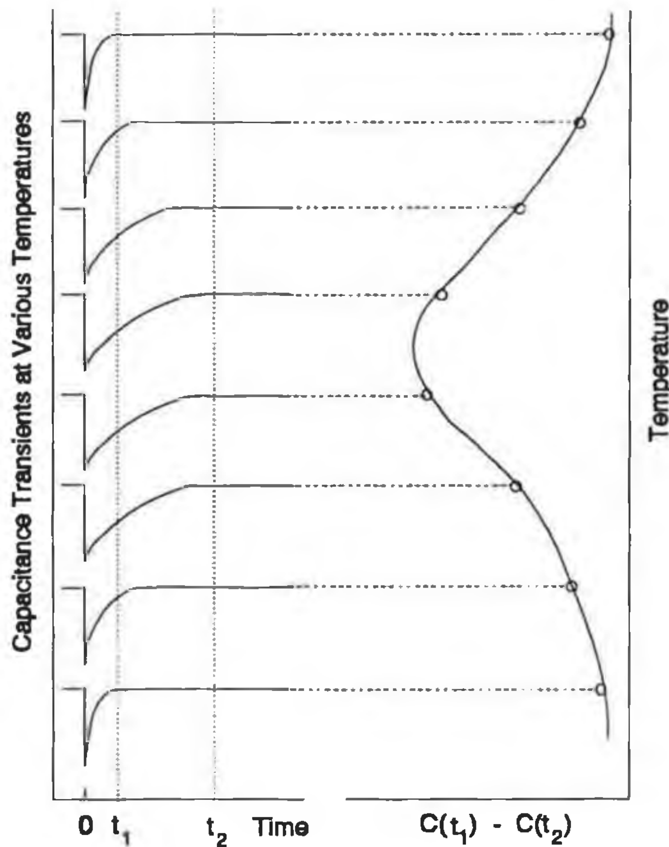

Figure 3.6. DLTS spectrum obtained by the application of an emission rate window.

Although the main information yielded is the temperature dependence of the emission rate e_n, several other important parameters regarding the nature of deep levels can be obtained from the DLTS spectrum, namely:

(i) the activation energy of the deep level, E_T i.e the position of the level, with respect to the conduction band, within the bandgap,

(ii) the capture cross section σ_n and

(iii) the concentration N_T of the deep level.

Furthermore, from equation 3.12, it can be seen that since e_n has a monotonic dependence on E and T, it follows that temperature scanning enables different portions of the energy range to contribute successively to the signal $\Delta C=C(t_1)-C(t_2)$ and therefore is equivalent to energy scanning.

The activation energy and capture cross section are obtained from an Arrhenius analysis of the emission rate e_n from equation 3.12 i.e.

$$e_n = BT^2 \exp\left(-\frac{E_c - E_T}{kT}\right) \tag{3.15}$$

where the relationships $N = 2(2\pi m^* kT)^{3/2}/h^3$ and $v_n = (8kT/\pi m^*)^{1/2}$. The measurement consists of recording the temperature dependence of the DLTS spectrum, as it sweeps through a peak, for different rate windows. At each peak, $e_0=e_n$ and thus a plot of $\ln(e_n/T^2)$ v^s $1/kT$, gives a straight line, the slope and intercept of which give the thermal activation energy E_T and the electron capture cross section σ_n respectively.

Since the change in capacitance ΔC is proportional to the emission of trapped electrons we may write:

$$\Delta C = C_0 \exp(t/\tau) \tag{3.16}$$

where C_0 is the amplitude of the capacitance transient at t=0. The trap concentration N_T can thus be determined by differentiating equation 3.10 and assuming constant bias conditions, i.e.:

$$\frac{\Delta C}{C} = \left(\frac{\Delta N_T}{N_D - N_T}\right) \tag{3.17}$$

Here, ΔC is the amplitude of the DLTS peak, i.e. $\Delta C = C_0$ at $t=\tau$.

3.2.4.2 Detection of Interface States

It is clear from the last section the conventional reverse-bias mode of DLTS discussed above provides both valuable qualitative and quantitative information on

deep traps within the semiconductor. However, no information is yielded on the presence of interface states. This is because, unlike deep traps which are isoenergetic within the depletion region, interface states can have a range of energies distributed throughout the bandgap within the intrinsic depletion region. Because the fill pulse remains at the same amplitude for a particular DLTS scan, usually 0 V, so too does the quasi Fermi level. For this reason, interface state distributions within the intrinsic depletion region do not appear in a reverse bias DLTS spectrum when the magnitude of the fill pulse is 0 V.

Consider a Schottky diode with a continuous distribution of interface states at the metal-semiconductor interface. Figure 3.7 illustrates the qualitative features of the DLTS measurement. A reverse bias V_r applied to the junction keeps the interface states in depletion, shown in Figure 3.7(a). If a positive trapping pulse $V_p>0$ is imposed on the junction, such that the quasi-Fermi level ξ is moved to a position closer in energy to the bottom of the conduction band E_c, all interface states below ξ will fill with electrons, as illustrated in Figure 3.7(b). By quickly returning to the reverse bias condition, electrons begin to be emitted to the conduction band. It follows that electrons occupying interface states which are situated closer to the bottom of the conduction band will be emitted first. Thus, as the pulse voltage is increased, the DLTS peak corresponding to the interface states is seen to move to lower temperatures. Furthermore, because the interface state density is continuous up to the conduction band, the amplitude of the DLTS signal increases with pulse voltage. It is these properties that distinguishes a broad interface state distribution from a discrete bulk trap level, whose position is independent of pulse magnitude. A discrete level of interface states can also be detected by forward bias DLTS as a peak whose intensity does not saturate with increasing pulse voltage, provided it does not have the same energy as a bulk trap.

3.3 Surface Science Studies

3.3.1 Photoemission

Photoemission has become one of the most widely used experimental techniques used for the study of solid surfaces. The principle of photoemission is in effect straight forward; monochromatic light is allowed to hit a sample and the energy distributions of the photoemitted electrons are then measured. Photoemission is thus an excitation

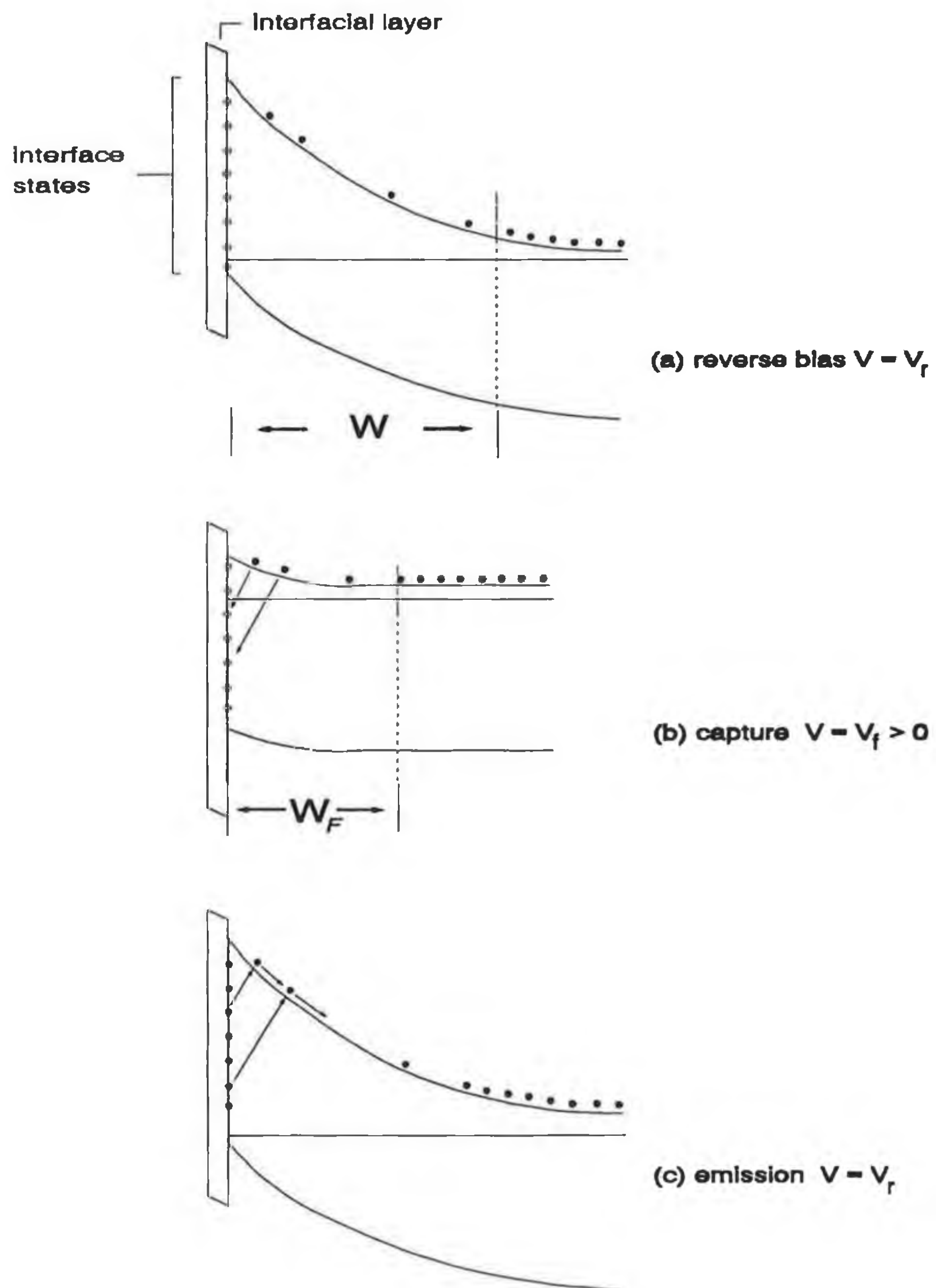

Figure 3.7. Interface state detection by forward bias DLTS. (a) SBD under reverse bias V_r. (b) Capture process $V=V_f$. (c) Emission process $V=V_r$.

process and the basic quantity from which information about the electronic structure can be extracted is the probability N(hυ,E) for a photon of energy hυ to excite an electron from an initial state E_i to a final state $E_j = E + E_i$. A typical energy distribution curve (EDC) is shown in Figure 3.8. Such a spectrum may be recorded in either angle integrated mode, whereby the photoelectrons are collected over all angles, or in angle-resolved mode, whereby photoelectrons are collected from a small cone of emission, the latter mode giving a more well defined structure.

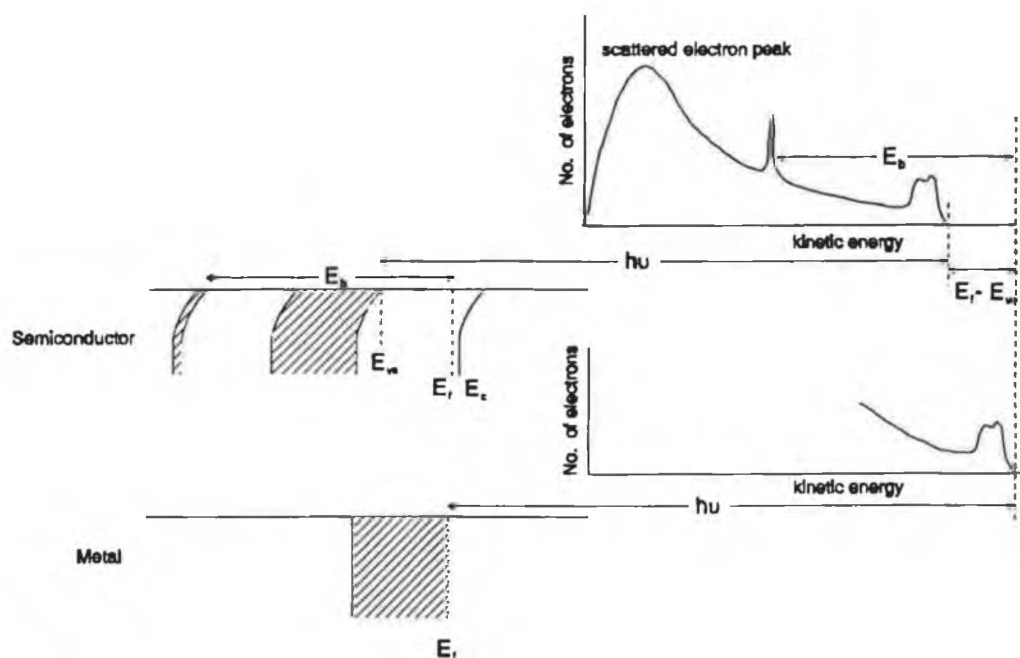

Figure 3.8. Energy band diagrams for semiconductor and metal and corresponding EDC curve. (After reference 1.)

Typically, optical excitation extends about 100Å into a solid, depending on the material and photon energy. The escaping electrons must pass through the solid before reaching the surface from which they enter vacuum. One of the fundamental problems in interpreting the photoemission spectra is that of separating the primary unscattered core level electrons from the inelastically scattered ones (see Figure 3.8). One of the most popular theoretical models used to interpret the photoemission event is the "three-step model", first proposed by Berglund and Spicer[5]. Within this model, the photoemission process is viewed as consisting of three independent events. The

first event is the optical excitation, and the second is the transport of the electrons to the surface during which they suffer from inelastic scattering processes. The third event is the escape of electrons across the surface potential barrier into vacuum. This is shown schematically in Figure 3.9.

Although the three-step model has been successfully used to explain photoemission data, it does suffer some conceptual deficiencies in that it assumes that the electrons in the solid are free-electron like and that surface effects are neglected.

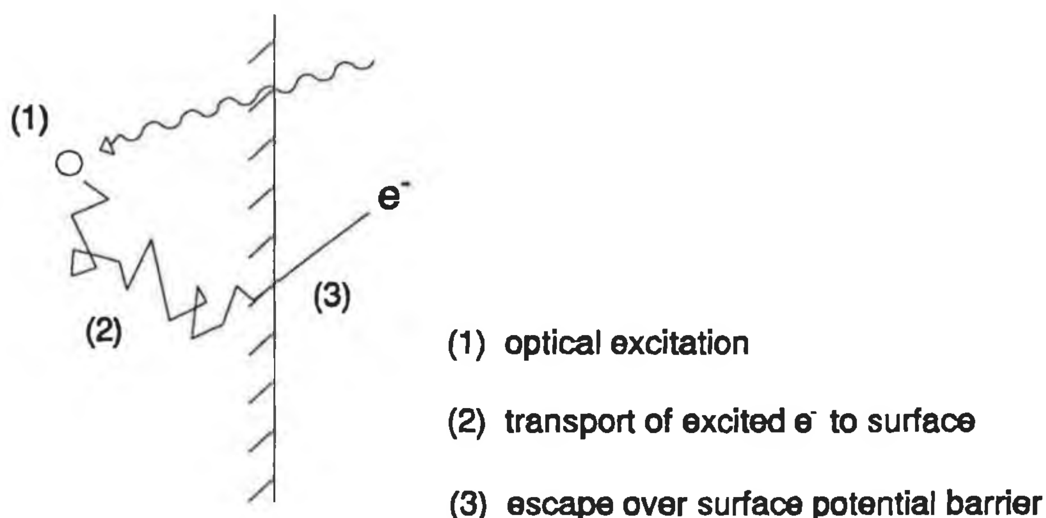

Figure 3.9. Schematic diagram illustrating the three-step model of photoemission. (After reference 6.)

In a more sophisticated model, the photoemission process is viewed as a one-step quantum-mechanical event. The electron wave function for the event is written as $\chi = \chi^0 + \chi'$, where χ^0 is the central-site contribution (direct wave) and χ' takes account of the surrounding atoms. By breaking up the wave function into these two parts, both single and multiple scattering processes are included. Although this model is more accurate in describing the photoemission process it is also more complicated, with the result that it has only been preformed for simple systems.

3.3.1.1 Binding Energy Measurement

The energy of the core level E_b in Figure 3.5 with respect to the vacuum level E_{vac} is referred to as the binding energy. If E_j is the energy of the emitted electron corresponding to this level following photoexcitation of energy $h\upsilon$ then:

$$h\upsilon - E_j = E_{vac} - E_i \tag{3.18}$$

where E_i is the initial state energy of the system. Assuming E_{vac} - E_i = E_b, then:

$$h\upsilon - E_j = E_b \tag{3.19}$$

The above is commonly referred to as the one-electron approximation. It does not take into account the fact that after excitation of the photoelectron, the remaining electrons can "relax" towards the hole created. What is measured is the difference in energy between the N-1 electrons in their final state and the N electrons in their initial state. It is this energy that is given to the escaping photoelectron. Another assumption when using equation 3.19 to determine the binding energy is that when an electron is removed from an N-electron atom, the energies associated with the orbitals of the ion are the same as that in the neutral atom. This result is known as Koopman's theorem[7]. In reality however, the relaxation energy cannot be measured since it is simply a theoretical concept which makes use of the one-electron approximation for an N-electron system.

Difficulties in determining core-level binding energies can arise for many reasons. For instance, the relaxation energy in molecules is nearly always larger than that for atoms. Relaxation shifts can occur when atoms are adsorbed onto solid surfaces. This makes the interpretation of photoemission spectra difficult as binding energies of core levels in adsorbed atoms generally differ with corresponding atoms the gas phase. As well as relaxation effects, chemical bonding of adsorbates onto surfaces induce "chemical shifts" in adsorbate core level binding energies. This phenomenon forms the basis of the photoemission results in this thesis and is discussed in section 3.3.1.3.

3.3.1.2 Reference Level

Clearly, one must have a reference in order to determine the binding energy of a core level. For the case of metals, this level is taken as the Fermi level which is well

defined. The case for a semiconductor is more difficult however, since factors such as the dopant type and concentration can result in different Fermi energies, and the presence of bulk or surface states and adsorbates can cause band-bending at the semiconductor surface. For this reason, it is more accurate to use the region that will give the highest kinetic energy photoelectrons as the zero or reference, namely the valence band edge.

3.3.1.3 Chemical Shifts

The exact value of the binding energy measured for a given element depends on the chemical environment. A change in binding energy due to an altered chemical state gives rise to a chemical shift. The importance of such shifts was realised by Siegbahn and co-workers[8], who derived the acronym ESCA (Electron Spectroscopy for Chemical Analysis). They showed that core electron binding energies in molecular systems exhibit chemical shifts that are related to the covalency.

Chemical shift data is widely used to identify the chemical environments of an element by comparing the binding energies of a set of reference compounds involving the same element. The physical and chemical information contained in and the factors affecting the chemical shifts are of further importance. The basic physics involved in a change in binding energy is relatively straight forward. The energy of an electron in a tightly bound core level is determined by the attractive potential of the nuclei and the screening potential due to the repulsive core Coulomb interaction with all other electrons. A change in the chemical environment of a particular atom involves a spacial rearrangement of the valence electrons of this particular atom and all the other atoms in the compound. The change in binding energy and therefore the chemical shift ΔE_i experienced by an atom i in two different compounds A and B with valence charges q_i^A and q_i^B respectively can be expressed by the relationship:

$$\Delta E_i^{A,B} = k(q_i^A - q_i^B) + (V_i^A - V_i^B) \qquad (3.20)$$

where k is a coupling constant which relates the interaction between the core and valence electrons and V_i is the Madelung potential. The first term on the right-hand side of equation 3.20 takes account of the fact that an increase in binding energy is accompanied by a decrease in valence electron density on atom i. The second term is a measure of the potential due to the other atoms which surround atom i. For

most solids, both terms are of the same order of magnitude, ≈10 eV[7] such that they partially cancel, with the result that values of chemical shifts are of the order of a few eV or less. This therefore emphasises the need for accurate determination of core level binding energies if one is to derive reliable information from chemical shifts.

3.3.1.4 Surface Sensitivity

Surface sensitivity refers to the probing of the outermost atomic layers of a surface. A major factor influencing the degree of surface sensitivity is that of wave matching of the electron states across the solid-vacuum interface. This can be explained using a quantum-mechanical approach. The wave mechanical coupling between Bloch waves in initial states in the solid with a continuum of electron plane waves in final states in vacuum is illustrated in Figure 3.10. All states above the vacuum level are

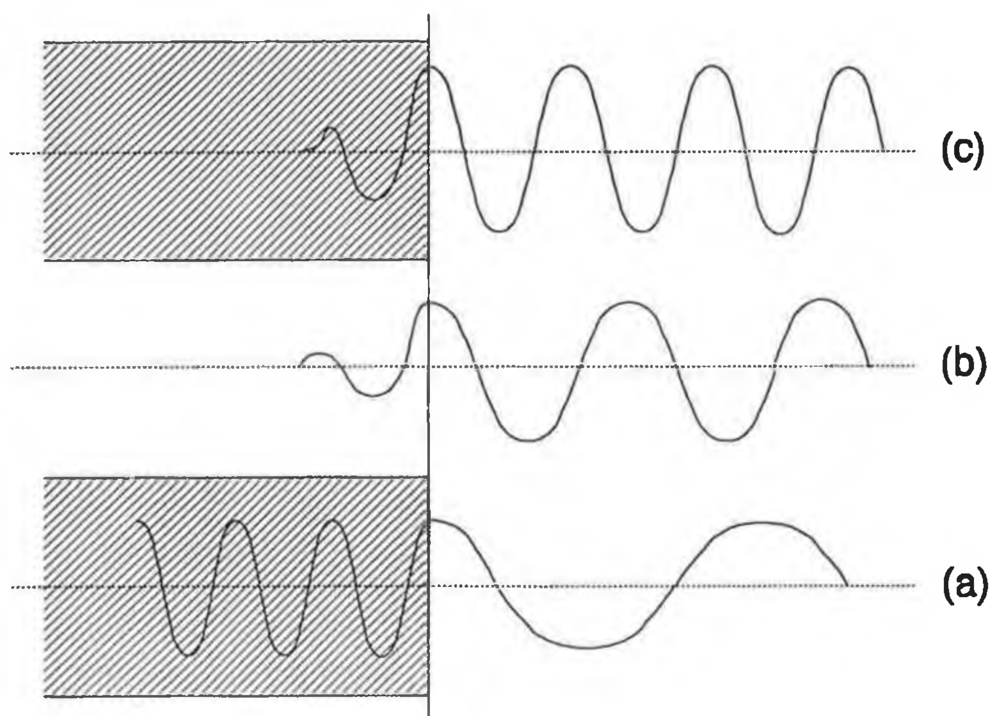

Figure 3.10. Wave matching across the interface for different cases (see text).

free electron states whereas below there exists bandgaps where no electron states may exist. Three different cases can arise. When the mean free path or escape depth of the electron is large (i.e. damping of the excited electron is small) then it is possible to match the free electron state in the vacuum to a Bloch state in the solid

as in Figure 3.10(a). If, on the other hand, there exists an energy gap in the solid, then the electron wave will decay exponentially over the distance of an atomic layer. This case is important as it means that photoemission is always possible from states that are localised at the surface. The third case involves the situation where there is strong inelastic scattering (i.e. damping of the excited electron is large), then the free electron wave in the vacuum couples to a decaying wave in the solid. In the first case, photoemission bears information on bulk properties of the solid whereas in that latter two cases, information is carried on the immediate vicinity of the surface. It is clear therefore, that photoemission spectra may contain a complex mixture of bulk and surface emission.

A second factor which gives rise to surface sensitivity is the inelastic scattering of the photoexcited electrons as they move towards the surface of the solid. The mean free path of these photoexcited electrons is strongly dependent on the electron energy. In a first approximation, the scattering probability can be defined in terms of a scattering length L(E) (escape depth) i.e.

$$S(E,x) = \exp\left(-\frac{x}{L(E)}\right) \tag{3.21}$$

where x is the distance travelled before scattering and E is the electron energy. Electron scattering between the excited electron and the valence electrons and electron-phonon scattering within the crystal lattice are the two most important processes giving rise to the scattering probability. Losses due to the latter however are small whereas electron-electron scattering energy losses can be considerably larger. Figure 3.11 shows the variation in mean free path for inelastically scattered electrons as a function of electron energy. As can be seen, the general behaviour of the escape depth as a function of electron energy is first a sharp decrease with increasing electron energy, then a fairly flat minimum in the 20-200eV range, with extremely small escape depths and finally an increase with electron energy.
It is clear that by working around the minimum of the curve, extreme surface sensitivity can be achieved with the result that it is possible to probe just the first few atomic layers of a solid.

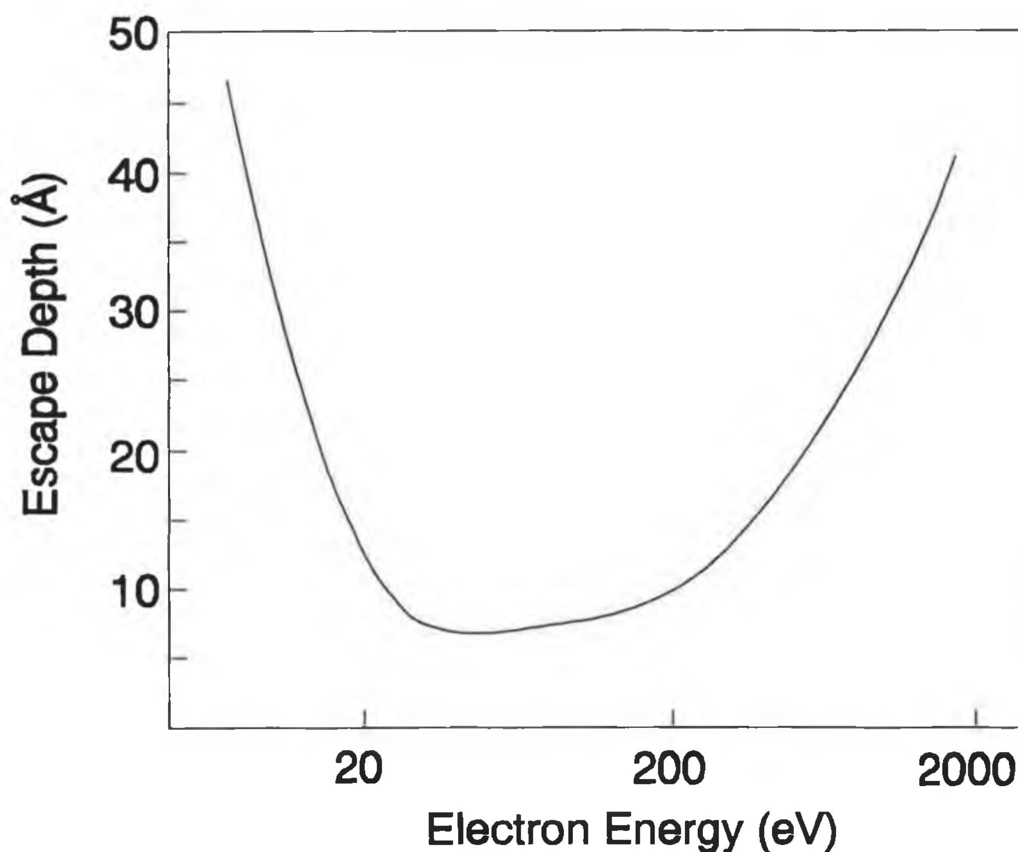

Figure 3.11. Plot of escape depth Vs energy

3.3.1.5 Photoionisation Cross-section

In addition to surface sensitivity, the photoionisation cross-section for a particular level in a solid is an important component in the photoemission process. In simple terms, it is related to the accessibility of the energy levels of the elements of the solid. The character of these levels, based on their principal quantum numbers, varies, as does the proximity of the photon energy to the photoemission threshold for the various levels. It is these parameters which affect the photoionisation cross-section.

Photoionisation cross-sections are usually calculated using the Golden rule[9] that the emission rate is proportional to the square of the matrix element $\langle f|\mathcal{H}|i\rangle$ where $\mathcal{H}$ is the interaction between the electron and $|f\rangle$ and $|i\rangle$ are the final and initial state wave functions. In practice, these states are many-electron wave functions and the

interaction must be summed over all electrons. However, it is more usual to calculate cross-sections assuming one-electron wave functions only.

It has been shown by Cooper[10] that the photoionisation cross-section for a particular level is highly energy dependent and goes through a minimum. This is known as the Cooper minimum. The main advantage of this result is that conditions can be chosen so as to maximise or minimise the sensitivity of a particular level. This may be achieved with a tunable source, such as a synchrotron.

3.3.1.6 Synchrotron Radiation

Synchrotron radiation, originally a by-product of high energy physics, is the electromagnetic radiation emitted when a beam of relativistic electrons undergo centripetal acceleration in a synchrotron. The radiation produced is well collimated, high energy continuum radiation with energies ranging from X-ray to radiofrequency. In addition to the above characteristics, there are several properties which make synchrotron radiation unique, particularly for photoemission studies. When used with a suitable monochromator, synchrotron radiation essentially becomes a high intensity tunable source, making it possible to optimise both photoionisation cross-section and surface sensitivity for the particular material being studied. Typical photon energies range from 40-200 eV[11].

Synchrotron radiation has other properties such as high resolution and stability and a high degree of polarisation. The latter property is particularly important for angle resolved studies, but is not used in the experiments presented in this thesis.

3.3.2 Low Energy Electron Diffraction

The coherent scattering of a low monoenergetic beam of electrons incident on a crystalline solid is referred to as Low Energy Electron Diffraction (LEED). First suggested by Ehrenberg[12], LEED reveals the geometry of a crystalline surface as a projection of the reciprocal lattice which in turn is related to the real surface geometry according to the Bragg relationship[13]. Thus, a LEED pattern results in a projection of a series of diffracted beams, the periodicity of which is dependent on the incident energy, the two dimensional symmetry of the surface and the angles of the diffracted beams. Typical incident electron beam energies ranging from 10-200

eV means that the mean free path for inelastically scattered electrons is at its minimum value of around 5 Å . These electrons have a high probability of losing energy and being lost from the elastically scattered electron flux. Of equal importance is the fact that elastic back scattering is very strong. Hence, successive surface layers contribute less to the elastic scattering as they receive smaller incident electron flux. It is these two effects which give rise to the extreme surface sensitivity of the LEED technique.

While the LEED pattern provides information on the periodicity of the crystal surface, the structure and position of atoms in the scattering system can be obtained by analysis of the diffracted beam intensities[14]. However, such analysis is extremely complicated, having to take into account the combined effects of ion core, multiple and elastic scattering as well as temperature effects. The restriction to the analysis of the LEED pattern however is very useful in itself. As a technique which gives information on the short range order of the surface being studied, it can thus be used to monitor the change from clean surface conditions to the ordered or dis-ordered adsorption of different atoms.

3.3.3 Auger Electron Spectroscopy

The ionisation of an atomic core level by an electron of sufficient energy can lead to two competitive processes. In one process, the core hole produced is filled by an electron from a shallower level, with the subsequent emission of a photon. Indeed, this process is the basis of X-ray generation. A second process can occur by which the energy released from filling the core hole with a shallow level electron can be given to another shallow level electron, which is then emitted. This radiationless process is termed the Auger effect, after its discoverer, Pierre Auger, and is shown schematically in figure 3.12, together with notation for an Auger transition.

The cross-section for Auger ionisation is energy dependent and reaches a maximum at three to five times the threshold energy for ionisation, typically around 3-5 keV. The Auger electrons emitted are characteristic of the excited atom and provided the valence electrons are not involved, these electrons exhibit features which are characteristic of their parent elements. Such fingerprints are useful for elemental composition analysis and have been catalogued by Davies *et al*[15]. Another attribute

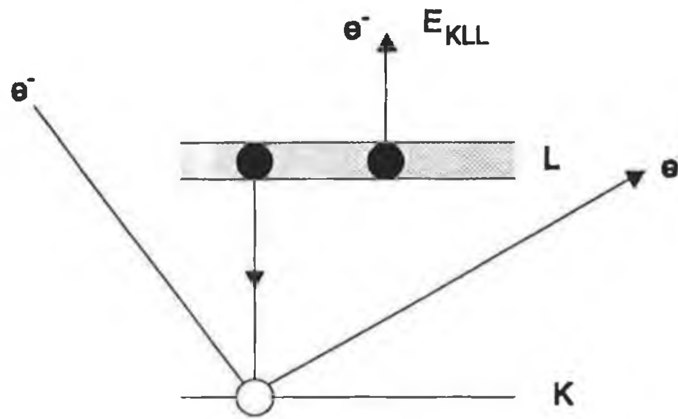

Figure 3.12. The Auger process, showing an Auger electron emitted from the L shell.

of the Auger process is that no variation in the Auger electron energy occurs for a variation in the incident electron energy. The surface sensitivity of the Auger technique arises due to the short mean free path of the Auger electrons, making it a valuable surface science technique.

In the electron yield curve of backscattered electrons, Auger electrons appear as a broad peak with structure at the low energy side due to numerous loss process. These Auger features are small in amplitude but can be enhanced dramatically by differentiation, usually by electronic modulation techniques.

References

[1] Rhoderick E.H. and Williams R.H., Metal-Semiconductor Contacts, 2nd Edition, Oxford Science Publications (1988).

[2] McLean A.B., Dharmadasa I.M. and Williams R.H., Semicond. Sci. Technol. (1986) **1**, 137.

[3] Lang D.V., J. Appl. Phys. **45** (1974) 3023.

[4] Platen W., Schmutzler H.-J., Brauchle K.-A. and Wolter K., J. Appl. Phys. **64** (1988) 218.

[5] Berglund C.N. and Spicer W.E., Phys. Rev. A. **136** (1964) 1030.

[6] Hughes G.J., PhD. Thesis, (1983) 25.

[7] Cardona M. and Ley L. eds., "Photoemission in Solids I", (Springer-Verlag 1978) 62-65.

[8] Seigbhan K., Nordling C., Fahlman A., Nordberg R., Hamerin K., Hedman J., Johannson G., Bergmark T., Karlsson S.E., Lindgren I. and Lindberg B., ESAC: Atomic, Molecular and Solid State Structure Studied by Means of Electron Spectroscopy, Nova Acta Regiae Sci. Ups., Ser. IV, **20** (1967).

[9] Woodruff D.P. and Delchar T.A., Modern Techniques of Surface Science, (Cambridge University Press, 1986).

[10] Cooper J.W., Phys. Rev. **128** (1962) 681.

[11] Howells M.R., Norman D., Williams G.P. and West J.B., J. Phys. E: Sci. Instrum. **11** (1978) 199.

[12] Ehrenberg W., Phil. Mag. **18**, 878 (1934).

[13] Bragg W.L., Proc. Cambridge Phil. Soc. **17** (1912) 43.

[14] Pendry J.B., "Low Energy Electron Diffraction" (Academic Press, London, 1974)

[15] Davies L.E., MacDonald N.C., Palmberg P.W., Riach G.E. and Weber R.E., Handbook of Auger Electron Spectroscopy (Physical Electronics Industries Inc., Eden Prairie, MN, 1976).

Chapter 4 Experimental Methods

4.1 Introduction

Numerous experimental techniques exist nowadays for investigating the properties of metal-semiconductor interfaces and since no one technique can provide a complete picture of the interface, it is advantageous to employ as many different techniques as are available. This chapter describes the experimental apparatus and methods used to obtain the results presented in this thesis.

Two experimental UHV systems were required during the course of this work, the first system, used in our home laboratory, was used for fabricating GaAs Schottky barrier diodes for electrical studies. The second system was located at the synchrotron radiation source (SRS) in Daresbury Laboratory and was used for surface science analysis. These systems, together with their related techniques are described in sections 4.2 and 4.3 respectively.

4.2 Electrical Studies

Figure 4.1 shows schematically, the typical steps involved in the fabrication of Schottky barrier diode's for characterisation by electrical techniques.

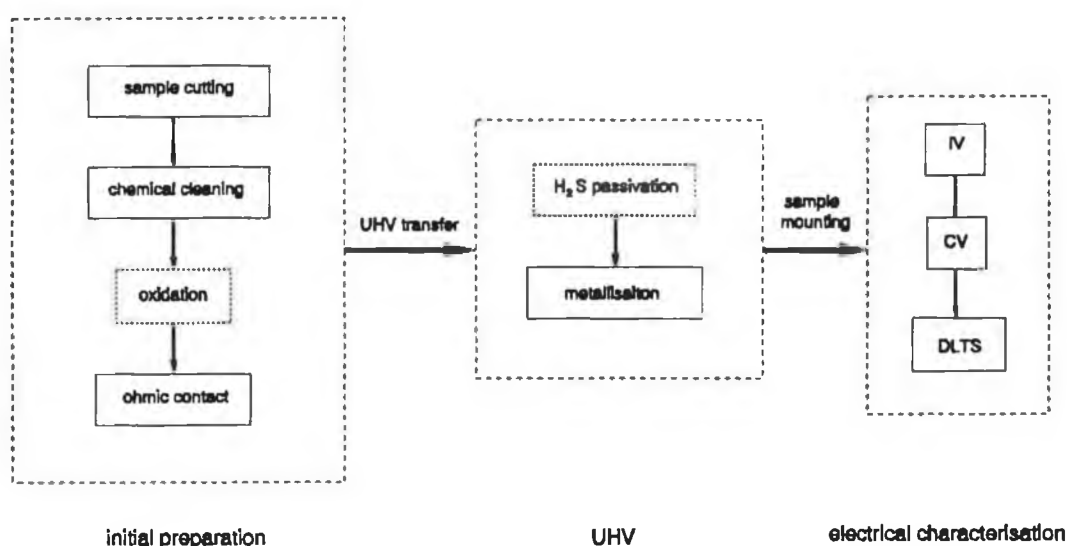

Figure 4.1. Block diagram of fabrication steps for electrical characterisation.

4.2.1 UHV System 1

Figure 4.2 shows the home built UHV system, UHV system 1. This system was used to prepare semiconductor surfaces with H_2S and molecular sulphur prior to *in situ* metal evaporation and consists of a stainless steel cylindrical main chamber 12" in diameter and 18" in height, the top and base of which have ports of 6" and 8" diameter, respectively. There are two experimental working levels, the top level of which is shown in Figure 4.3(a). The upper working level contains five 23/4" ports, four of which are at right angles to each other. The fifth is connected to the preparation chamber via a MDC sliding gate valve. Two 6" ports located on this level, at right angles to eachother, served as viewing ports while an 8" port allowed for the future attachment of a LEED/Auger apparatus. A Tekscan manipulator, located on the top 8" port allowed sample rotation about a vertical axis as well as movement in three orthogonal planes. A six way cross piece with a fast entry lock, to which an MDC magnetically coupled linear translator is attached, served as the preparation chamber. This was connected to the main chamber through the gate valve.

The pumping arrangement for this vacuum system is illustrated in Figure 4.2(b). Initial pumping of the system was achieved using a Leybold-Heraeus turbomolecular pump connected to the preparation chamber via a 1.5" diameter bellows. This was backed by a Leybold-Heraeus direct drive rotary pump. At suitably low pressures the Varian ion pump was switched on. Base pressures of 10^{-10} mbar in the main chamber were achieved following bakeout at 180 °C for eight hours. A titanium sublimation pump which was screened from the main chamber area by a stainless steel shield helped to retain this base pressure throughout the experiments. Pressures were monitored by Vacuum Generators ion gauges both in the main chamber and preparation chamber. A Hiden Analytical quadrupole mass spectrometer connected to the main chamber at the lower level allowed both the detection of leaks and the monitoring of the purity of gases being adsorbed on the sample surfaces.

4.2.2 Sample Preparation and Transfer

The samples used in these experiments were cleaved from Si-doped n-type GaAs(100) (N_D-N_A = $4x10^{16}$ cm^{-3}) wafers which were grown by the Czochralski method, one side which was polished to give a mirror-like surface. Samples were

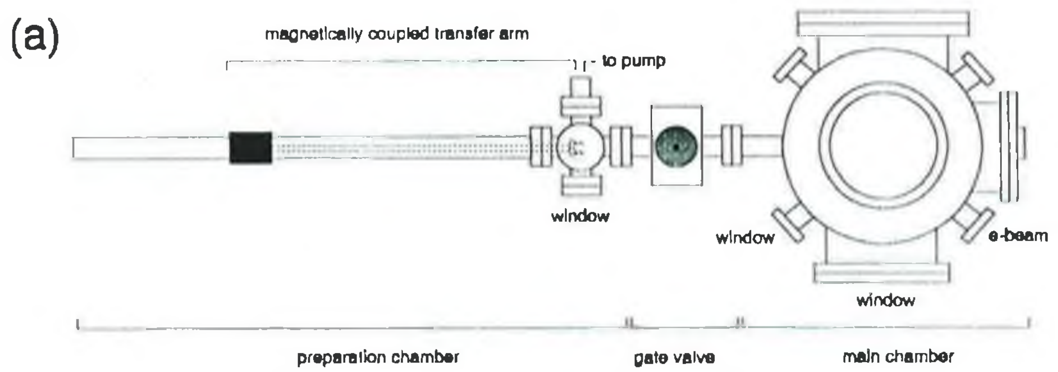

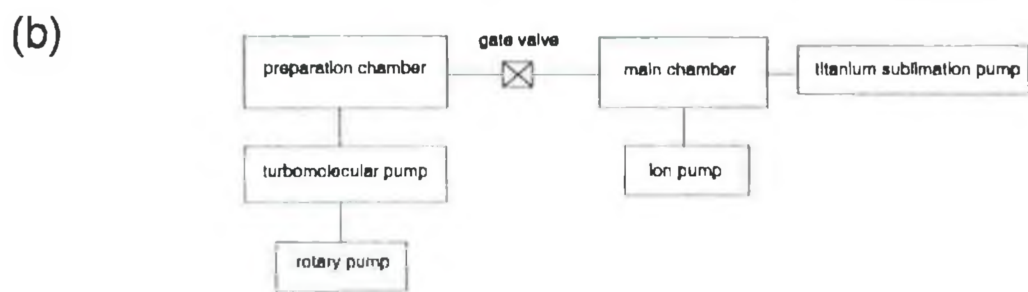

(c)

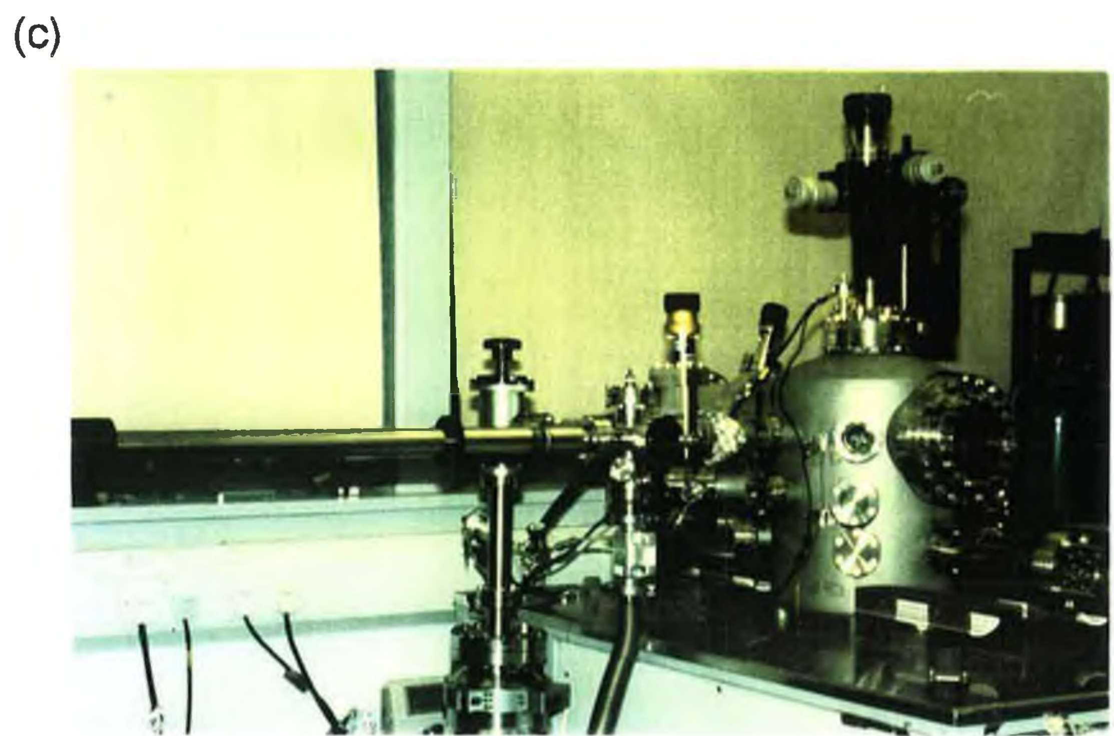

Figure 4.2. (a) UHV system 1 showing upper level of main chamber and preparation chamber. (b) Pumping arrangement for UHV system 1. (c) Photograph of UHV system 1.

prepared by placing the wafer on a flat surface and by positioning a stainless steel ruler 5 mm from the wafer edge, a scribe was used to make a small indent in the wafer along the ruler edge, parallel to the cleavage plane. Upon lightly tapping the wafer, it cleaved along the indent. The same procedure was used in a direction perpendicular to the first indent, so that small rectangular samples were formed. Typical sample dimensions were about 5mm x 6mm. The samples were then ready for chemical cleaning. This was carried out by first degreasing the samples using acetone followed by methanol. The samples were then transferred to the etch solution H_2SO_4 : H_2O_2 :H_2O (5:1:1) and etched for 2 minutes typically. In this etch, the H_2O_2 oxidised the GaAs surface and the H_2SO_4 dissolved the oxidation products. This was followed by a de-ionised water rinse, which removed the excess As and Ga oxides and ceased the etching reaction. The samples were then dried in a flow of inert N_2 gas. Contacts were made to the unpolished side of the samples by coating with InGa alloy and initial preparation was completed by annealing the alloy into the sample to form an ohmic contact. Earlier experiments necessitated that samples be annealed in a furnace at temperatures of 670K for 15 minutes in an N_2 atmosphere. However, modifications to the experimental apparatus, described below, permitted sample annealing to be carried out in UHV. This minimised the time during which samples were exposed to air.

Sample transfer was achieved by placing a sample on a specially designed sample holder. This is shown in Figure 4.3. The latter was then loaded onto a pair of pins located on the end of the linear translator. Having pumped the preparation chamber to a suitable pressure, the gate valve could then be opened and the sample transferred to the main chamber.

4.2.3 Sulphur Passivation

While a number of methods were used to sulphur passivate the GaAs samples, the main methods focused on either the exposure to hydrogen sulphide gas or the deposition of molecular sulphur in the form of S_2 from an electrochemical cell. The latter method, used in conjunction with surface science techniques to monitor the evolution of the passivated GaAs surface, is described in section 4.3.3. In the first method, high purity compressed H_2S cylinder was attached to one end of a 1 m length of stainless steel tube of 5 mm inner diameter. The other end of the tube was

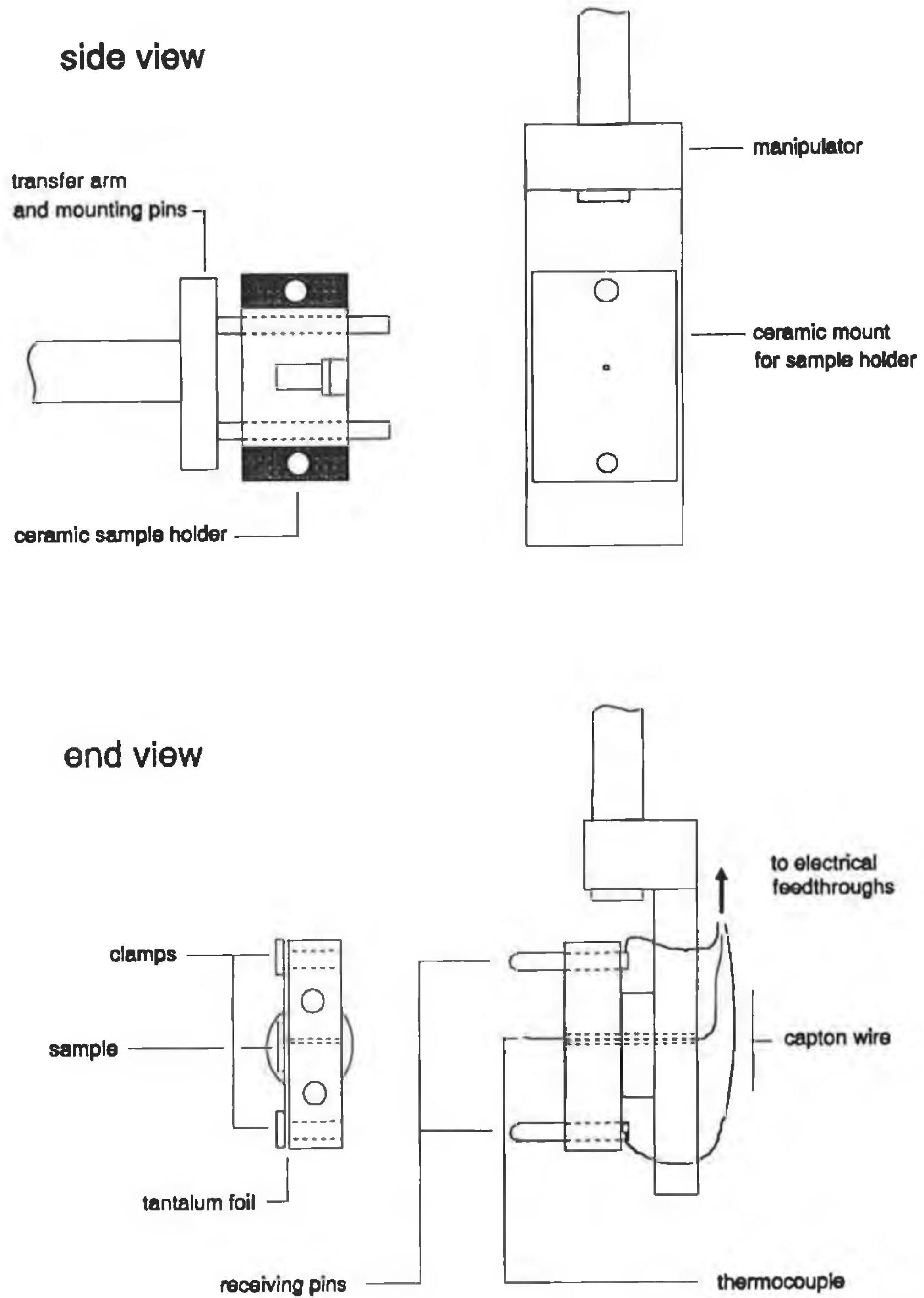

Figure 4.3. Sample holder design and transfer arrangement

fastened to a leak valve which was located on a 23/4" port on the preparation chamber. Before loading and exposing a sample, the stainless steel tube was first pumped out by opening and closing the H_2S cylinder thus allowing the gas to fill the tube. The leak valve was then opened fully and the H_2S, together with any other residual gases in the line, was pumped out. This procedure was carried out a number of times to ensure that the H_2S gas in the line was of high purity. It was also possible to bake the tube to 180 °C using special heating tape. Having loaded the sample into the preparation chamber and pumping the latter to UHV. H_2S passivation could be carried out. Exposure was measured in units of Langmuirs (L), where 1L = $1x10^{-6}$ Torrsec. For higher exposures i.e. up to $2x10^{12}$ L, the H_2S cylinder valve and leak valve were opened without pumping the preparation chamber.

4.2.4 Metal Evaporation

The basic experimental arrangements used for metal evaporation is illustrated in Figure 4.4(a). For metals which evaporated relatively easy, e.g. Au, Ag, Fe or when no stringent conditions were placed on the thicknesses of Schottky contacts, resistively heated filaments made from single diameter 0.1mm strand tungsten wire wound into coils were used. Newly made filaments were given an initial outgassing in the preparation chamber. Ultra pure metals which came in wire form of 0.5 mm diameter were cut and wound into small loops which were placed evenly around the filament. Metals such as Fe had to be cut into small rectangular strips from an Fe sheet. These strips were wrapped around the filament spirals. Alternatively the tungsten filament was wound into a vertical spiral boat, so metals could be placed into the boat without falling off.

Filament evaporation normally took place in the preparation chamber. Before evaporating a sample, currents of 4-5 Amps were rapidly and repeatedly passed through the filament, so that both filament and metal could be outgassed. During this time, small spherical beads of metal formed on the filament. Typical evaporation currents of 3-4 Amps were passed through the filaments for various lengths of time depending on the metal to be evaporated. A stainless steel cylindrical shaped shroud with a square exit slit placed over the filament ensured that metal evaporation was restricted to the sample, thus minimising exposure to the preparation chamber walls. Typical GaAs samples measured 5mm x 6mm in area. Thus, by placing a stainless

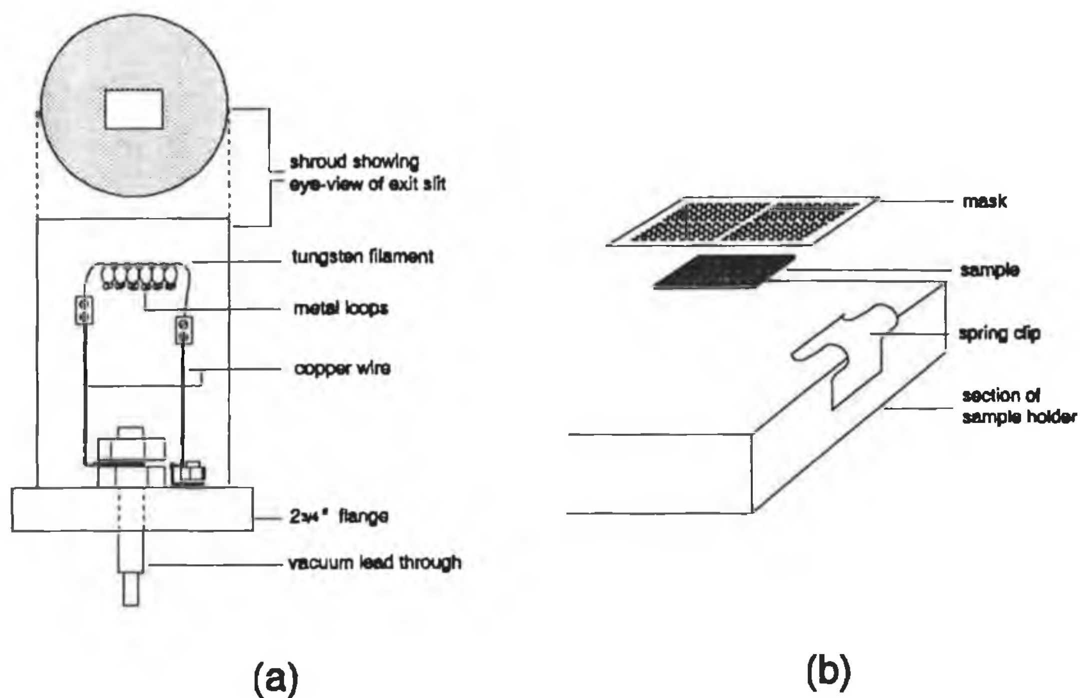

Figure 4.4. (a) Arrangement for metal evaporation from a tungsten filament. (b) Position of mask for filament evaporation.

steel shadow mask with a regularly spaced array of circular holes in close contact with the sample during evaporation, several Schottky barrier diodes could be fabricated on one sample. This is illustrated in Figure 4.4(b) Schottky barrier diodes of diameter 0.6 mm were fabricated in this fashion. For routine electrical studies, no special constraints were placed as regards the thickness of the deposited metal overlayers, and it was sufficient to ensure that contacts were thick enough so that they could be seen by eye and couldn't be easily pierced when probed.

Metal deposition by electron beam evaporation was used in cases where controlled deposition rates of thin metal overlayers was required. A schematic diagram of the VSW ME10 electron beam evaporator is shown in Figure 4.5. The principle of operation is based on the evaporation by electron bombardment of a metal held at high positive voltage. It was the main means of evaporation of titanium used in these experiments, where deposition rates of as low as 0.01 Å per min could be

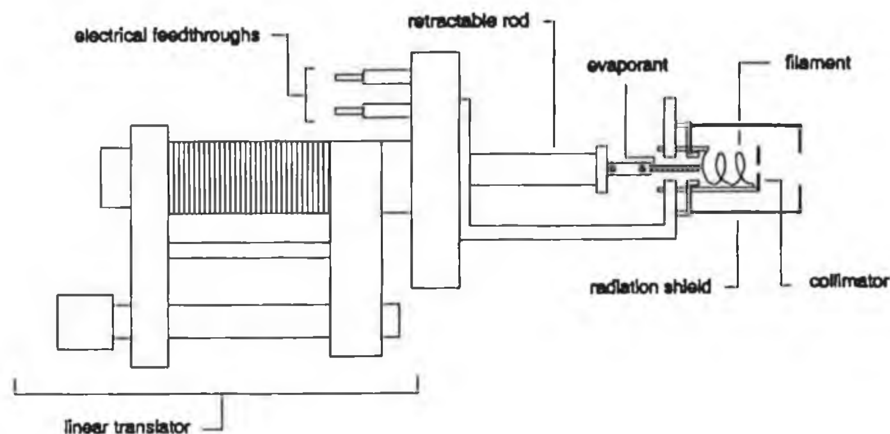

Figure 4.5. Diagram of VSW ME10 electron beam evaporator

achieved. The metal to be evaporated came in the form of a 1mm diameter wire which was cut into a 25mm rod and filed flat at one end. The other end was clamped into a retractable tube and the latter adjusted so that it was situated in a central position at the base of the helical filament. A collimating plate and a tungsten radiation shield placed over the filament ensured that the evaporating metal was directed at a small area. Before metal deposition, both the filament and metal were outgassed. Pressures of $<10^{-8}$ mbar were required in order to minimise high voltage breakdown during routine evaporation. In normal operation, a high positive voltage of 2.5 kV was applied to the metal. Electrons from the heated filament bombarded the metal tip causing a temperature rise and hence evaporation. By using a linear translator, the metal tip could be moved so that it remained at the base of the filament as it shortened, thus prolonging metal evaporation and minimising the need to vent the vacuum chamber. The rate of metal evaporation was monitored using a water-cooled Intelemetrics quartz crystal thin film thickness monitor. Thickness measurement was achieved by moving the crystal using a linear translator to a position just behind the sample in direct line with the emerging metal beam. As the quartz crystal was located at a greater distance from the electron beam evaporator than the sample a $1/r^2$ relationship was used to determine precise metal coverages.

4.2.5 DLTS Sample Mounting

A Biorad LN_2 cryostat was used to house samples for electrical measurement and although primarily intended for DLTS characterisation, it could easily be connected for I-V and C-V measurements with a minimum of external rewiring. Illustrated in Figure 4.6, the cryostat is cylindrical in design of diameter 200mm and height 100mm. A removable top cover allowed sample transfer and electrical probing to be carried out with relative ease. Samples were placed on a T-shaped Cu-Ni alloy sample stage. A stainless steel block located immediately underneath the stage containing both a LN_2 cold finger and a resistive heater allowed sample cooling and heating for DLTS operation. Consequently, sample evacuation to about 10^{-2} mbar was required and was achieved using an Edwards rotary pump connected to the base of the cryostat. Sample temperature was monitored by a platinum resistance thermometer which was attached to the top of the stage adjacent to the sample. Two gold probes attached to two separate xyz- translation stages enabled electrical contact to be made to both the top(rectifying) and back(ohmic) sides of the sample. These probes were connected to the centre pins of two BNC sockets located on the outside of the cryostat. The sample stage was earthed through the BNC ground.

Before being transferred to the cryostat, samples had first to be suitably mounted so that both rectifying and ohmic contacts could be probed. A thin sheet of mica acted as an electrically insulating but thermally conductive base, onto which a small amount of colloidal silver paint was applied. The sample was then placed with the ohmic contact face down onto the silver paint which was subsequently dried using a hot air gun. A small quantity of thermally conductive grease spread onto the stage was required, particularly for DLTS operation, as it provided good thermal contact to be made between the sample and the stage.

4.2.6. I-V and C-V Measurement

An automated measurement system, utilising the input/output capabilities of an Advantech PC-712 Multi-lab card, was used to measure both I-V and C-V characteristics of Schottky barrier diodes. Block diagrams of the experimental arrangements used for these measurements are shown in Figure 4.7. The voltage across the sample is provided for by a high-precision OP-07 operational amplifier which is driven by the PC via the 12-bit digital to analog converter (DAC) on the lab

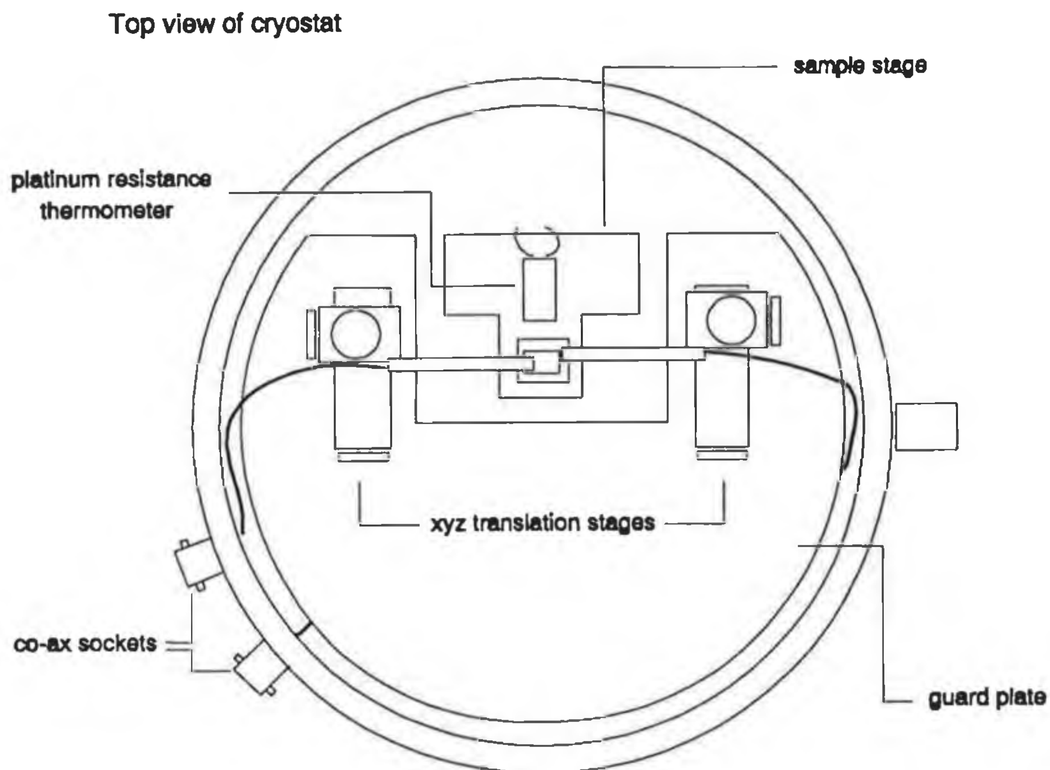

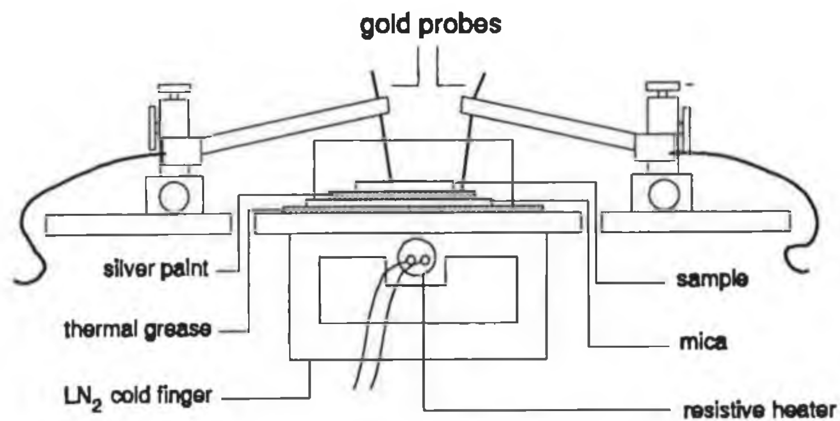

Figure 4.6. Diagram of the LN_2 cryostat used for electrical studies and the sample mounting arrangement.

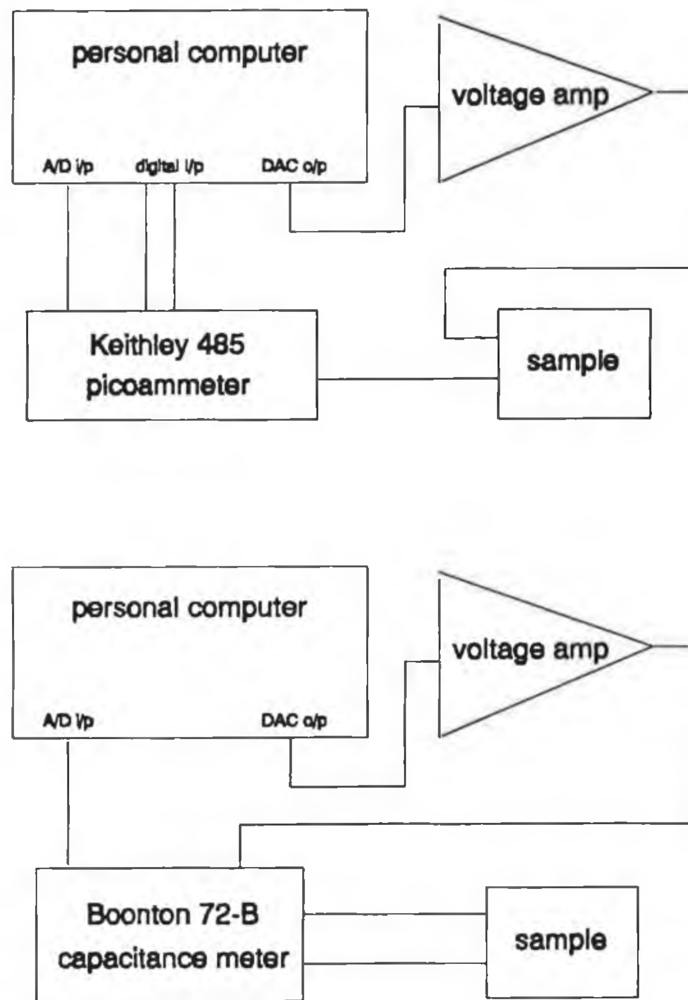

Figure 4.7. Block diagram of the I-V and C-V measurement used to characterise GaAs Schottky barrier diodes.

card. The diode current is measured by a Keithley 485 picoammeter, which gives a 0-2 V dc output for each of six 20nA, 200nA, 2μA, 20μA, 200μA and 2mA current ranges. The picoammeter output and current range status are fed to the lab card 12-bit analog to digital converter (A/D) and digital input port respectively. Software was written in the computer language C to provide both hardware control and data acquisition and manipulation. Characteristic I-V and lnI vs V curves could be plotted from which the ideality parameter n and the barrier height ϕ_B^{IV} could be determined from a least squares analysis of the lnI vs V characteristic curve.

With the substitution of a Boonton 72-B capacitance meter for the picoammeter, C-V measurements can be taken. In this case, a reverse bias is applied to the sample via the DAC and the resultant differential capacitance is measured by the Boonton, which gives a 0-3 V dc linear output. This is applied to the A/D on the PC. Similar software to that written for I-V measurements enabled a $1/C^2$-V analysis to be performed, from which the barrier height ϕ_B^{CV} and carrier concentration N_D could be determined. Although I-V and C-V measurements were essentially straight forward techniques, both offered different means of determining the barrier height ϕ_B, which was useful for the purpose of cross correlation. The value of N_D obtained from a $1/C^2$-V plot could be compared with the value quoted by the semiconductor manufacturer. As an indication of the quality of the Schottky barrier diodes, I-V and C-V measurements could also determine whether further electrical characterisation such as DLTS was to be carried out.

4.2.7. Deep Level Transient Spectroscopy

A Biorad S4600 DLTS system was used for DLTS characterisation of Schottky barrier diodes in these experiments. The S4600 is modular in design, consisting of a bias pulse generator and timer, a signal processor and master clock, a capacitance meter and a temperature controller. Temperature output and DLTS signals are applied to the lab-card via a home-built interface so that automated data collection and manipulation can be achieved. A block diagram of the DLTS system is shown in Figure 4.8(a). The pulse generator provides the necessary reverse bias and fill pulse sequences of variable width and amplitude to the sample located in the LN_2 cryostat, via the Boonton capacitance meter. The resulting capacitance transient measured by the capacitance meter is fed to the signal processor. The master clock, which controls the fill pulse sequence generated by the pulse generator, also provides the appropriate timing for each of the twelve preset emission ratewindow settings available on the S4600. These are listed in Figure 4.8(b). The signal processor module contains a triple boxcar averager which effectively allows sampling of the transient at three intervals t_1, t_2 and t_3, where t_2 - t_1 and t_3 - t_2 each represent a emission ratewindow setting. Consequently, two ratewindows can be imposed on the capacitance transient to produce two separate DLTS signals. This concept is illustrated in Figure 4.8(c). The temperature controller module, in addition to monitoring sample temperature, also provides controlled sample heating from 77 K

(a) S4600 DLTS system

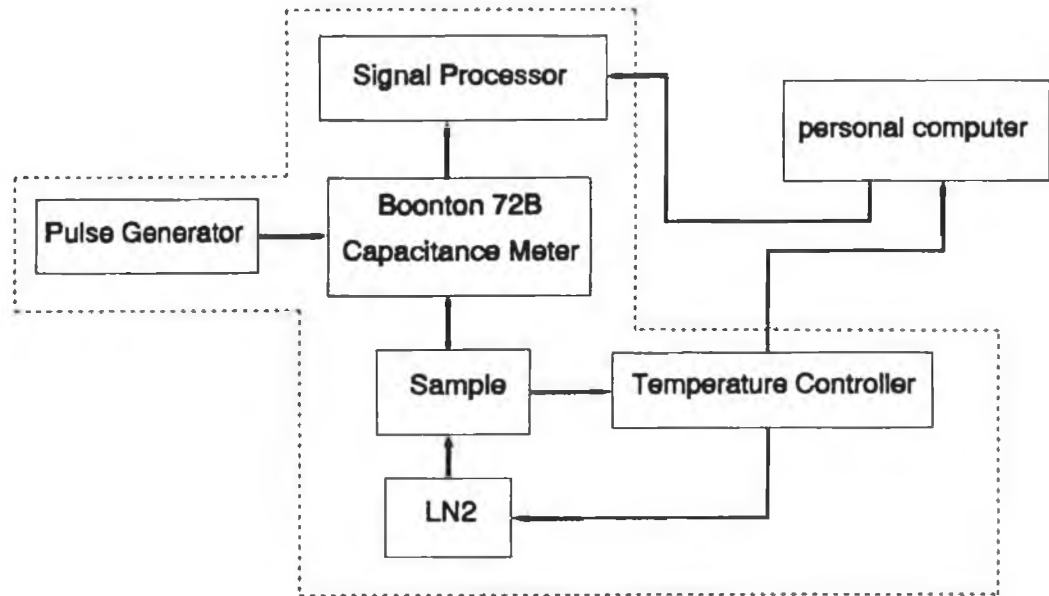

(b)

B	0.4	2	8	40	200	1000
A	1	5	20	100	500	2500

preset emission ratewindows (s^{-1})

(c)

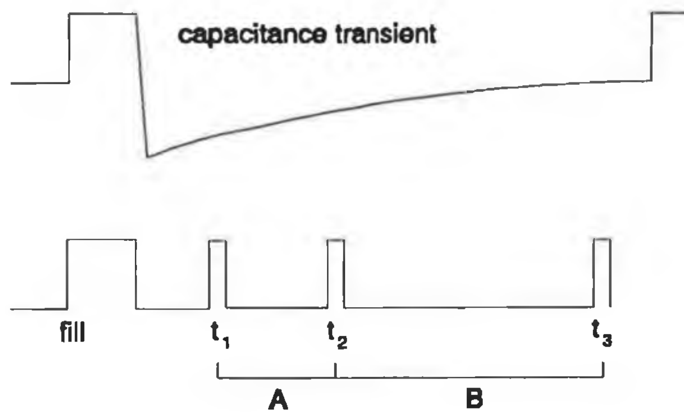

Figure 4.8. (a) Block diagram of DLTS system. (b) Preset emission ratewindows for S4600. (c) Implementation of two ratewindows A and B simultaneously.

up to 450 K. This is achieved by a feedback arrangement which combines the flow of LN_2 via an Archimedes screw to the cold finger with resistive heating of the sample. Temperature ramp rates of as low as 0.1 K/sec are possible.

In a routine DLTS measurement, the required rate windows were selected and suitable reverse bias and fill pulse of appropriate amplitude and width were applied to the sample to obtain a capacitance transient. This was carried out at room temperature. Increased sensitivity could be achieved by adjusting a range select switch on the capacitance meter. The initial and final temperatures were selected on the temperature controller and a suitable temperature ramp rate was chosen to ensure that no hysteresis or thermal lag by the sample could occur. The sample was then cooled rapidly to the required initial temperature and a short time was allowed to elapse in order that the sample could reach thermal equilibrium. A DLTS scan could then be taken.

Two distinct modes of DLTS operation were employed. In one mode, reverse and fill pulse voltages were kept constant and several DLTS spectra were taken at different emission rate window settings. For each temperature at which a peak occurred, a corresponding emission rate could be calculated. Consequently, an Arrhenius analysis enabled the determination of both the activation energy and capture cross section of particular, and usually well documented electron traps. This mode of DLTS operation was used when quantitative information on deep traps within semiconductor bulk was required. The second mode involved varying the fill pulse voltage amplitude, typically from 0 V up to the barrier height of the Schottky barrier diode, while keeping both reverse bias and ratewindow setting constant. By taking a DLTS spectrum at several fill pulse voltages, a profile of interface state distributions, if any, unfolded, yielding detailed information as regards the quality of the metal-GaAs interface. By taking spectra at different rate window settings, activation energies and capture cross sections corresponding to the interface states could be determined by the same method as that used for bulk traps. This mode of operation was used extensively to compare the concentrations of interface state distributions detected on Schottky barrier diodes which exhibited near-ideal and highly non-ideal I-V characteristics.

4.3 Surface Science Studies

4.3.1 UHV System 2 and Related Techniques

The second UHV system is a standard Vacuum Generators ADES 400 system with modifications to allow it to couple with the grazing incidence monochromator, GIM6, on beamline 6.1 at the Synchrotron Radiation Source, SRS, at Daresbury. The system consists of a non-magnetic μ-metal main chamber in the form of a bell-jar to which a stainless steel preparation chamber is attached. A photograph of the entire system is shown in Figure 4.9.

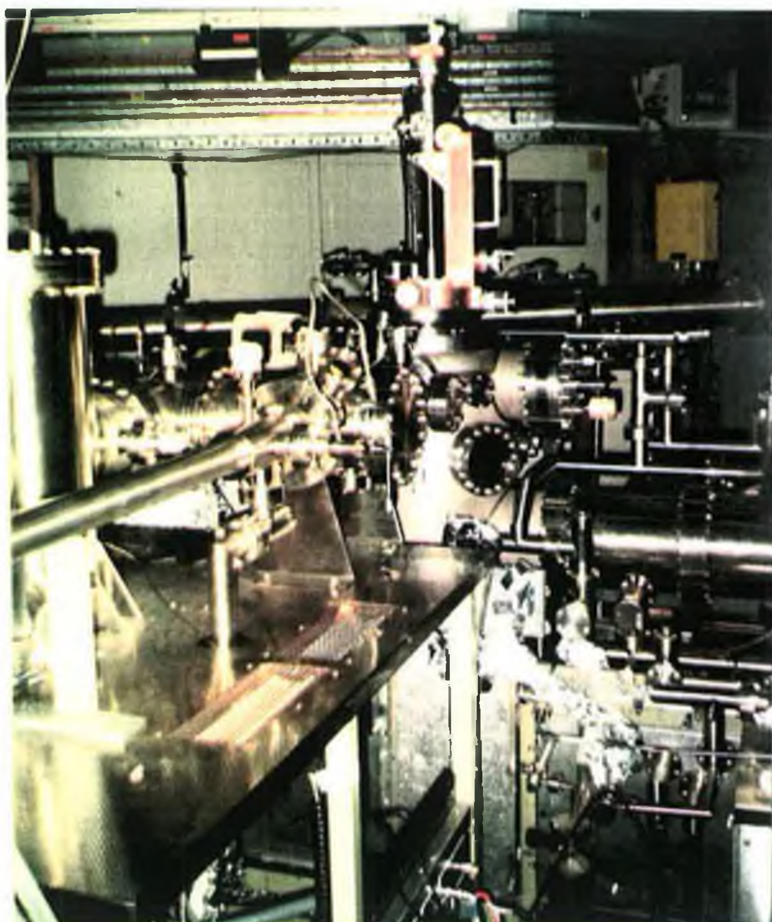

Figure 4.9. Photograph of UHV system 2.

Measuring 14" in diameter and 36" in height the main chamber is mounted on a 17" base flange, just above which an 8" port leading to the pumping system is located. This chamber has two experimental working levels shown schematically in Figure 4.10, with a 8" top port on the chamber axis. The upper working level has seven

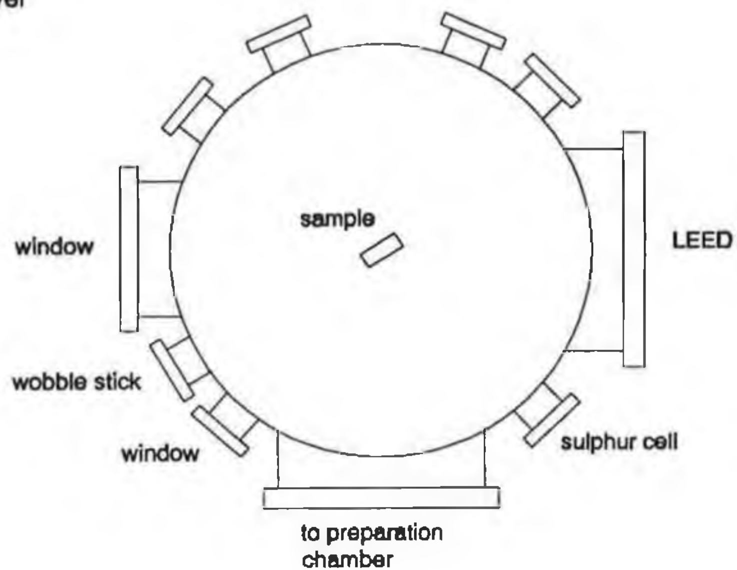

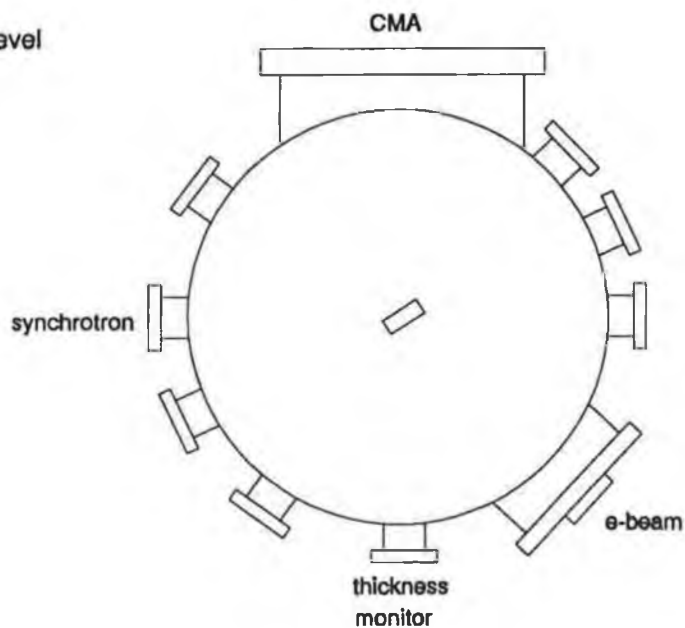

Figure 4.10. Schematic representation of upper and lower levels of UHV system 2.

23/4" ports positioned radially around the chamber, an 8" port for LEED optics opposite a 6" window, on an axis parallel to the beam line, and an 8" port for attachment of the preparation chamber. The sulphur cell (described in section 4.3.3) was mounted at this level. The lower working level contains eight 23/4" ports mounted radially around the chamber, a 6" viewing port and an 8" port to which the cylindrical mirror analyzer, CMA, was attached. It was at this level that synchrotron radiation from the monochromator entered the chamber. The e-beam evaporator and thickness monitor described in section 4.2.4 were also mounted at this level. A Vacuum Generators UMD20 universal manipulator located on the top 8" port allowed sample rotation about a vertical axis, azimuth rotation about an axis normal to the sample surface and movement in three orthogonal planes.

The preparation chamber, a top view of which is illustrated in Figure 4.11, was connected to the main chamber upper level, perpendicular to the incoming synchrotron radiation, via an 8" port, as mentioned above. Samples were loaded into this chamber for transfer to the main chamber. This horizontally mounted chamber of diameter 8" and length 24" contains eleven 23/4" ports and three 4" ports placed radially along its circumfrence. An 8" side-port located opposite an 8" viewing window led to the pumping system for the chamber. Isolation from the main

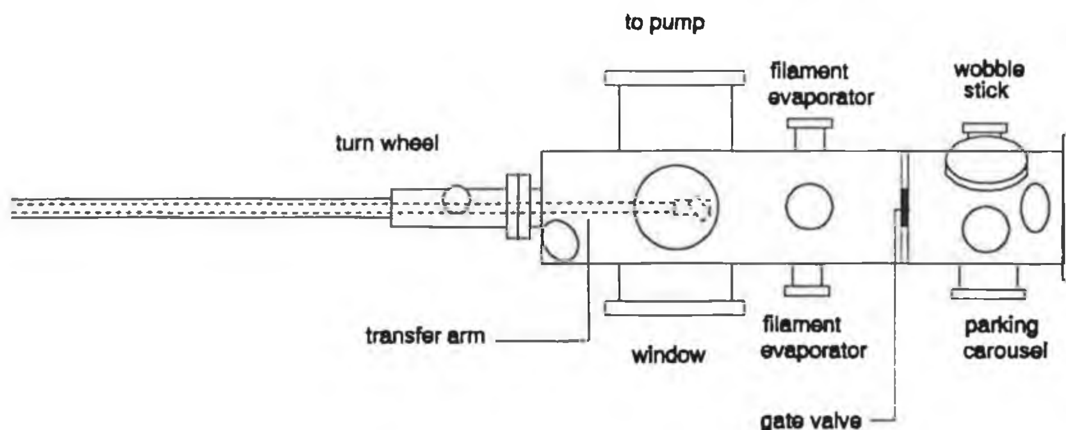

Figure 4.11. Schematic diagram of the top view of the preparation chamber.

chamber is achieved via a 23/4" spring-loaded sliding gate valve located as shown in Figure 4.11. Filament evaporators described in section 4.2.4 were mounted in this chamber. In order to make efficient use of the allocated beam time it was necessary to use a system whereby several sample transfers could be made without breaking vacuum. A stainless steel carousel type sample holder, capable of holding two samples, was designed for this purpose[1]. The sample holder, described in section 4.3.2, was mounted on a Vacuum Generators linear translator which was attached to a 4" diameter flange at the end of the preparation chamber. Movement of the linear translator was achieved by turning a cog wheel which engaged a set of teeth positioned along the length of the translator.

The pumping arrangement for the system 2 is shown schematically in Figure 4.12. The preparation chamber is pumped by a Balzers turbomolecular pump which is backed by an Edwards EMD6 rotary pump. Further pumping is achieved using a Vacuum Generators LN_2 cooled vapour trap and a titanium sublimation pump. The main chamber is pumped by a Balzers turbomolecular pump, backed by an Edwards rotary pump. The turbomolecular pump is at the base of a Vacuum Generators LN2

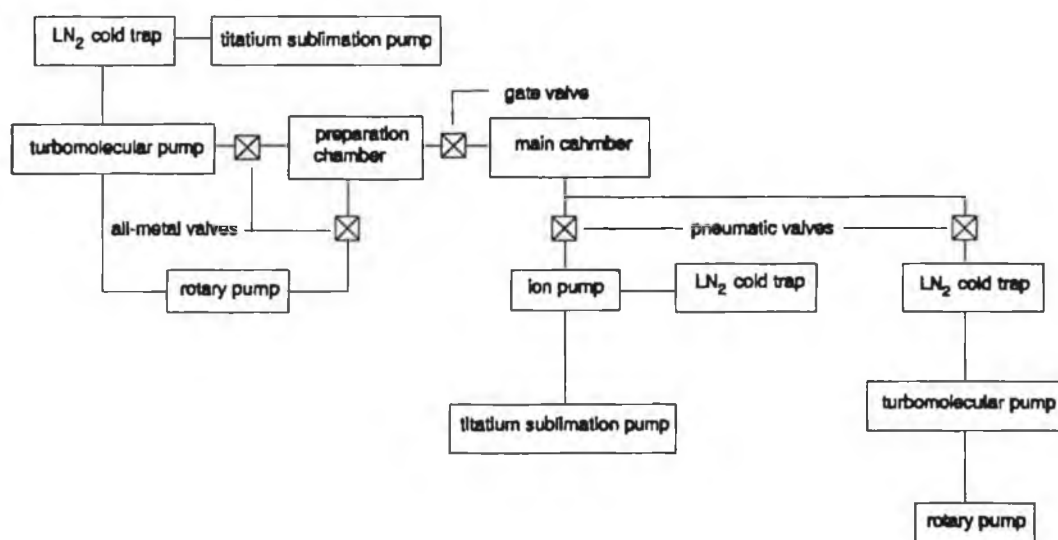

Figure 4.12. Pumping arrangement for UHV system 2.

cold trap. Evacuation from atmosphere for both chambers was achieved using the preparation chamber rotary pump which was connected to a 23/4" port on the preparation chamber. The entire system was surrounded by bake-out ovens allowing it to be baked at 180 °C. Ultimate pressures of better than 1 x 10^{-10} mbar were monitored by Vacuum Generators ion gauges both in the main chamber and preparation chamber. A Vacuum Generators SX200 quadrupole mass spectrometer connected to the main chamber at the lower level allowed both the detection of leaks and the monitoring of any residual gases present in the chamber following bakeout.

4.3.1.1 Electron Energy Analyzer

A Perkin-Elmer double-pass cylindrical mirror analyzer (CMA) was used measure the energy distribution of electrons emitted from the sample surface. This analyzer had two modes of operation, namely XPS and Auger. In XPS mode, it served to collect and energy analyze photoelectrons which were emitted from the sample. The analyzer operates by electrostatically focusing incoming electrons in such a way as that only those with energies within a certain range $E_0 + \Delta E$, selected by the exit slit, form an image of the entrance slit at the detector. Illustrated in Figure 4.13(a), the analyzer consists of a set of concentric cylinders which accepts electrons into a conical annulus of approximately ±6° about a mean angle of 42°. With the inner cylinder at ground, a negative potential V applied to the outer cylinder creates an electrical field with cylindrical symmetry. Incoming photoelectrons, with initial kinetic energy $E_e=eV_e$, are accelerated or retarded to the pass energy E_0, and deflected towards the inner cylinder by an amount depending on their kinetic energy. The double-pass design reduces background noise generated by secondary electrons within the analyzer by imposing two stages of filtering, with the first stage operating at low resolution. By sweeping the potential on the outer deflection cylinder from zero to the photon energy and hence, varying E_0, an energy spectrum is obtained. The energy resolution $\Delta E/E_0$, determined by the analyzer dimensions, is constant.

Having passed through the analyzer, the photoelectrons are collected and amplified by a channeltron electron multiplier, whose output is proportional to $N(E).\Delta E$, or $E_0.N(E)$, since ΔE E_0, where N(E) is the electron energy distribution. The channeltron output pulses are fed via a dc isolating capacitor to a Vacuum Generators pulse counting unit. A mini-computer provided suitable data acquisition and

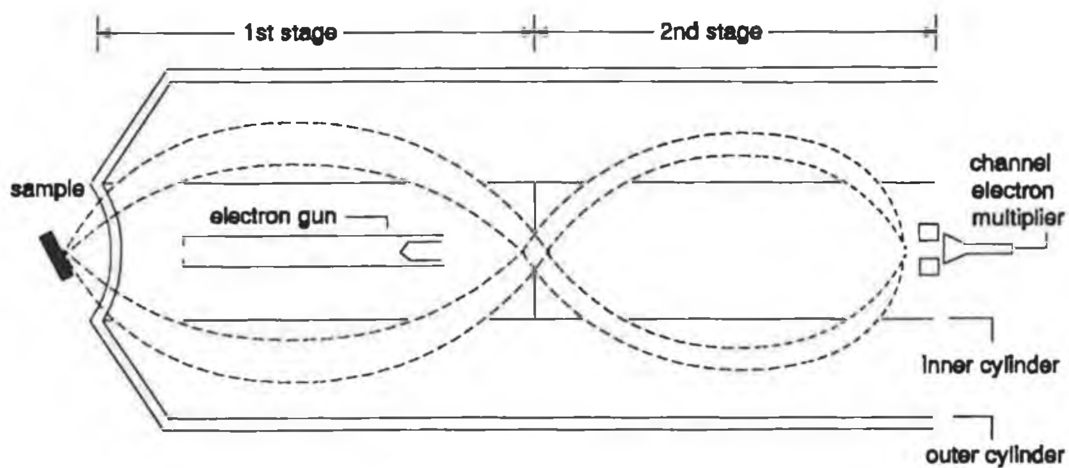

(a)

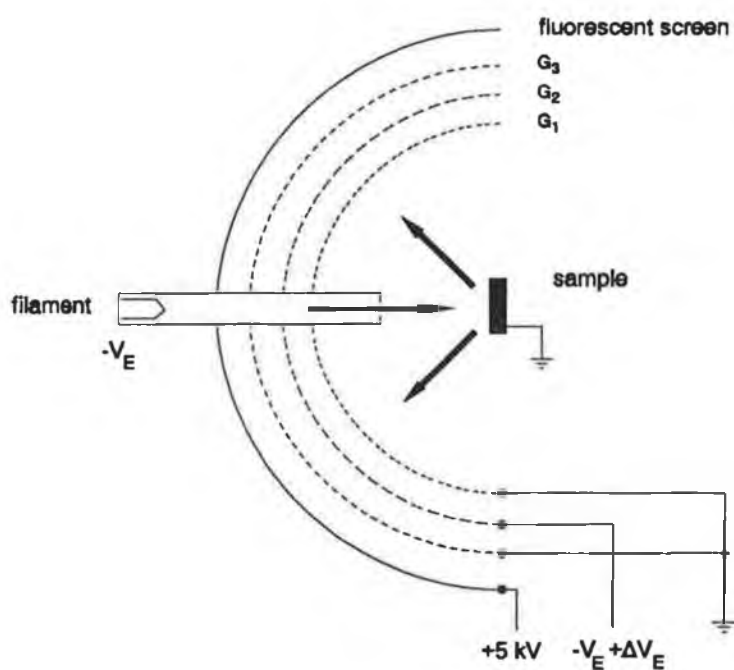

(b)

Figure 4.13. Schematic representations of (a) Perkin-Elmer double-pass cylindrical mirror analyzer (CMA); (b) Varian 3-grid LEED optics.

hardware control. The CMA can easily be switched over to operate as an Auger system. In this mode of operation, an electron gun which is mounted coaxially inside the CMA is used to direct an electron beam, with energies ranging from 3 to 5 keV, at the sample. A negative voltage ramp V is applied to the outer deflection cylinder together with a modulation signal $V_m \sin\omega t$. The current collected by the CMA then contains a component at the modulation frequency ω, given by:

$$I(\omega) \propto \frac{dN(E)}{dE} \qquad (4.1)$$

Thus, by using phase sensitive detection dN(E)/dE can be obtained directly.

4.3.1.2 LEED System

A Varian 3-grid retarding field analyzer (RFA), illustrated in Figure 4.13(b), was used to observe LEED patterns. The system consists of three concentric stainless steel mesh grids, together with an fluorescent screen, all of which form a hemisphere around a radially mounted electron gun. The electron gun delivers a fine beam of monoenergetic electrons of approximately 1 μA in the energy range 20 - 1keV to the sample, which is held at ground. With grid G_1 also at ground, backscattered electrons travel through a field free region of space to grid G_2. A potential is placed on this grid, such that all electrons other than those which have been elastically scattered by the sample, are retarded. These elastically scattered, diffracted electrons pass through grid G_3, which is connected to grid G_1, and are accelerated towards the fluorescent screen which is held at a high positive potential of 5 kV. Grids G_1 and G_3 act to shield grid G_2 from field penetration from the screen. The LEED patterns produced were observed though a 6" window directly opposite the LEED system.

4.3.1.3 Monochromator

The synchrotron radiation was rendered monochromatic by a grazing incidence monochromator which was constructed at Daresbury laboratory[2]. The arrangement of the monochromator at zero order is indicated in Figure 5.14. One of the principal features of the design is that only two reflections are required to monochromate the radiation. The plane grating, manufactured by the National Physical Laboratory is a "laminar grating" which was originally developed for use in the X-ray region. The concave mirror occupies a fixed position along the lower line and the grating is

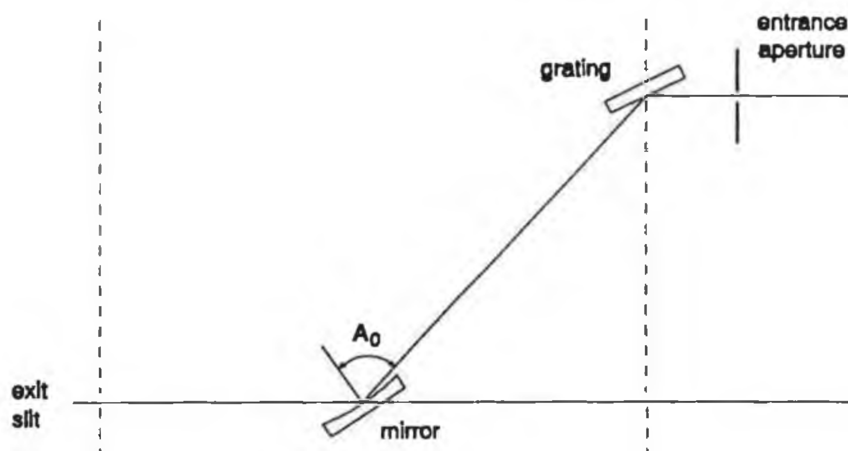

Figure 4.14. Optical arrangement of the monochromator in zero order position. (After reference 2.)

simply rotated to scan wavelength. It has been shown[2] that two values of A_0, and hence two points on the mirror, correspond to a focus position. In order to solve the problem of contamination of the monochromated beam by higher orders, two mirrors of different radius of curvature were used, with the ability that they could be interchanged where appropriate along the lower axis. Since each mirror had two positions of focus, a total of four wavelength regions were available. This corresponded to a total energy range of 40-200 eV thus making a large number of core levels as well as valence bands accessible.

4.3.2 Sample Preparation and Manipulation

MBE GaAs epi-layers, doped with Si atoms to $4x10^{16}$ cm^{-3} and subsequently capped in situ with a protective layer of As, were used for surface science analysis. These 2μm thick epilayers were grown on a GaAs n^+ substrate requiring little or no processing other than the thermal removal of the As layer in UHV, to produce oxide free clean surfaces. The GaAs crystals were cut from wafers to dimensions of typically 10 mm x 5 mm. Having coated the unpolished "substrate" side with InGa alloy to provide a suitable ground, each sample was fixed to a stainless steel spade by means of a tantalum spring clip, before being mounted onto the sample holder. This carousel type sample holder, mentioned in section 4.3.1, and illustrated in Figure 4.15, was shaped in the form of a rectangular block with recessed slots running anti-

parallel along opposite sides to receive the sample spades. A stainless steel shaft with a flat head passed through a vertical hole in the centre of the block and was fixed to a bracket which was located on the linear translator. This shaft acted as an axle on which the carousel could rotate. Small strips of tantalum foil spot welded to the sides of the carousel allowed sample spades to be guided and fixed securely into place. A second identical carousel was located on a specially adapted 4" flange in the preparation chamber, but on the main chamber side of the gate valve. Samples were transferred between the carousel on the linear translator and this "parking" carousel by means of a wobble stick. In this way, up to four samples could be analysed without venting or rebaking the system.

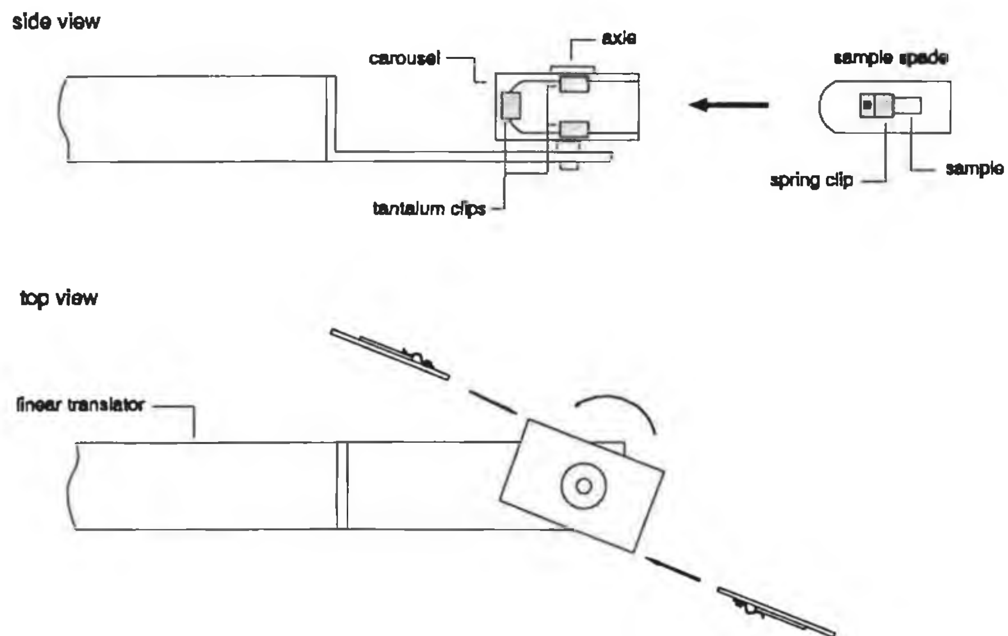

Figure 4.15. Illustration of carousel and sample loading arrangement.

Sample transfer to the main chamber was achieved by moving the translator to a position adjacent to the UMD20 manipulator. A wobble stick was used to withdraw the sample spade from the carousel and slide it into the holder located at the base of the manipulator, after which the translator was withdrawn.

Thermal decapping of the protective As layer was accomplished by means of a resistive heater positioned on the sample holder underneath the sample spade. Typically, two to three heating cycles at temperatures of between 300 and 450 °C, as measured by a thermocouple, were sufficient to remove the cap. Moreover, the ratio of the As to Ga atoms in the topmost layers could be precisely controlled by monitoring the decapping process using PES and AES.

4.3.3 Sulphur Passivation

The deposition of sulphur in the form of a molecular S_2 beam from a electrochemical sulphur cell provided a novel "dry process" approach to sulphur passivating the GaAs surface. The sulphur flux is generated by the electrochemical decomposition of silver sulphide, Ag_2S, at temperatures of around 300 °C, using the $Pt/Ag/AgI/Ag_2S/Pt$ cell[3-5] shown schematically in Figure 4.16. The electrolyte array was prepared by fusing powders of silver, silver iodide and silver sulphide, together with a sheet of platinum mesh, in a KBr press under 1 Tonne of pressure to form a cylinder of approximately 1 cm in both length and diameter. A silver disc placed next to the fused silver powder provided electrical contact for the silver iodide cathode, while the platinum mesh made contact with the silver sulphide anode. The cell was then fitted tightly into a glass tube, one end of which had a 4 cm long

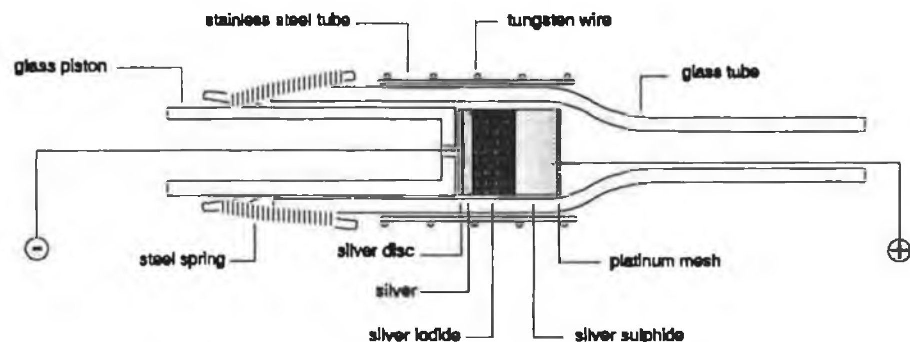

Figure 4.16. Schematic representation of electrochemical sulphur cell.

capillary with a 5mm i.d. orifice through which the sulphur effused. External electrical contact from the anode and cathode was made via platinum leads. Sufficient pressure contact was maintained on the cell by means of a glass piston which was secured to the tube using steel springs. A sheet of stainless steel together with several windings of tungsten wire provided uniform heating of the electrolyte array, the temperature of which was monitored by a thermocouple. The entire cell was mounted on a 23/4" flange thus providing a vacuum compatible sulphur source.

The principle of operation of the cell is based on fact that at elevated temperatures, the application of an emf changes the chemical potential and therefore the activity of the sulphur in the silver sulphide. Furthermore, silver iodide is an ionic conductor and acts as a source or sink to the silver ions by transporting them from the silver sulphide to the silver. Thus an ionic current flows due to the effusion of sulphur from the orifice.

References

[1] Caffolla A.C., private communication.

[2] Howells M.R., Norman D., Williams G.P. and West J.B., J. Phys. E.:Sci. Instrum. **11** (1978) 199.

[3] Heegeman W., MeisterK.H. Bechtold E. and Hayek K., Surf. Sci. **49** (1975) 161.

[4] Wagner C., J. Chem. Phys. **21** (1953) 1819.

[5] Davies G.J. Andrews D.A. and Heckingbottom, J. Appl. Phys. **52** (1981) 7214.

Chapter 5 An Investigation of Metal-GaAs(100) Interfaces by Deep Level Transient Spectroscopy

5.1 Introduction

Over the past two decades, studies of both the chemical and electrical properties of metals deposited on III-V compound semiconductors, in particular, Schottky barrier diodes, have focused on GaAs interfaces, primarily because of their device applications[1,2]. Of considerable importance is the role of both bulk and surface defects. It is widely accepted that bulk defect levels can inhibit as well as enhance the performance of such a device depending on the precise function of the semiconductor bandgap in the operation of the device. For example, the well characterised EL2 bulk trap is known to play an important role in the semi-insulating properties of GaAs[3]. Furthermore, the existence of defect states at the metal-semiconductor interface can have a detrimental effect on the electrical and optical properties of various devices because of their location in the semiconductor bandgap. Moreover, the concentration of such interface states has been found to be very much dependent on device preparation and processing. In sufficient densities, they can result in Fermi level pinning at the metal-semiconductor junction[4-6], thus preventing the metal from influencing the Schottky barrier height. It is therefore important to characterise these states experimentally and theoretically.

The DLTS technique developed by Lang[7] and described in Chapters 3 and 4 has been widely used to characterise the nature of bulk defects in GaAs[8,9]. This technique has also been shown to be capable of detecting interface states at semiconductor-insulator[10,11] and metal-semiconductor interfaces[12-14]. As explained in Chapter 3, interface states can be unambiguously distinguished from bulk states in the intrinsic depletion region by monitoring the DLTS peak position as a function of forward bias. For interface states with a broad range of energies within the bandgap, the DLTS peak maximum shifts to lower temperature with increasing forward bias, while for bulk traps the peak position is found to be independent of forward bias magnitude. Moreover, deviations of the I-V characteristic from ideal behaviour have also been attributed to the presence of interface states[15]. The I-V characteristics of metal-semiconductor diodes can be termed "ideal" if they can be solely described in terms of the thermionic emission of conduction electrons across the interfacial barrier. The

presence of a high density of interface states at a junction can provide an additional current path across the interface and thereby lead to non-ideal electrical characteristics[16]. The primary objective of the work presented in this chapter was to attempt to establish a correlation between the non-ideal behaviour of GaAs Schottky barrier diodes as determined from the current voltage characteristic and the presence of interface states as detected by DLTS. In addition, from the measured values of barrier heights of non-ideal diodes, efforts were made to investigate if Fermi level pinning occurred at the metal-GaAs interfaces studied. If so, could the density of interface states determined from DLTS spectra compare with values predicted by the interface theories discussed in Chapter 2 for effective Fermi level pinning?

For the purpose of comparison, both ideal and non-ideal diodes were prepared for experimental investigation. Reference diodes exhibiting ideal characteristics were fabricated by metal deposition immediately following chemical etching and ohmic contact formation as described in Chapter 4 Section 4.2.2. Non-ideal diodes were prepared by chemical etching followed by oxidation in hydrogen peroxide for 20 seconds prior to metal deposition. Of the metals deposited (Ag, Ti, Au, Fe, Ga) during the course of this work, two have been selected for detailed study. Au is known to be relatively unreactive and results in a high barrier on clean GaAs(100) surfaces whereas Fe-GaAs is reactive and gives a lower barrier on the same surface[17,18]. The ideality parameter for both unoxidised (ideal) and oxidised (non-ideal) diodes were determined by I-V measurements. Barrier heights were calculated both from C-V and I-V characteristics. As a typical sample contained between 10 and 20 diodes, it was possible to obtain an average ideality and barrier height for a particular sample. C-V measurements also enabled the determination of the effective dopant density in the intrinsic depletion region. For DLTS measurements all diodes were subjected to a reverse bias of -1.0 V, and a forward pulse voltage which was varied between 0.0 and +1.0 V. A pulse bias width of 80 μs was found to completely fill all deep levels. Activation energies and capture cross-sections for both bulk levels and interface states were calculated from Arrhenius plots as described in Chapter 3 Section 3.2.4.1. Rate windows of 8, 20, 40 and 100 s^{-1} were used in all measurements.

In this chapter the results of investigations into metals deposited on unoxidised and H_2O_2 oxidised GaAs(100) surfaces will be presented in sections 5.2 and 5.3, respectively. In section 5.4, a detailed discussion of these experimental studies is given. Special consideration is devoted to the models for Schottky barrier interfaces as well as comparative studies carried out by other researchers. Finally, a summary of the findings is presented in section 5.5.

5.2 Metals on Unoxidised GaAs(100)

5.2.1 I-V Measurements

I-V measurements for both Au- and Fe-GaAs reference samples were taken at 300 K. The resulting data was analysed according to equation 3.3:

$$I = I_s \exp\left(\frac{qV}{nkT}\right)\left[1 - \exp\left(-\frac{qV}{kT}\right)\right] \tag{3.3}$$

which assumes thermionic emission as the main current transport mechanism. Plots of I/(1-exp(-qV/kT) vs V for both contacts are shown in figure 5.1. For each plot, the ideality factor n was found from the slope, while the saturation current I_s and hence the barrier height ϕ_B^{IV} was determined from the intercept, by applying a least squares fit to the data[16]. As can be seen from the figure, the characteristics are linear across the range -0.6 V to +0.4 V, with the deviation from linearity above 0.4 V being due to series resistance[19]. Average ideality factors of 1.04 and 1.07 were calculated for Fe- and Au-GaAs respectively, indicating that thermionic emission is indeed the dominant means of current transport. Taking into account a correction of 0.04 eV due to image force lowering of the barrier[16,17], I-V barrier heights of 0.73 eV for Fe-GaAs and 0.83 eV for Au respectively were extracted from the intercept with the current axis. While the value for Fe-GaAs agrees, within an experimental error of ±0.01 eV, with that of 0.72 eV from works by Waldrop on GaAs(100) diodes with the same donor concentration[17,18], the I-V barrier height for Au obtained in this study is somewhat lower than that of 0.89 eV reported by the same author. A possible reason for this might lie in the observation that the acidic etch used in this study is known to leave excess As on the GaAs surface[20] which has been shown to produce lower barriers at Au-nGaAs interfaces[21,22].

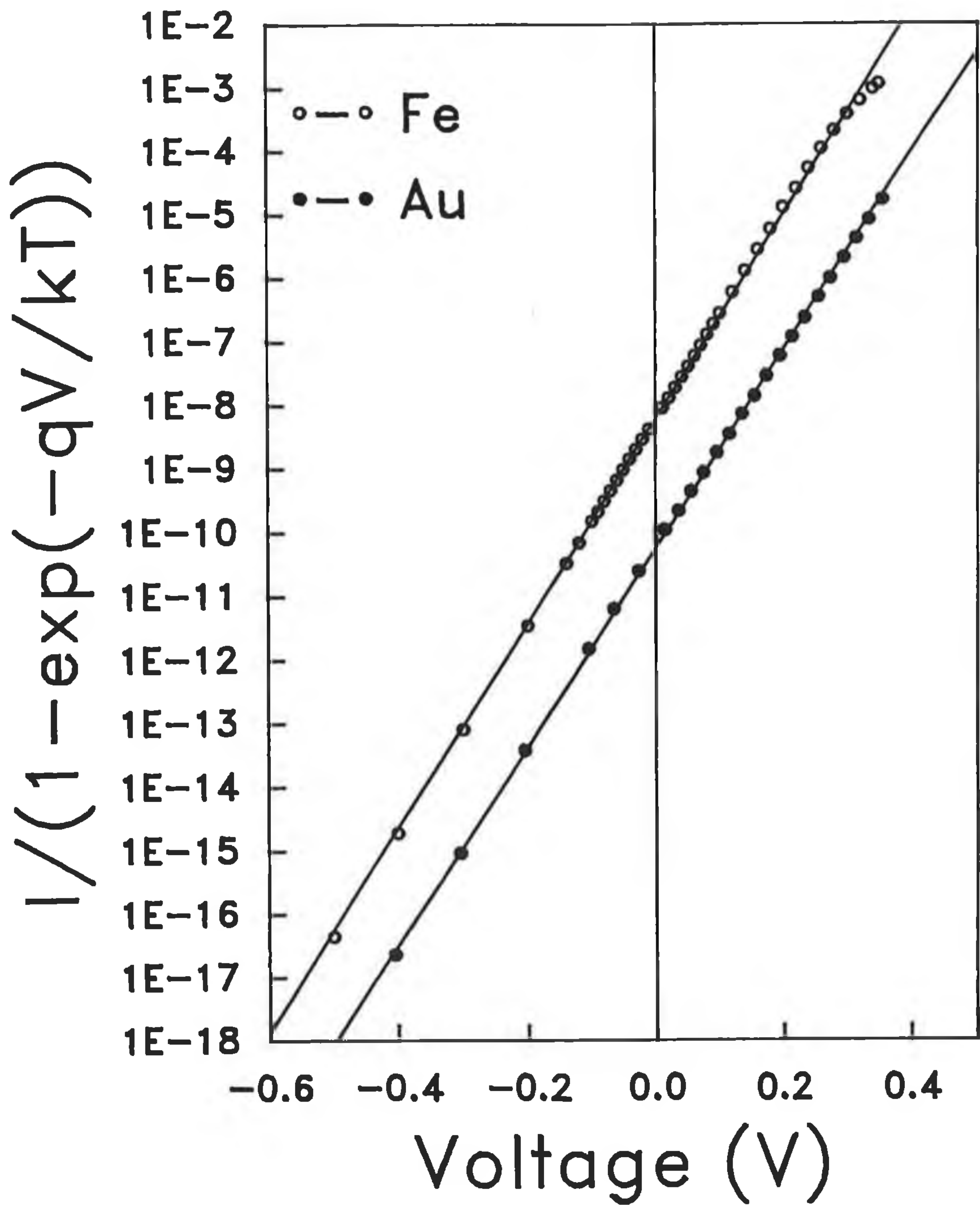

Figure 5.1. I-V characteristics of unoxidised samples. Open circles: Fe-GaAs n=1.04, ϕ_B^{IV}=0.73 eV; filled circles: Au-GaAs n=1.07, ϕ_B^{IV}=0.83 eV.

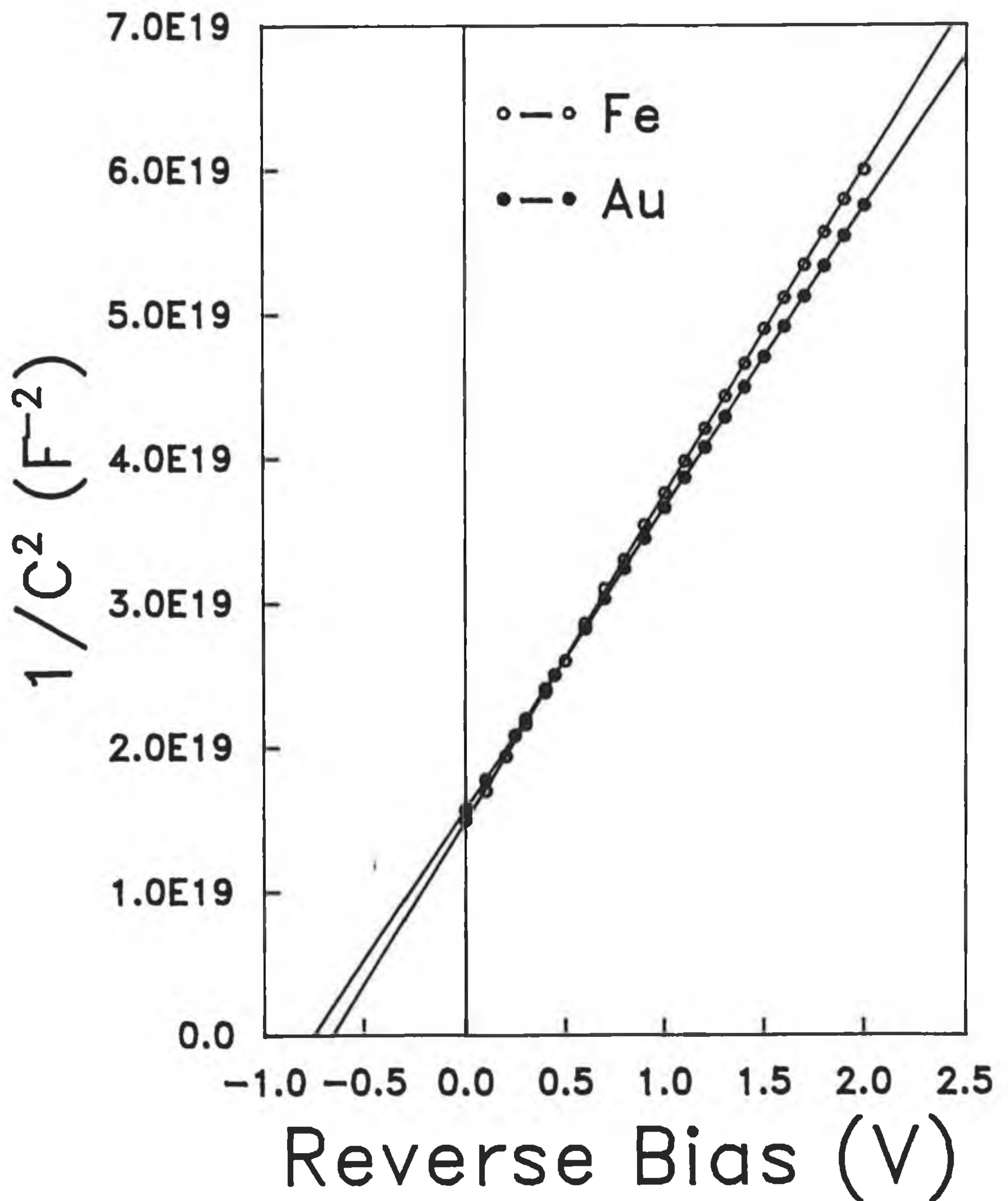

Figure 5.2. C-V characterictics of reference samples. Open circles: Fe-GaAs ϕ_B^{CV}=0.74 eV, filled circles: Au-GaAs ϕ_B^{CV}=0.83 eV.

5.2.2. C-V Measurements

The C-V data, taken at 300K, were plotted as $1/C^2$ vs V and analysed by a least squares fit according to equation 3.6:

$$\frac{1}{C^2} = \left(\frac{2}{S^2 q N_d \varepsilon_s}\right)\left[\phi_B - V_n - V_r - \frac{kT}{q}\right] \qquad (3.6)$$

All points were found to lie in a straight line over the measurement range of 2.0 V to 0.0 V reverse bias as shown in figure 5.2 for both metals. The effective donor concentrations, calculated from the slopes of the graphs were 6.0×10^{16} cm^{-3} and 6.5×10^{16} cm^{-3} for Fe-GaAs and Au respectively. The diffusion (built-in) potential and C-V barrier height, determined from the intercept with the x-axis, were 0.66 V and 0.74 eV for Fe-GaAs and 0.75 V and 0.83 eV for Au-GaAs, respectively. As can be seen, the values for C-V barrier height compare very well with those from I-V measurements, suggesting that, in the context of the models used, the interfaces are electrically abrupt. The discrepancy of 0.01 eV for Fe-GaAs, lies within the estimated experimental error of ±0.01 eV. It is thought that this variance arises out of the different methods of measurement; the I-V method measures the zero-bias barrier height whereas the C-V method measures the flat-band barrier height. Compared with Waldrop's value of 0.75 eV for Fe-GaAs, the value in this study agrees within experimental error, while his value of 0.87 eV for Au-GaAs is again higher.

5.2.3 DLTS Studies

Figures 5.3 and 5.4 show the DLTS spectra taken at different ratewindow settings for the unoxidised Au-GaAs and Fe-GaAs samples respectively. For each deep level an activation energy E_T and majority capture cross section σ_n was determined from an Arrhenius plot of $\ln(e_0/T^2)$ vs 1/T, as shown in Figure 5.5. In determining the results, the following criteria were taken into account. An error of ±0.02 eV was estimated for the activation energy. It was assumed that the capture cross section was independent of trap energy[23]. The most prominent traps are located at 0.82, 0.55 and 0.32 eV below the conduction band. The properties of these electron traps are summarised in Table 5.1, where a correlation with those characterised by other workers is also given[9]. From reference 8 and 9 and the measured activation energies in this work, it is clear that these defects can be identified as the EL2, EL3 and EL6

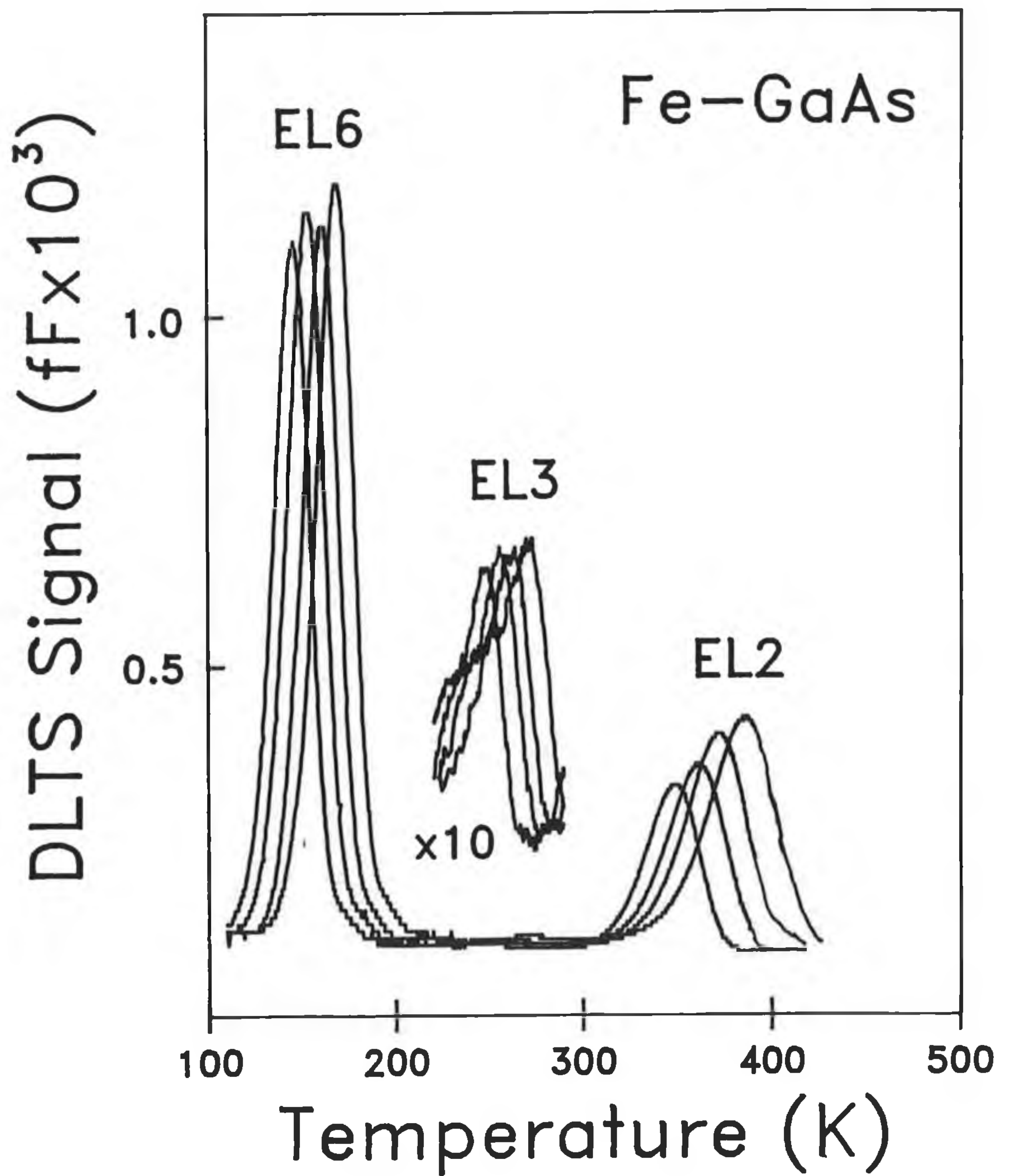

Figure 5.3. DLTS spectra taken of unoxidised Fe-GaAs sample for ratewindows of 8,20,40 and 100 s^{-1}. V_r=-1.0 V, V_p=0.0 V.

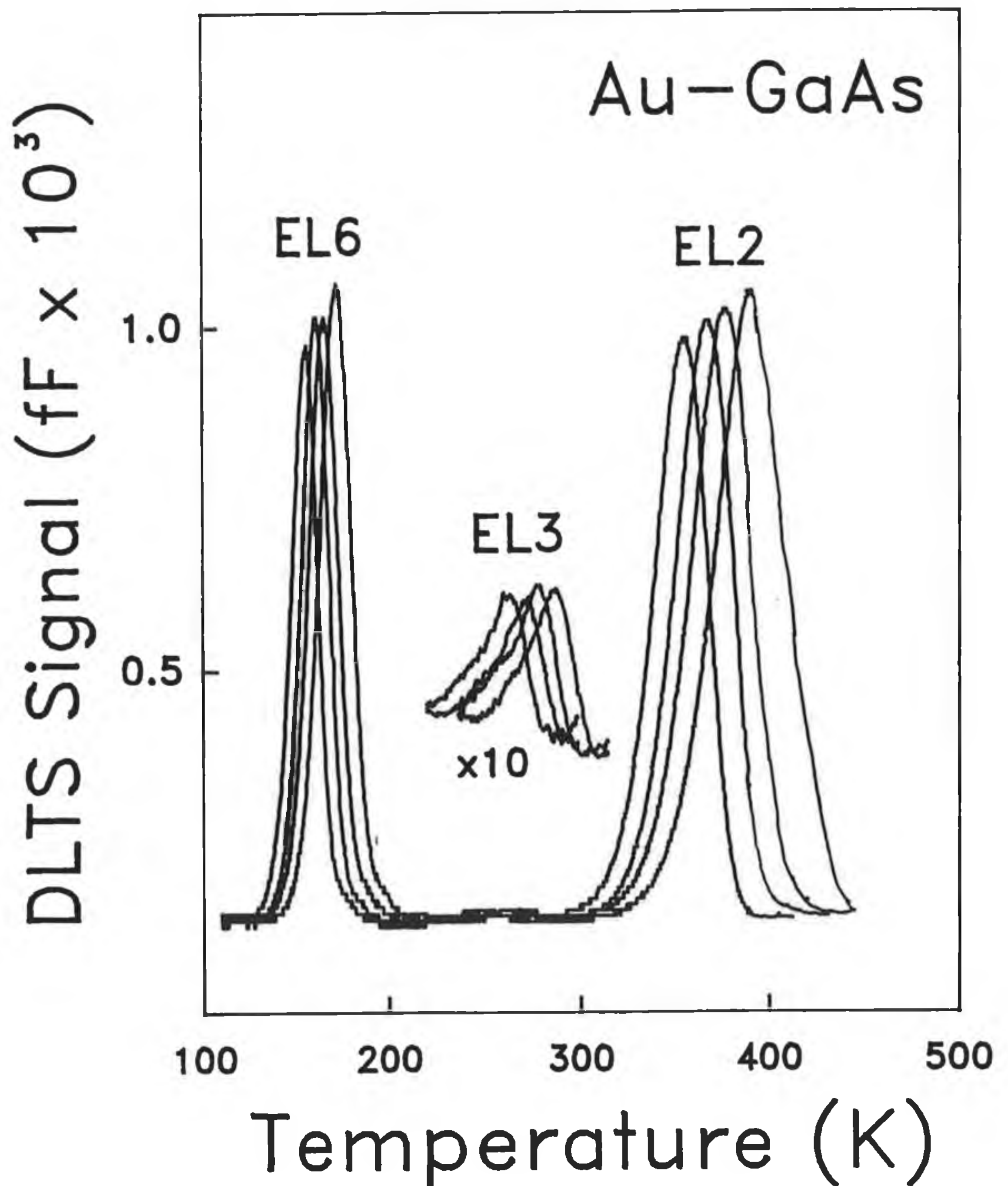

Figure 5.4. Spectra of unoxidised Au-GaAs sample. Ratewindows of 8,20,40 and 100 s^{-1} used to obtain E_a and σ_n for all traps. V_r=-1.0 V, V_p=0.0 V.

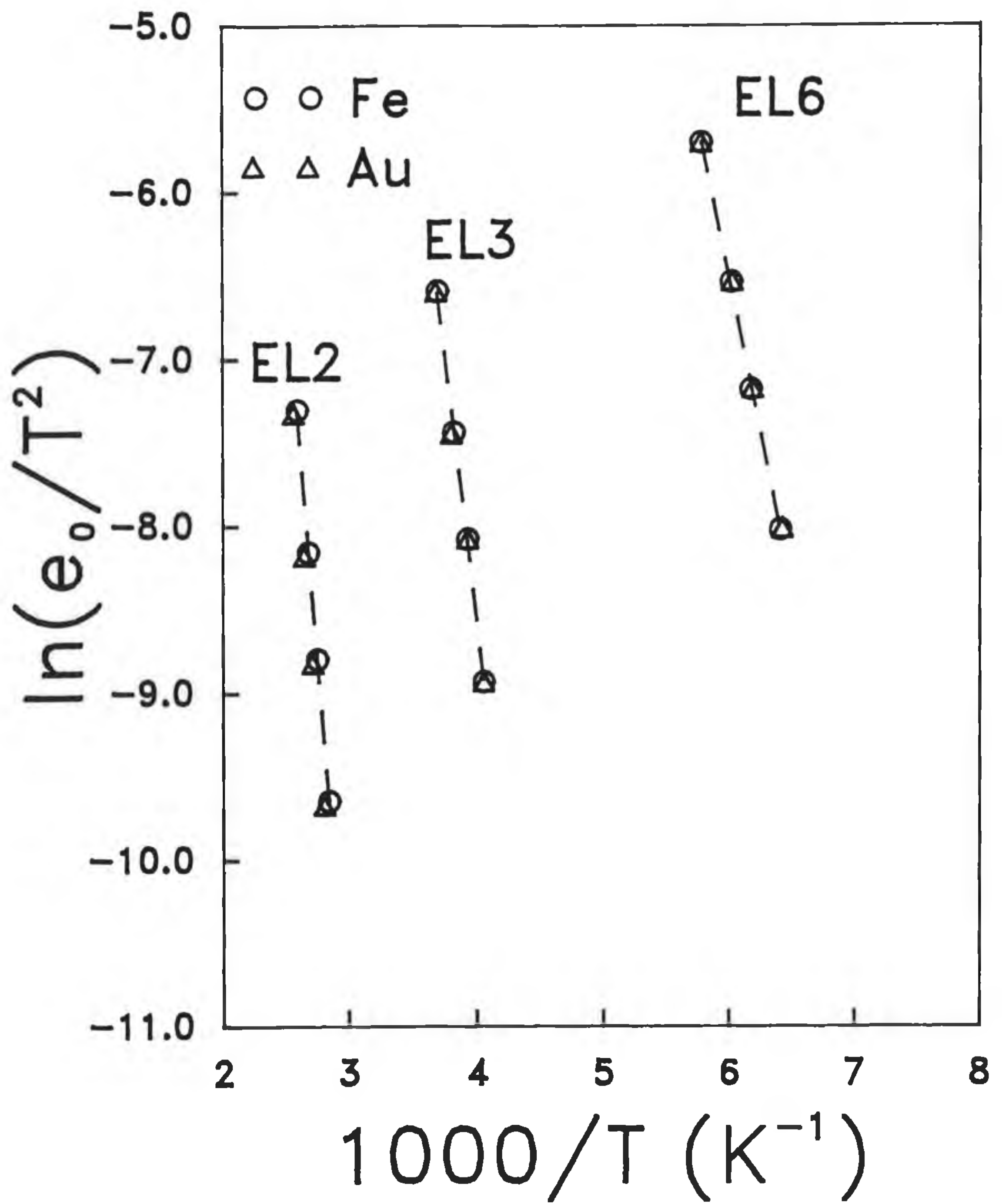

Figure 5.5. Arrhenius plots of $\ln(e_o/T^2)$ vs 1000/T for EL2, EL3 and EL6 bulk deep levels.

Table 5.1. Properties of EL2, EL3 and EL6 bulk deep levels in nGaAs(100)

	This study		Reference 9	
Defect	Activation Energy E_T (eV)	Capture Cross Section σ_n (cm^2)	Activation Energy E_T (eV)	Capture Cross Section σ_n (cm^2)
EL2	0.81	1×10^{-13}	0.81	1×10^{-13}
EL3	0.55	1×10^{-13}	0.52	5×10^{-14}
EL6	0.32	5×10^{-14}	0.34	1×10^{-13}

bulk levels commonly referred to in the literature. The nature of these defects is considered briefly.

The EL2 defect at 0.81 eV has been well characterised[24]. Originally thought of as been related to the substitution of O atom on an As site, O_{As}[25], there is evidence to suggest that it is a complex native defect consisting of an As anti-site defect associated with a native point defect, As_{Ga} - V_{As}[26,27]. The EL6 deep level with activation energy at 0.32 eV has been related to As excess in LEC crystals grown under As overpressure[28] and the EL3 level at E_T=0.55 eV has been associated with a Ga-O-Ga centre[29]. The concentrations of each deep level for both samples within a region 0.11 - 0.18 μm into the bulk is shown in Table 5.2. The most obvious difference between the two samples is the concentration of the EL2 trap, also seen graphically by comparing the spectra in Figures 5.3 and 5.4. This has been previously observed and an explanation has been proposed in terms of the relative position of the Fermi level with respect to the EL2[30]. When the barrier height is low, as for the Fe-GaAs diodes (ϕ_B^{IV}=0.72 eV; ϕ_B^{CV}=0.74 eV), the EL2 level (E_T=0.81 eV) lies almost totally below the quasi-Fermi level and therefore its occupancy is almost unchanged by a bias pulse sequence, hence only a small EL2 peak is observed. However, when the barrier height is higher (ϕ_B^{IV}=ϕ_B^{CV}=0.83 eV) as for the Au-GaAs diodes, the EL2 level is above the quasi-Fermi level, and during the pulse bias sequence the occupancy is significantly altered thereby giving rise to a larger EL2 peak. This is graphically illustrated in Figure 5.6. Of further importance was the observation that by increasing the reverse bias while keeping the fill pulse bias constant at some arbitrary positive voltage, say 0.5 V, it was found that the EL2 concentration increased i.e. the EL2 concentration increases going into the material,

Table 5.2 Trap concentrations of the EL2, EL3 and EL6 deep levels in Fe- and Au-GaAs(100)

Defect level	Trap concentration N_T	
	Fe	Au
EL2	1.5×10^{14}	4.8×10^{14}
EL3	1.5×10^{13}	1.0×10^{13}
EL6	5.0×10^{14}	4.7×10^{14}

while both the EL3 and EL6 levels showed no change, indicating that the latter defects may have a contribution to physical or chemical effects at the GaAs surface.

Figure 5.7 illustrates the DLTS spectra recorded for both the Fe-GaAs and Au-GaAs diodes for fill pulse voltages of 0.0 V and +0.8 - +1.0 V, thereby probing the distribution of defects within the intrinsic depletion region. The EL2 and EL6 are used here as reference features in the study. The upper curves show the spectra taken at pulse voltages above flat-band for both diodes. The increase in the EL2 and EL6 peak heights is to be expected as they are both assumed to have some concentration within the intrinsic depletion region. However, it can be seen that there is no evidence of interface states of the form described in section 3.2.4.2 as detected by DLTS for this forward bias pulse sequence.

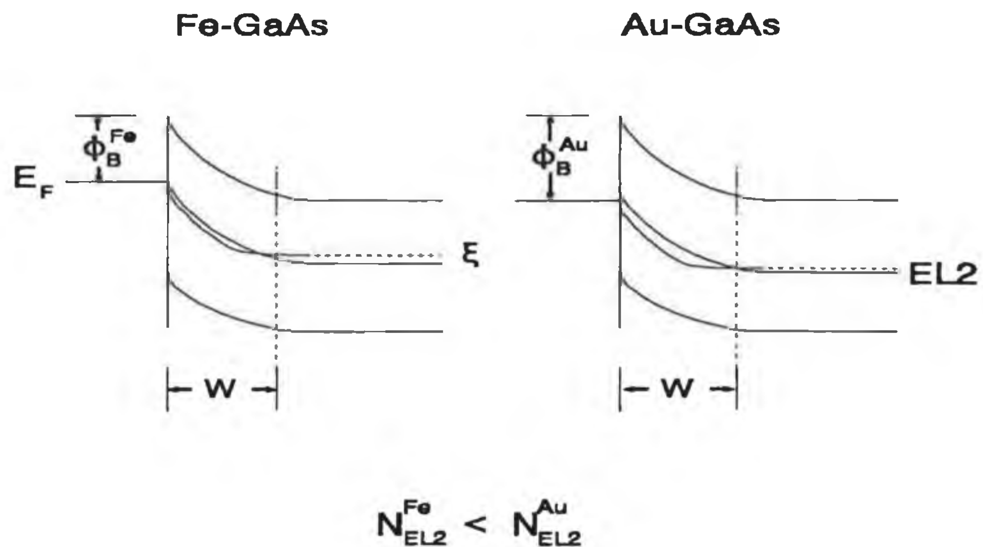

Figure 5.6. Graphical illustration of the variation of EL2 trap concentration, N_{EL2}, with the barrier height of iron and gold diodes, as seen by DLTS.

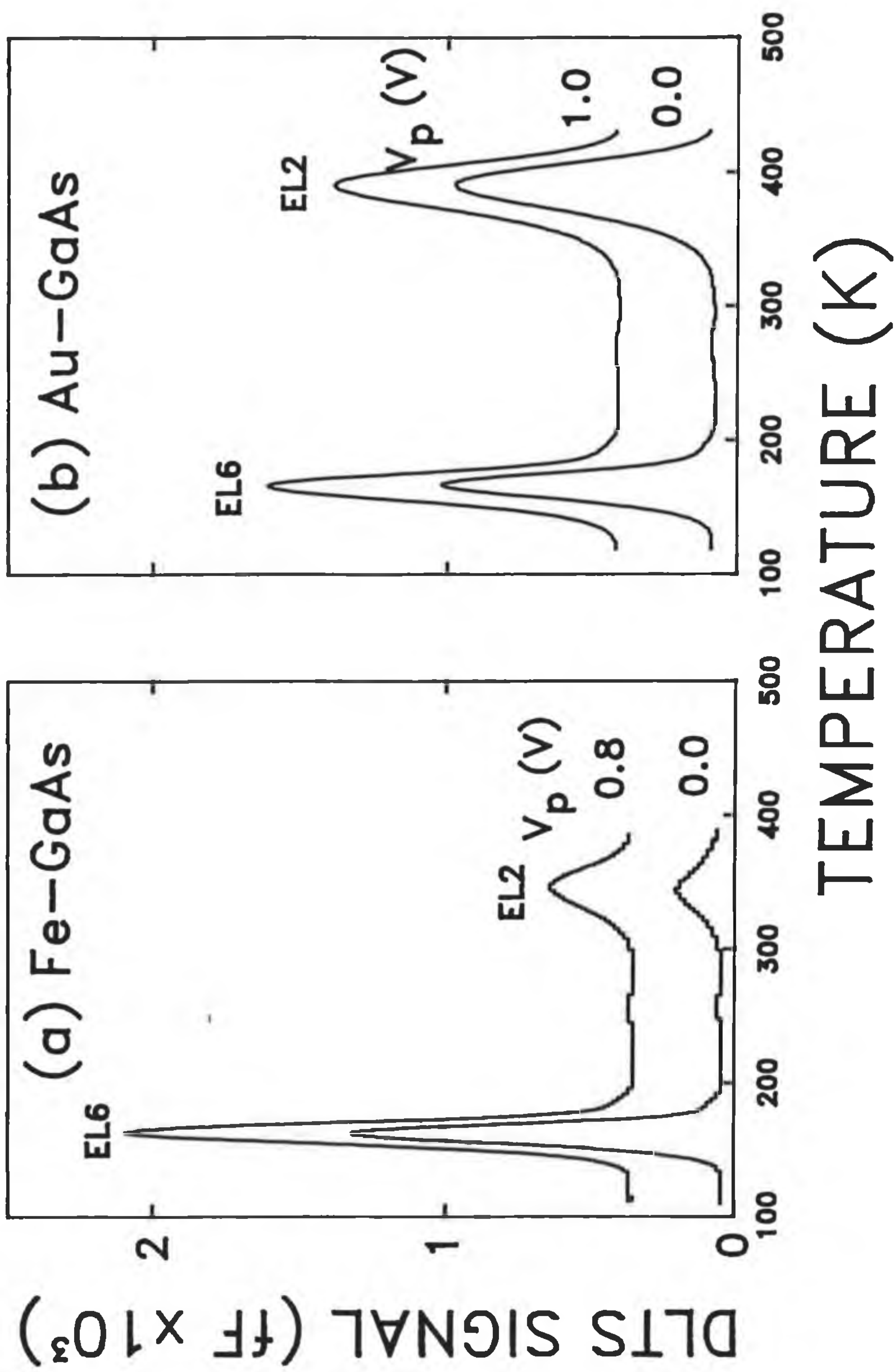

Figure 5.7. DLTS spectra of unoxidised samples: (a) Fe-GaAs (n=1.04), V_r=0.0 V, V_p as shown. (b) Au-GaAs (n=1.07), V_r=0.0 V, V_p as shown.

5.3 Metals on H_2O_2 Oxidised GaAs(100)

5.3.1 I-V Measurements

Figure 5.8 shows a plot of ln[I/1-exp(-qV/kT)] vs V for the H_2O_2 oxidised Fe-GaAs and Au samples. It can be seen that the plot for Au-GaAs is linear over the voltage region 0.1 - 0.35 V. At both reverse and high forward voltages there was significant current leakage. Using this region of the plot a barrier height of 0.91 eV was obtained. The plot for Fe-GaAs is highly non-linear in the forward voltage region. By applying the thermionic emission equation and using linear least squares fits to the data points, average ideality factors of 1.4 and 1.8 were determined for the Fe-GaAs and Au-GaAs samples respectively. At higher voltages, the ideality increases due to the fact that the Fermi level is moved to a high density of states as will be discussed in section 5.3.3.

It can be observed from Figure 5.8 that while the linear least squares method fits the data points for the Au-GaAs sample, it is not as reliable for the Fe-GaAs data. In an attempt to overcome this problem, which could lead to erroneous results for the saturation current and hence the barrier height, a computer model, based on a non-linear least squares fit of equation 3.4, was employed. Described by McLean *et al*[16], the model proposes fitting the I-V data by the addition of a recombination current term to that for thermionic emission such that the current I is expressed according to equation 3.4 but with the inclusion of a series resistance term R_s:

$$I = I_s\left(\exp[\alpha(V-IR_s)] - 1\right) + I_r\left(\exp[\alpha/2(V-IR_s)] - 1\right) \qquad (5.1)$$

where I_s and I_r are the saturation and recombination currents respectively and α=q/kT. This fit, however, was only valid for V>0, and so to include I-V values for V<0, the data was also fitted according to the equation:

$$I = \frac{2\sinh(\alpha V/2)\,[I_s\exp(\alpha V/2) + I_r]}{1 + \alpha R_s[I_s\exp(\alpha V/2) + I_r\cosh(\alpha V/2)]} \qquad (5.2)$$

with the constraint that $\alpha IR_s \ll 1$. To assess the integrity of the models, each was applied to the "ideal" I-V characteristic of the unoxidised Fe-GaAs sample as well as the oxidised Fe-GaAs sample. The results of both fits are illustrated graphically in Figure 5.9, where it can be seen that while both models work extremely well for the ideal diode, only moderately good fits are obtained on the oxidised sample when

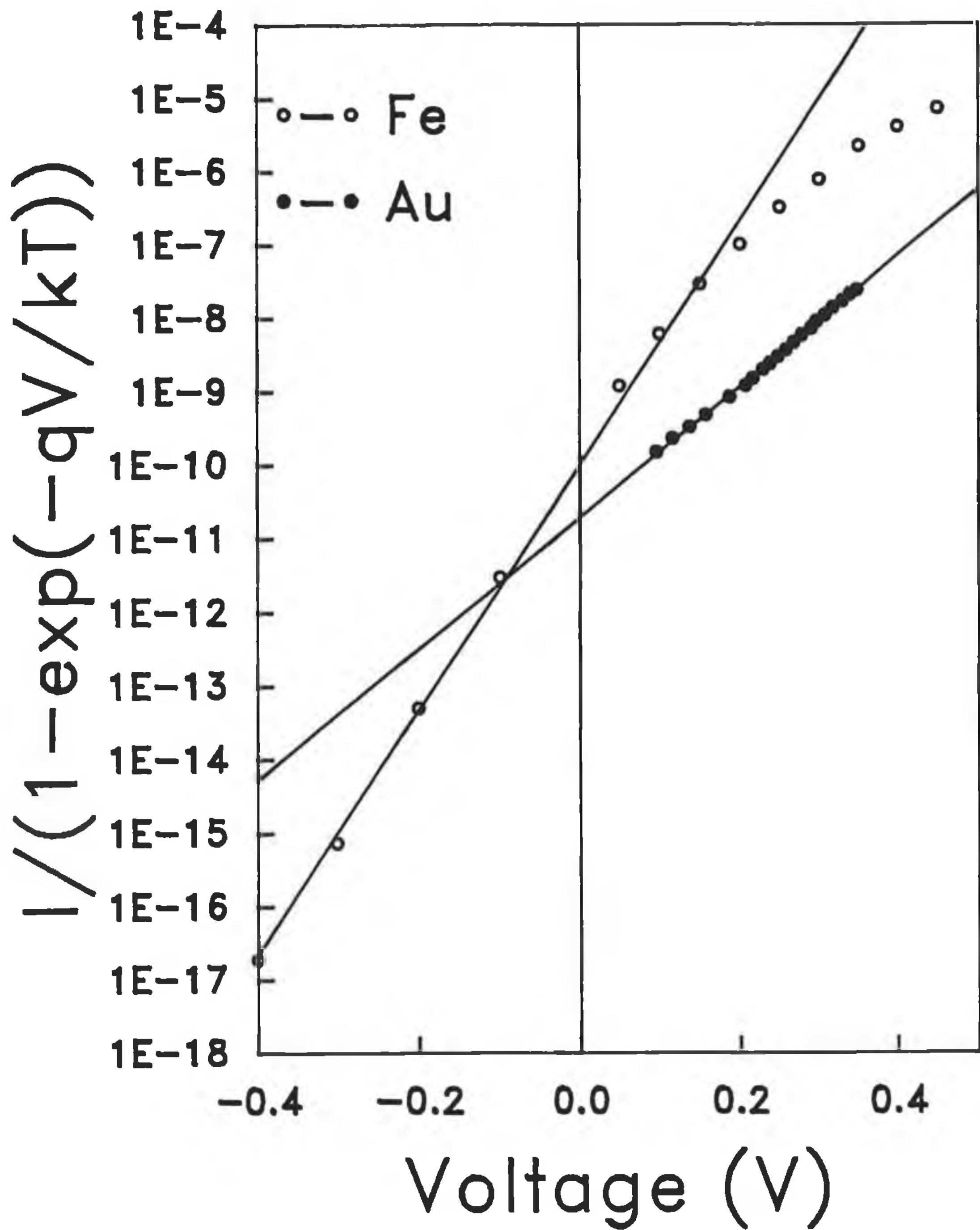

Figure 5.8. I-V characteristics of oxidised samples. Open circles: Fe-GaAs n=1.4, ϕ_B^{IV}=0.83 eV; filled circles: Au-GaAs n=1.8, ϕ_B^{IV}=0.91 eV.

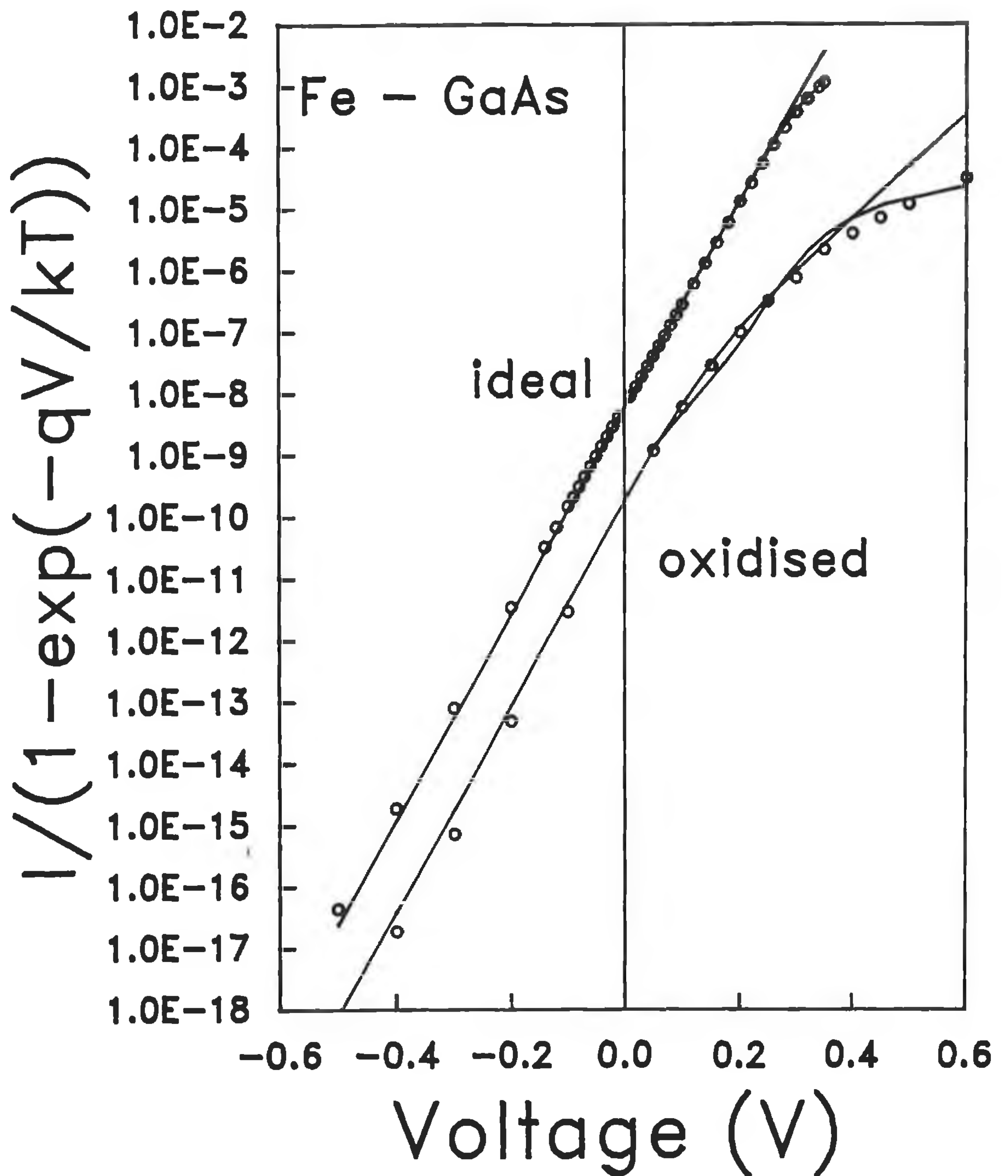

Figure 5.9. Results of the fitting the Fe-GaAs I-V data points using equations 5.1 and 5.2.

the parameter R_s is unconstrained, to the point that the values become unrealistic. Table 5.3 shows the results of the non-linear fits for both ideal and non-ideal Fe-GaAs samples together with the results of the linear least squares fit. From the calculated values of saturation current I_s, the extracted barrier heights range from 0.85 - 0.87 eV; from the linear least squares method a value of 0.83 eV is obtained. The lack of a good fit to the data by either model suggests that the I-V characteristics of the oxidised sample are not governed purely by thermionic emission and recombination and that some other physical process must also be occurring at the interface. Nevertheless, the application of the thermionic emission alone gives a quantitative measure through the ideality parameter of the degree of deviation from ideal behaviour and it is only in this context that the ideality parameter is quoted.

Table 5.3. Results of the fits to the Fe-GaAs I-V data points using the computer models

	Unoxidised sample			Oxidised sample		
	I_s(A)	I_r(A)	R_s(Ω)	I_s(A)	I_r(A)	R_s(Ω)
Computer model 1(McLean)	$6x10^{-9}$	$2x10^{-9}$	90	$2x10^{-11}$	$6x10^{-10}$	$9x10^{3}$
This work	$6x10^{-9}$	$2x10^{-15}$	20	$6x10^{-11}$	$2x10^{-14}$	$1x10^{5}$
Thermionic emission	$6x10^{-9}$	...	...	$4x10^{-11}$	...	...

5.3.2 C-V Measurements

C-V measurements were taken on the oxidised Au- and Fe-GaAs are shown graphically in Figure 5.10. In comparison with the C-V plots for the unoxidised samples, the oxidised C-V data points lie in a straight line over the measurement range. Effective dopant concentrations of $6x10^{16}$ cm^{-3} and $4x10^{16}$ cm^{-3} were extracted from the slopes of the graphs. By extrapolation to the voltage axis, diffusion potentials of 0.78 and 0.93 V and C-V barrier heights of 0.86 and 1.01 eV were obtained for Au-GaAs and Fe-GaAs samples respectively. This clear deviation from corresponding values for I-V barrier heights is suggestive of highly non-abrupt interfaces. Moreover, it can be observed that both I-V and C-V barrier heights are consistently higher than those of the unoxidised samples. These matters will be considered further in section 5.4. A summary of the I-V and C-V characteristics of both unoxidised and oxidised samples is presented in Table 5.4.

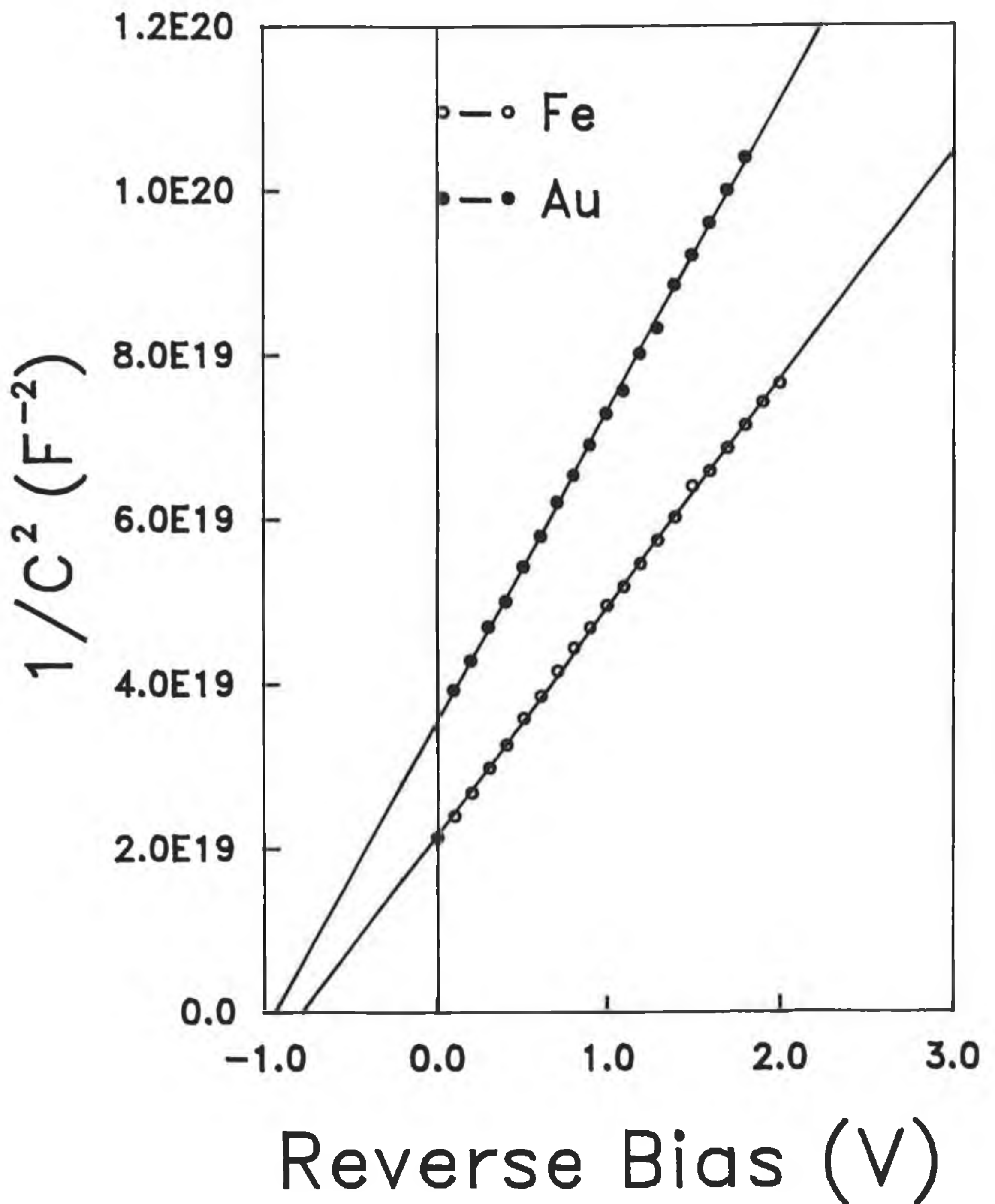

Figure 5.10. C-V characterictics of oxidised samples. Open circles: Fe-GaAs ϕ_B^{CV}=0.87 eV, filled circles: Au-GaAs ϕ_B^{CV}=1.01 eV.

Table 5.4. Ideality parameters and Schottky barrier heights (in units of eV) for unoxidised and oxidised samples.

	Reference samples			Oxidised samples		
	n	ϕ_B^{IV}	ϕ_B^{CV}	n	ϕ_B^{IV}	ϕ_B^{CV}
Fe	1.04	0.73	0.72	1.4	0.83	0.87
Au	1.07	0.83	0.83	1.8	0.91	1.01

5.3.3 DLTS Studies

Figure 5.11 shows the DLTS spectra taken on the H_2O_2 oxidised samples. The spectra of Fe-GaAs on oxidised GaAs (Figure 5.10(a)) exhibit two distinct additional spectral features compared with the unoxidised sample. The peak at 250K which is observed in the conventional reverse bias mode of DLTS operation can be correlated with the bulk EL3 level. In addition, the spectral feature at 290K is seen to increase in magnitude and the peak maximum shifts to lower temperatures as a function of increasing forward bias. This feature shows no saturation for pulse voltages up to +0.9 V. The spectra for the oxidised GaAs surfaces with Au Schottky contacts are shown in Figure 5.11(b). There are similarities with the results observed for Fe-GaAs diodes in that the idealities have increased and an additional spectral feature was observed in the forward biased DLTS spectra. Again, as for the Fe-GaAs diodes, no saturation of this interface state feature was observed up to a pulse voltage of +0.8 V. Activation energies and capture cross sections corresponding to each of the interface state peaks at $V \geq 0.4$ V were calculated by Arrhenius plots of the thermal emission rates by the same technique as that used in the case of bulk traps[10]. Energy distributions and capture cross sections of E_a= 0.65 - 0.59 eV and 3 - 7x10^{-16} cm^{-2} for Fe-GaAs and E_a=0.63 - 0.54 eV and 2 - 5x10^{-16} cm^{-2} for Au-GaAs were obtained.

5.4 Discussion

For both systems investigated, distinct differences are observed in the DLTS spectra for diodes of different idealities. Two additional features are observed in the spectra of Fe-GaAs diodes fabricated on the H_2O_2 oxidised GaAs surface. The peak assigned EL3 with activation energy 0.55 eV is significantly larger on the oxidised surface when compared with the unoxidised sample. The fact that it is also observed in the reverse bias mode would indicate that it extends a substantial distance (> 0.3 μm)

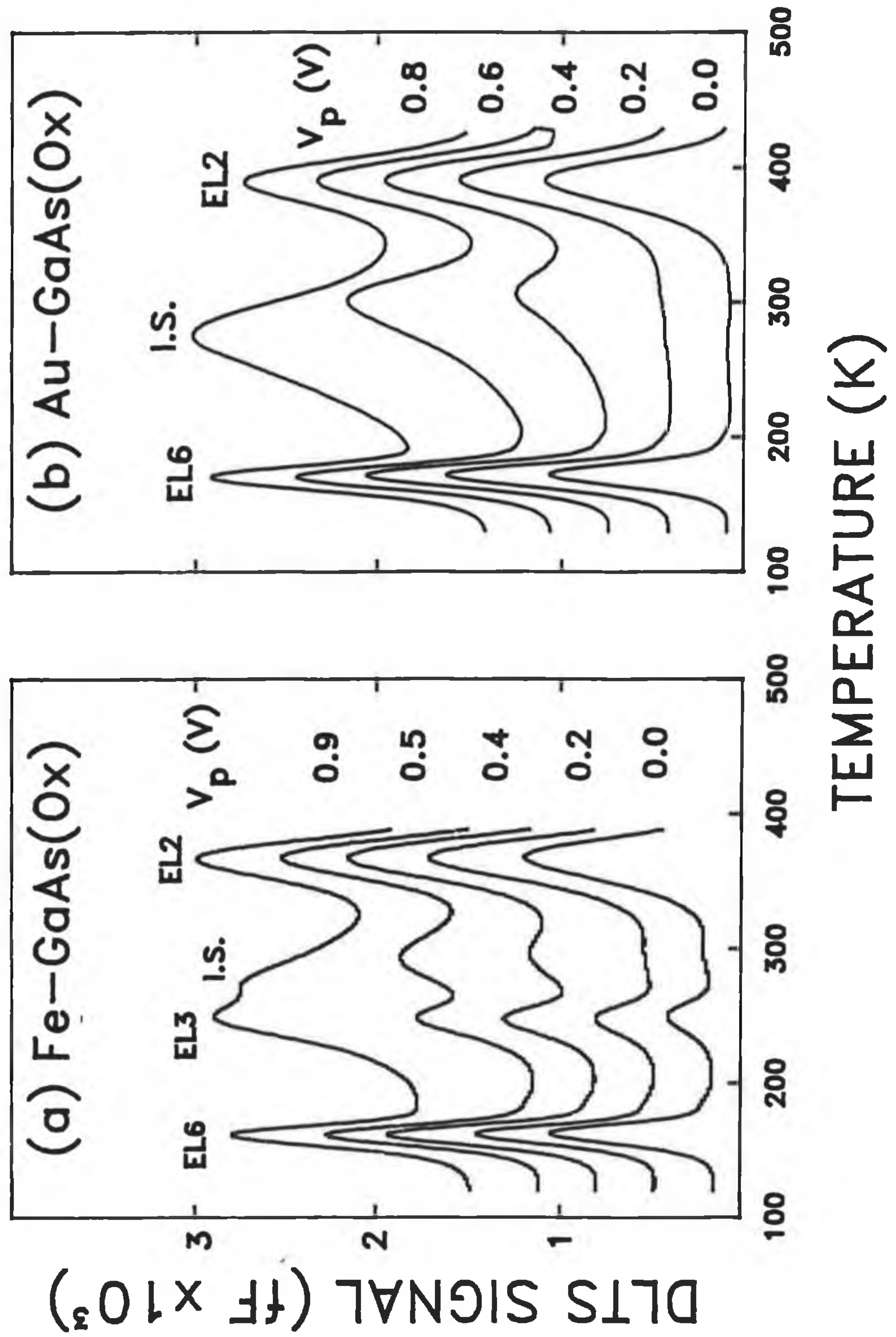

Figure 5.11. Spectra of oxidised samples: (a) Fe-GaAs (n=1.4). (b) Au-GaAs (n=1.8). V_r=-1.0V, V_p as shown. I.S. denotes interface states

into the bulk. In spite of this, two points suggest that the peak may be also related somehow to the oxidation of the surface. Firstly, Neild *et al*[29], using DLTS, have observed a level with activation energy 0.55 eV which they associate with the presence of a defect centre in GaAs samples which were intentionally doped with oxygen. Together with FTIR measurements they identified the level as being related to a Ga-O-Ga defect. Secondly, by carrying out bulk defect concentration measurements on undoped bulk-grown GaAs wafers, Auret and co-workers[9] found that the EL3 defect concentration decreased when going into the material, whereas the EL2 and EL6 showed the opposite effect. Based on this observation they suggested that this level may be surface related. However, EL3 features of comparable magnitude have been observed from other samples analysed in this work which exhibit near-ideal I-V characteristics. For this reason it is not thought that the EL3 contributes to the poor electrical characteristics of the oxidised samples.

The other feature at 290K, which only appears in the forward bias pulse sequence, increases in magnitude and moves to lower temperature with increasing forward bias pulse voltage. The fact that the magnitude of this peak does not saturate up to the flat-band voltage indicates that the electron traps related to this feature have a continuous range of energies throughout the semiconductor band-gap, in contrast to the well defined energy of a bulk defect level[30]. The diodes which display these features have been found to have significantly higher idealites than unoxidised reference diodes. The DLTS spectra for gold are broadly similar. Again it is possible to fabricate an interface with near ideal behaviour as determined from the I-V characteristics. These diodes only display the characteristic bulk deep-level electron trap features in forward bias. The oxidised Au-GaAs diodes have higher idealities and a feature attributable to interface states can clearly be detected in the forward bias scans. This interface state distribution has the same form as that observed for the oxidised Fe-GaAs.

The fact that interface states are not observed by DLTS at the unoxidised metal-GaAs interfaces does not necessarily mean that no interface states are present. It is well known that even at intimate metal-semiconductor junctions fabricated in UHV, interface states are present in sufficient densities to pin the Fermi level[31]. However, as explained by Platen *et al*[30], the intimate contact allows emission from the interface

states into the metal at a rate which is too fast to be detected by DLTS. In these experiments, even samples which were metallised immediately following etching, a thin interfacial surface oxide will be present which decouples the semiconductor from the metal. Indeed, deviations from ideal behaviour resulting in n values of 1.1-1.2 have been observed on such diodes, however, the oxide layers were obviously not thick enough to cause major disruption of the GaAs surface resulting in an interface density detectable by DLTS measurements. This leads to an important distinction; the presence of interface states as detected by DLTS implies that the diode exhibits non-ideal I-V characteristics. On the other hand, non-ideal I-V characteristics do not always indicate that DLTS will detect interface states.

In contrast, the exposure of the GaAs samples to H_2O_2 results in the formation of a thick interfacial oxide being formed, and therefore a potential drop across the layer. Examination of the GaAs oxide composition by Garner *et al*[32] revealed by AES and XPS the presence of both Ga_2O_3 and As_2O_3 after treatment with H_2O_2. It has also been shown that As_2O_3 is unstable in the presence of GaAs and forms elemental As and Ga_2O_3[20]. Furthermore, Miller and Stillman[33] have shown by experiment that As_2O_3 is completely immiscible in H_2O_2. Thus the H_2O_2 treatment should be capable of producing elemental As at the interface. Garner and co-workers studied the I-V properties of interfaces resulting from the interaction of H_2O_2 and concluded that the presence of high concentrations of As oxides produced traps in the oxide which led to the non-ideal electrical behaviour observed in Schottky barriers. It is believed that the interface states detected by DLTS on the the oxidised iron and gold samples are of a similar nature as the traps discussed by Garner.

A number of groups have derived parameters relating to interface states from DLTS spectra. Zhang *et al*[13] investigated interface state distributions of Al on n-type GaAs Schottky contacts, whereby the GaAs surface was prepared by chemical etching. For the calculation they proposed that in forward bias, the interface states are in equilibrium with the semiconductor electron quasi-Fermi level whereas in reverse bias the electron quasi-Fermi level is pinned to the metal Fermi level. However, in their derivation they assumed an intimate contact, even though the GaAs surface was prepared in air. Taking account of the results of spectra taken on reference and oxidised GaAs surfaces it is believed that the existance of a interfacial layer as

discussed above is necessary for interface states to be detected by DLTS.

Yamanski *et al*[10] have derived an approximation which relates the density of interface states $N_{IS}(E)$ at the interface to the capacitance of the interfacial layer C_{ox} and the DLTS signal ΔC as:

$$N_{IS}(E) = \frac{C_{ox}N_D}{C^3(t_1)kTln(t_2/t_1)}\Delta C \qquad 5.5$$

where $C(t_1)=C_{rev}$ at the peak temperature T, C_{ox} is the capacitance of the oxide layer and t_1 and t_2 are the DLTS sampling times. The ratio $t_2/t_1=2.5$ is set by the DLTS system. C_{ox} is measured from the forward capacitance C_{total} by:

$$C_{ox} = (1/C_{total} - 1/C_{sc})^{-1} \qquad 5.6$$

where C_{sc} is the capacitance of the space charge region and is given by:

$$C_{sc} = S\left(\frac{qN_D\varepsilon_s}{2(V_i + V_R)}\right)^{0.5} \qquad 5.7$$

In deriving equation 5.5, an energy independent capture cross section is assumed. Since the measurement error for σ_n is usually large, the values obtained above can be considered constant within the measurement error[30].

Figure 5.12 shows the energy distribution of the interface states for the iron and gold GaAs interfaces. It can be seen that for both interfaces, the density of interface states increases monotonically with energy toward the conduction band. The energy range over which the DLTS apparatus detects these interface states is limited at the shallower energies by the response time of the capacitance meter (1 ms) and at deeper levels by the overlapping emission from the EL2 bulk trap, which as can be seen in Figure 5.11(a) and (b) is much stronger than that for interface states. As expected, the densities, of the order of 0.4 - 1.6×10^{12} states/eV/cm^2 for iron and 0.7 - 4.6×10^{12} /eV/cm^2 for gold diodes are consistant with the higher n values obtained from I-V characteristics.

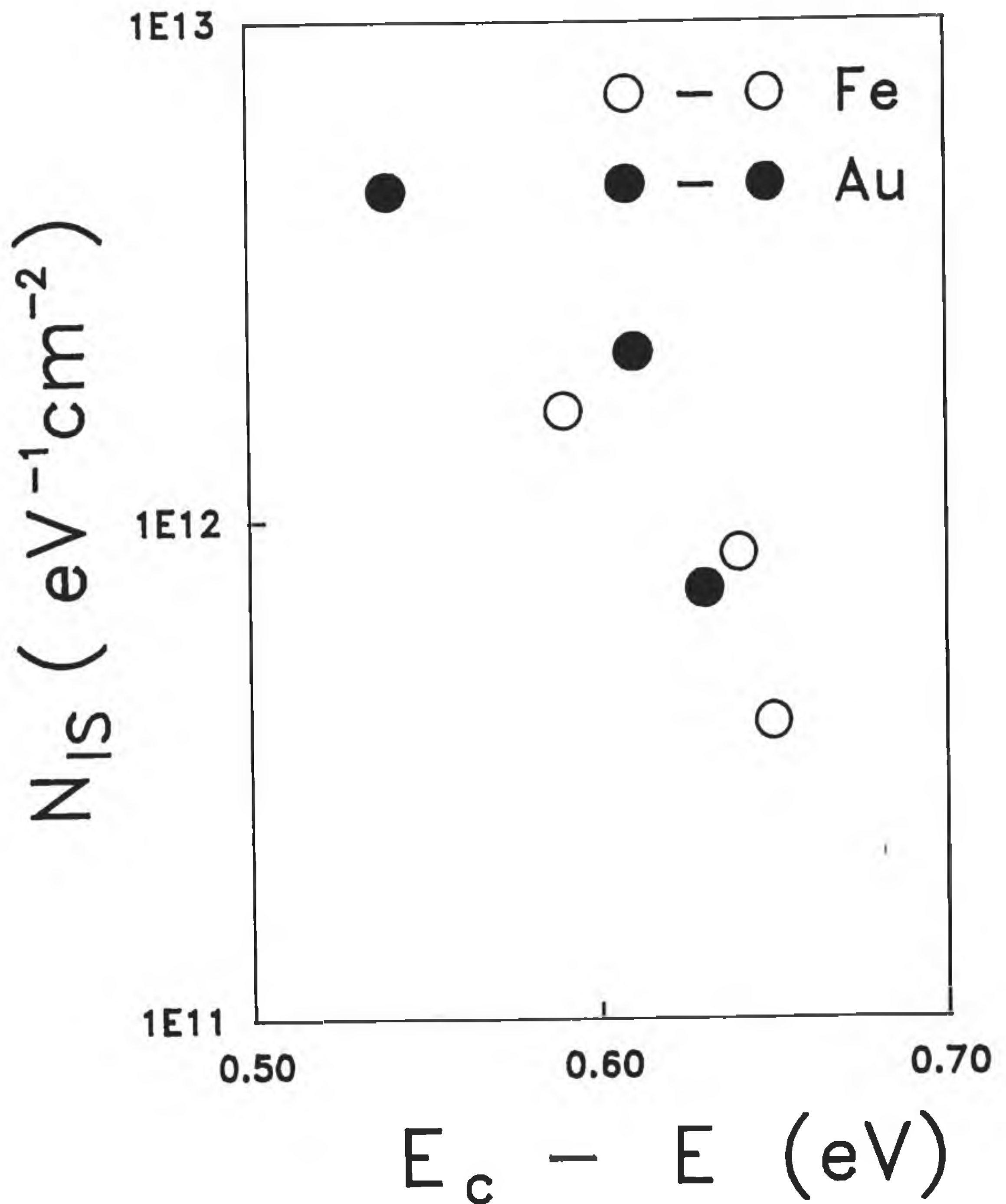

Figure 5.12. Plot of the density of interface states N_{IS} vs energy.

The difference in the measured values of barrier height by C-V and I-V methods for the oxidised surfaces in particular warrants consideration. It has been shown in these experiments that while both methods of determining the barrier height agree for metals which form an intimate contact with the semiconductor; those for oxidised surfaces do not. Therefore, it is clear that it is the effects of the interfacial layer that give rise to the discrepancy in ϕ_B^{IV} and ϕ_B^{CV}. This problem has been discussed by McLean *et al*[15]. They successfully modelled the I-V characteristics of diodes by the inclusion of a recombination current term in addition to the thermionic current and, in doing so, obtained values of ϕ_B^{IV} on non-ideal Fe-nCdTe diodes which were in closer agreement to ϕ_B^{CV} than would have been if the thermionic emission alone was used. It is clear, however, from the poor results obtained in attempting to fit the non-ideal diodes in this study with both computer models that thermionic emission and recombination do not completely govern the I-V characteristics and that some other factors such as the effect of interfacial layers has to be taken into account.

5.4 Summary

The results of the experiments presented in this chapter indicate that a correlation exists between the ideality factor as determined by I-V measurements and the presence of interface states as detected by DLTS. It is evident that the high density of interface states observed are due to defects induced by the oxidation of the GaAs surface prior to metal deposition. It has been found that a direct relationship exists, for the systems studied, between the measured density of interface states and the deviation of the ideality factor from n=1.

References

[1] Sinha A.K. and Poate J.M., in Thin Films - Interdiffusion and Reactions, Eds. Poate J.M., Tu K.N. and Mayer J.W., (Wiley-Interscience, New York, 1978) p. 407.

[2] Kowalczyk S.P., Waldrop J.R. and Grant R.W., Appl. Phys. Lett. **38** (1981) 167.

[3] Hasegawa F., Masaaki O., Mogi C. and Nannichi Y., Solid-St. Electron., **2** (1988) 223.

[4] Bardeen J., Phys. Rev. **71** (1947) 717.

[5] Spicer W.E., Liliental-Weber Z., Weber E., Newman N., Kendelwicz T., Cao R., McCants C., Mahowald P., Miyano K. and Lindau I., J. Vac. Sci. Technol. B **6**(4) (1988) 1245.

[6] Cowley A.M. and Sze S.M., J. Appl. Phys. **36** (1965) 3212.

[7] Lang D.V., J. Appl. Phys. **45** (1974) 3023.

[8] Martin G.M., Mitonneau A. and Mircea, A., Electron. Lett. **13**(7) (1977) 191.

[9] Auret F. D., Leitch A.W.R. and Vermaak J.S., J. Appl. Phys. **59** (1986) 158.

[10] Yamasaki K., Yoshida M. and Sugano T., Jpn. J. Appl. Phys. **18** (1979) 113.

[11] Murray F., Carin R. and Bogdanski P., J. Appl. Phys. **60** (1986) 3592.

[12] Roberts L. and Hughes G.J., Appl. Surf. Sci. **50** (1991) 424.

[13] Zhang H., Aoyagi Y., Iawi S. and Namba S., Appl. Phys. Lett. **50** (1987) 341.

[14] Platen W., Kohl D., Brauchle K.A. and Wolter K., Mater. Sci. Forum **10-12** (1986) 223.

[15] McLean A.B., Dharmadasa I.M. and Williams R.H., Semicond. Sci. Technol. **1** (1986) 137.

[16] Roderick E.H. and Williams R.H., Metal-Semiconductor Contacts, (OUP 1988).

[17] Waldrop J.R., J. Vac.Sci. Technol. B **2** (1984) 445.

[18] Waldrop J.R., Appl. Phys. Lett. **44**, (1984) 1002.

[19] Sze S.M., Physics of Semiconductor Devices, (Wiley, New York, 1981).

[20] Wilmsen C.W., Chap. 8, "Oxidation of GaAs", Gallium Arsenide Technology, ed. D.K. Ferry, (Howard W. James and Co., 1988), p. 358.

[21] Aydinli A. and Mattauch R.J., Solid-St. Electron. **25** (1882) 551.

[22] Spicer W., Chye P., Garner C., Lindau I., Pianetta P., Surf. Sci. **86** (1979) 763.

[23] Schlutz M. and Johnson N.M., Appl. Phys. Lett. **31** (1977) 622.

[24] Holmes D.E., Chen R.T., Elliot K.R. and Kirkpatrick C.G. Appl. Phys Lett. **40** (1982) 46.

[25] Mircea A, Mittoneau A., Hollan L. and Briere A, Appl. Phys. **11** (1976) 153.

[26] Li G.P. and Wang K.L., J. Appl. Phys. **53** (1982) 8653.

[27] Ruda H.E., Liu Q., Ozawa M., Zukotynski S., Parsey Jr. J.M., O'Neill T.J., Lockwood D.J. and Lent B., J. Phys. D:Appl. Phys. **25** (1992) 1538.

[28] Taniguchi M. and Ikoma T., J. Appl. Phys. **54** (1983) 6448.

[29] Nield S.T., Skowronski M. and Lagowski J., Appl. Phys. Lett. **58** (1991) 859.

[30] Platen W., Schmutzler H.-J., Kohl D., Brauchle K.-A. and Wolter K., J. Appl. Phys. **64** (1988) 218.

[31] Williams R.H., Physica Scripta **T1** (1982) 33 and references therein.

[32] Garner C.M., Su C.Y., Saperstein W.A., Jew K.A., Lee C.S. Pearson G.L. and Spicer W.E., J. Appl. Phys. **50** (1979) 3376.

[33] Miller W.R. and Stillman G.E., Appl. Phys. Lett. **57** (1990) 2934.

Chapter 6 Sulphur Passivation of the GaAs(100) Surface

6.1 Introduction

The development of a processing technique that electronically and chemically passivates the GaAs surface is of significant technological importance. The oxidation of GaAs in atmospheric conditions leads to the disruption of the surface structure increasing the density of states, which have a detrimental effect on device performance. Much interest has focused on the passivation of the GaAs surface by sulphur containing compounds and one of the first reports was given by Sandroff *et al*[1], whereby a solution of sodium sulphide, $Na_2S{\cdot}9H_2O$, used to treat the GaAs(100) surface, gave an improvement in photoluminescence (PL) intensity. Yablonovitch *et al*[2], who also treated GaAs surfaces with $Na_2S{\cdot}9H_2O$, reported a reduction in surface recombination velocity, thus indicating an improvement in surface quality. A major drawback of this treatment however, was that it was destroyed after being dipped in water[1]. More reproducible and dependable results were obtained by treatments with ammonium sulphide, $(NH_4)_2S$, and ammonium polysulphide, $(NH_4)_2S_x$ solutions. Of significant importance was the removal of the GaAs surface oxides[3]. Other effects such as enhanced PL intensity similar to that produced by the Na_2S treatment[4,5], better dependence of Schottky barrier height on metal work function[6-8] and a decrease in band bending[9], have been observed. In addition, by annealing $(NH_4)_2S_x$ treated GaAs surface Sugahara *et al*[9] found from photoemission results that S-Ga bonds become dominant and suggested that these bonds were the key to successful passivation.

Recently, Tiedje and co-workers[10] reported on the use of hydrogen sulphide, H_2S, as a means of sulphur passivation. In comparison with the inorganic sulphide solutions, a much higher fraction of sulphur bonding was found from photoemission studies of H_2S exposed GaAs surfaces. Their studies also indicate that the H_2S treated surface seems to be a better defined surface than those produced by either Na_2S or $(NH_4)_2S$ chemical treatments. Indeed, it has been speculated by Shin *et al*[11] that H_2S, which is given off by both solutions, may be involved in the formation of the S-GaAs interface. For these reasons, and from the point of view of *in situ* passivation, H_2S gas was chosen over chemical solutions as a means of sulphur treatment in these experiments.

For the majority of results reported thus far, an important point is that sulphur treatments indicate that the GaAs surface is covered with approximately one monolayer of sulphur atoms, which acts to reduce the density of surface states by providing a barrier to further oxidation. Furthermore, it has been seen in the previous chapter that oxidised GaAs surfaces lead to the appearance of a high density of interface states which may be detected by DLTS. The use of this technique to investigate the effectiveness of sulphur passivation in preventing an increase in the density of GaAs surface states which would otherwise be caused by oxidation therefore seemed a natural progression. The degree of passivation was determined by comparing spectra from both untreated and H_2S treated samples which had been subsequently exposed to air prior to Schottky barrier formation. Ideality parameters for treated and untreated samples were determined from I-V characteristics. The results of these investigations indicate that H_2S treatment prolongs the as-etched surface characteristics which quickly degrade in air in the absence of this treatment.

The majority of reports indicate that the S-GaAs interface forms by chemisorption and while the results from DLTS studies provide information in terms of the electronic properties of the passivated surfaces, little insight is given into the exact bonding nature of the sulphur adatoms to the GaAs surface. With the availability of synchrotron radiation, at a later stage in these studies, the chemistry of the passivated surface was investigated using the soft X-ray photoemission, (SXPS). AES was also used to study the elemental composition of the surfaces. A molecular sulphur beam, generated from the electrochemical cell described in section 4.3.3, served as a means of sulphur passivation in these experiments. In addition to being UHV compatible, this source is highly controllable and enables the study of the evolution of a sulphur-GaAs interface, therefore offering a considerable advantage over the use of H_2S.

Because the use of wet chemical surface preparation techniques do not ensure that the GaAs surface is contamination free, the starting surface before sulphur passivation is not well characterised. The use of UHV cleaning techniques such as Argon ion bombardment and annealing (IBA) can also leave the precise surface composition in doubt. As-capped GaAs samples[12], however, provide a very useful method of preparing an intrinsicly clean surface. Moreover, the composition of the topmost atomic layers can be accurately be controlled. This ability to predetermine

the surface composition is ideal for the studying the interactions of adsorbates with the surface.

The enhanced surface-sensitive capabilities of a synchrotron radiation source permitted both the measurement of sulphur coverages and accurate estimates of the chemical shifts caused by the bonding of sulphur adatoms to the GaAs surface. The precise control over the composition of the topmost atomic layer afforded by the use of As-capped GaAs surfaces, allowed the As/Ga surface ratio to be changed in a systematic manner. This added another degree of precision to these surface investigations which was previously only possible within a MBE facility.

The layout of this chapter is as follows. In section 6.2, the results of the H_2S passivation of GaAs(100) surfaces at room temperature are presented. The findings of the interactions of the clean GaAs(100) surface with electrochemically deposited sulphur are presented in section 6.3. A full discussion of the results is given in section 6.4, together with the results of related works. Finally, a summary of the findings is given in section 6.5.

6.2 H_2S Passivation

The GaAs(100) samples ($n = 5 \times 10^{16}$ cm^{-3}), similar to those used to obtain the results presented in chapter 5, were chemically cleaned as described in section 4.2.2. Ohmic contacts were made using In-Ga alloy and annealed at 400 °C in a nitrogen atmosphere. The samples were then directly inserted into the UHV preparation chamber where they were exposed to an atmosphere of H_2S for 30 min. Schottky diodes were fabricated on these samples by depositing gold contacts. In order to determine the effectiveness of the passivating procedure treated surfaces were exposed in air for periods up to 18 h prior to metal deposition. Electrical studies of both treated and untreated samples were carried by taking I-V measurements and DLTS spectra. On average, 10 individual diodes were tested on a sample; therefore any variations in the effective passivation across the surface could be detected.

Figure 6.1 illustrates the DLTS spectra obtained for the passivated and unpassivated GaAs samples. These spectra clearly show the well characterised EL2 and EL6 bulk electron trap features seen in results from chapter 5. The comparison is made

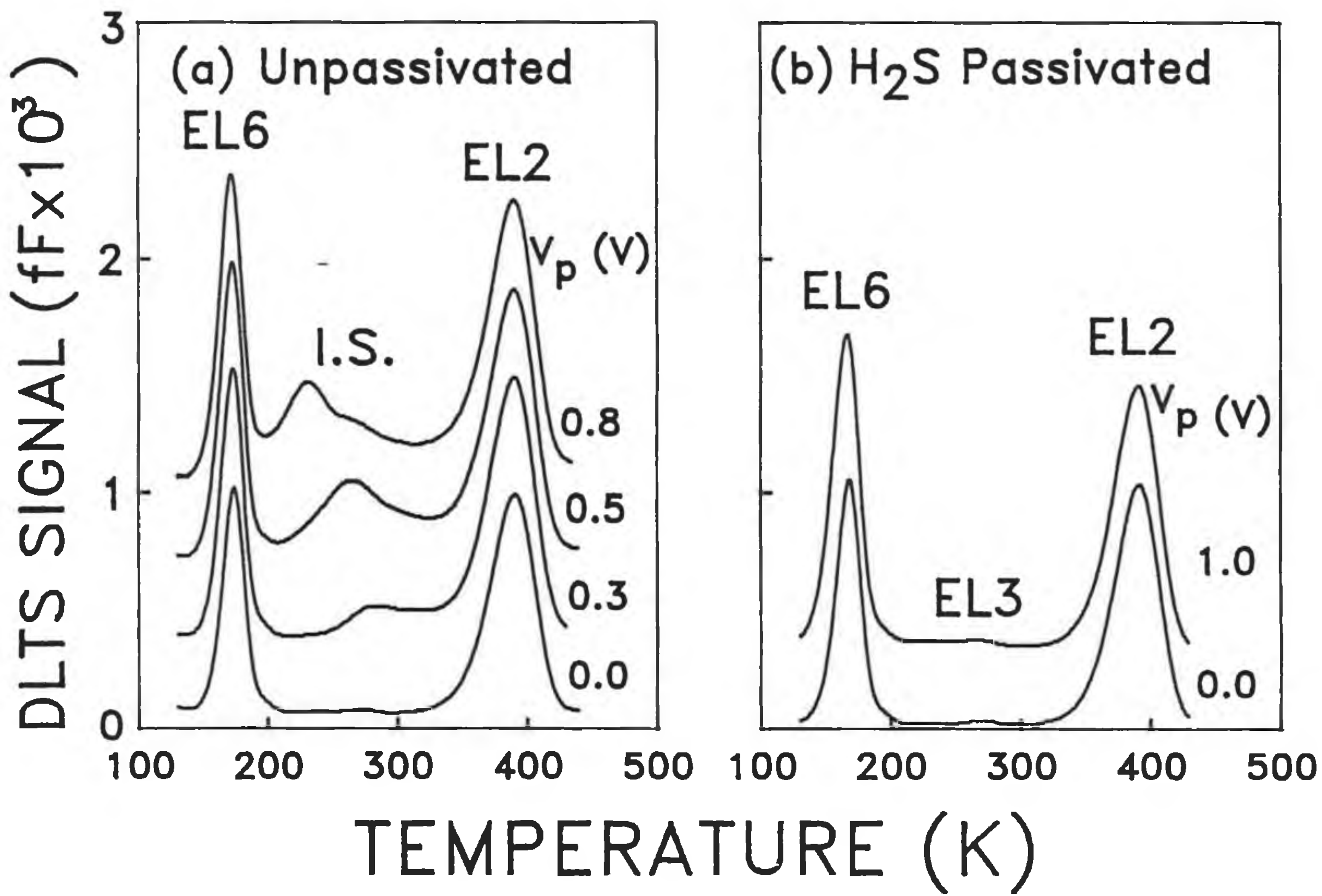

Figure 6.1. DLTS spectra of (a) unpassivated, n=1.6 and (b) H_2S passivated (n=1.1) GaAs, V_r= -1.00 V, V_p as shown. R/w is $100s^{-1}$. I.S.= interface state.

between two samples: one which was chemically etched and left in air for 1 h prior to gold deposition, and the other sample which was exposed to H_2S immediately after etching and then exposed to air for 1 h before a metal contact was deposited. The additional spectral features observed on the unpassivated GaAs surface are only detected in the forward-bias pulse sequence of the DLTS; therefore the electron traps corresponding to these features are located within the intrinsic depletion region of the diode. Two distinct overlapping peaks are clearly detected for high-forward bias voltages. It is clear both from the arguments presented in section 3.2.3.2 and the results in chapter 5 that these spectral features correspond to a broad distribution of interface states at the Au-GaAs junction. The ideality parameters derived from the I-V characteristics for the unpassivated sample are significantly higher ($1.6<n<2$) than for H_2S exposed surface ($n<1.1$). These latter idealities are similar to those routinely obtained for GaAs diodes where the gold overlayer is deposited immediately following etching. The DLTS spectra taken on these diodes exhibit characteristics similar to those of the passivated sample in that no interface states were detected during the forward-bias pulse sequence of a DLTS scan. Evidence of this may be seen by comparing the spectra shown in Figure 6.1(b) with those of Figure 5.6(b).

Figure 6.2 shows the DLTS spectra taken of a passivated sample which was subsequently exposed to air for 18 h prior to metal deposition. The idealities of the diodes fabricated on this sample were in the range n=1.1-1.2, and it may be seen from the Figure that there is some evidence of a feature attributable to interface states in the DLTS spectrum taken with a forward bias voltage, V_p, of 1.0 V . Nevertheless, by comparison with the spectra illustrated in Figure 6.1(a), it can be seen that there is a striking improvement in the quality of the passivated surface in terms of a reduction in interface state density.

6.3. Molecular Sulphur Passivation

The effectiveness of passivation using molecular sulphur was analysed using the surface science techniques described in section 3.3. For photoemission studies, a photon energy of 100 eV was chosen for all experiments. This provided maximum surface sensitivity with near identical escape depths for the photoemitted Ga and As *3d* electrons. The overall instrumental resolution at hν=100 eV was 0.45 eV;

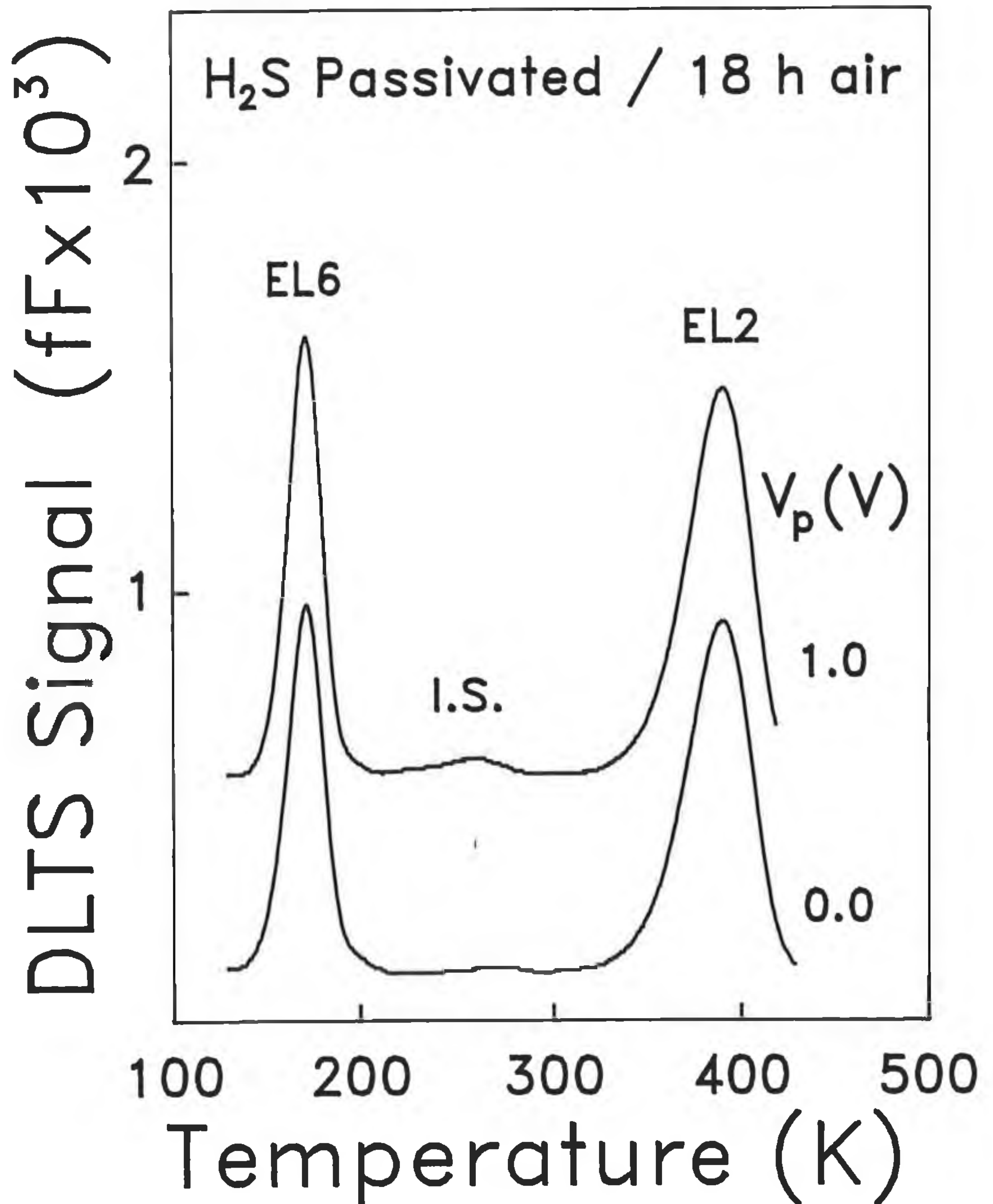

Figure 6.2. DLTS spectra of H_2S passivated GaAs surface after 18h exposure to air. V_r=-1.0V, V_p as shown. R/w is 100 s^{-1}. I.S. denotes interface states.

however, it was possible to reproducibly locate the position of a core-level to less than 0.1 eV. Throughout the experiments, the sulphur cell was operated under the conditions required to maintain a constant flux of almost exclusively S_2 molecules, as monitored by a mass spectrometer. For all samples, deposition of sulphur took place at room temperature with the cell operating at a current of 0.5 mA. AES was used to monitor the general cleanliness of the surfaces during the experiments. Initial preparation of the MBE samples ($n = 5x10^{16}$ cm^{-3}) involved the thermal decapping of the protective As overlayer as described in section 4.3.2. The ratio of the As-to-Ga surface atomic composition was controlled by annealing the surface to different temperatures during the decapping procedure[13]. The different surface compositions were monitored through variations in the surface structure as determined by LEED[14]. The As/Ga surface composition was determined from the relative intensities of the As and Ga *3d* core-levels taken at 100 eV photon energy[15].

Figure 6.3 illustrates "raw" photoemission spectra taken during a typical decapping procedure to obtain a clean GaAs surface. The quality of the As cap is demonstrated by the spectra in Figure 6.3(a) where it can be seen that only the As *3d* peak can be identified. The absence of the Ga Auger line at 1070 eV in AES studies gave further verification that the cap was intact. The shoulder to the high binding-energy side of the As *3d* is a result of oxygen bonded to the surface As atoms. The presence of oxygen, as well as other contaminants such as carbon and sulphur were also detected by AES. As mentioned above, the decapping process could be altered to produce clean GaAs surfaces of varying As content. Figures 6.3(b) and (c) show spectra taken of an As-rich and a Ga-rich surface, respectively. The observed core-level shift to lower binding-energy as seen by comparing the spectrum of the As capped surface with those of the As and Ga rich surfaces is indicative of the band bending induced by the desorption of both the As overlayer and As oxides. A recent analysis of clean GaAs surfaces prepared by thermal decapping indicated that the surface Fermi-level for n-type material is consistently found at 0.7 eV above the valence band maximum, regardless of surface As composition[13,15]. The investigations on the decapped surfaces in these studies are in agreement with this Fermi-level position to within 0.1 eV.

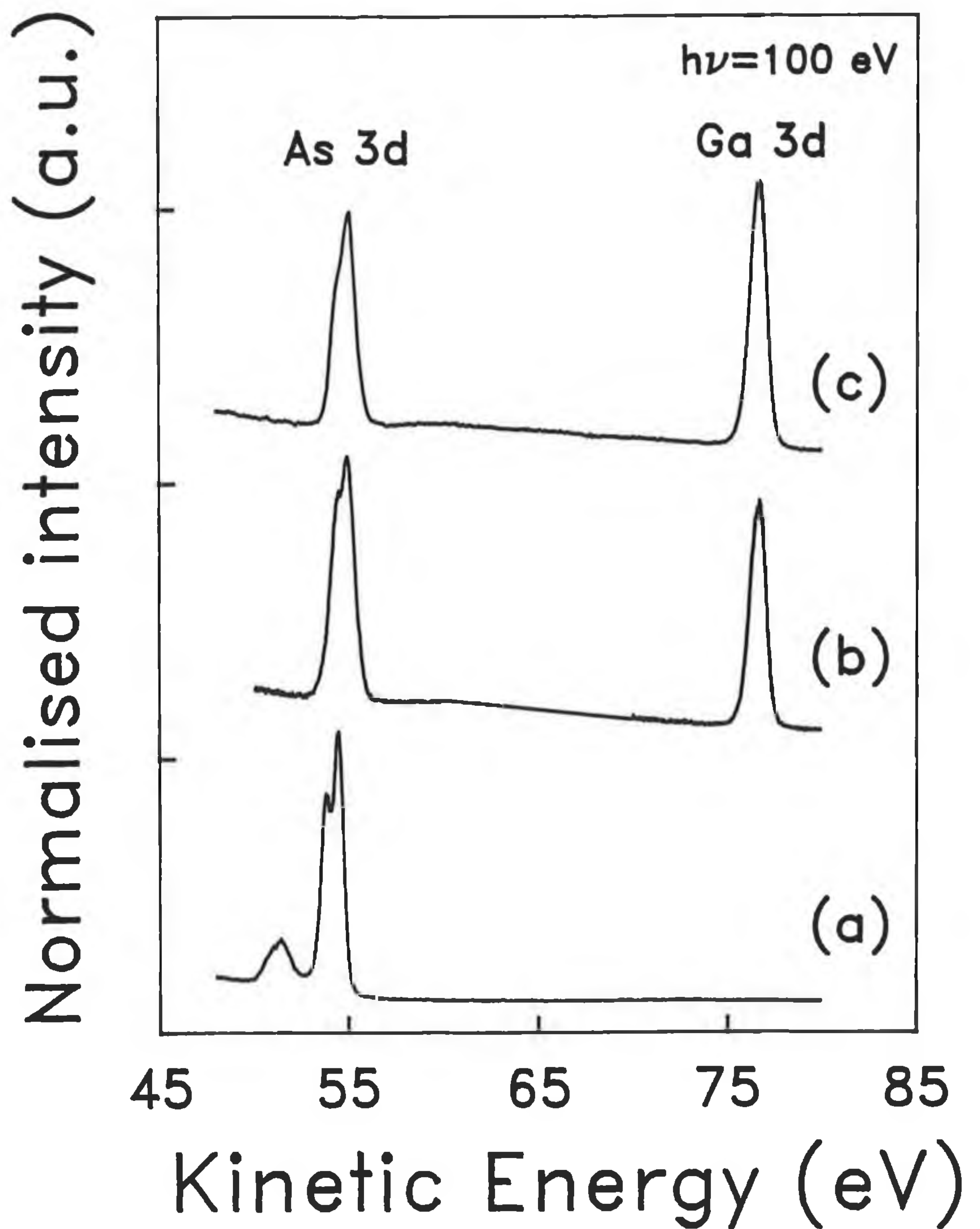

Figure 6.3. "Raw" SXPS spectra of (a) As capped GaAs surface. As-rich (b) and Ga-rich GaAs surface (c) were obtained during different stages of thermal annealing.

In order to obtain precise values for core-level binding energies as well as the chemically shifted As and Ga components, it was necessary to curve-fit the raw photoemission data. This was carried out by assuming a Voigt profile, i.e. a Lorentzian convoluted with a Gaussian lineshape, using a non-linear least-squares fitting routine[16]. The Lorentzian lineshape describes the natural lifetime broadening of a core-level, while the Gaussian form takes account of the effects of instrumental resolution.

Other parameters included were:

(i) spin-orbit splitting of both the As and Ga *3d* core-levels into *3d* $_{3/2}$ and *3d* $_{5/2}$ levels. This arises out of the loss in degeneracy of the core-level due the coupling between the spin and orbital angular momenta.

(ii) the relative intensities or branching ratios of the spin-orbit split terms.

(iii) the surface core-level shifts which arise due to the displacement of the surface As and Ga atoms from the bulk.

(iv) excess As binding-energy shift, when required, to account for the presence of free As atoms bonded to the GaAs surface.

The curve-fitting parameters that gave rise to the most consistent fits are shown in Table 6.1. Stringent conditions were placed on the number of fitting parameters used and the degree by which they were allowed to vary. The fixed parameters were the Lorentzian and Gaussian full-width-at-half-maximum (FWHM), the spin-orbit splitting and the branching ratios. These fitting parameters are within the range of the previously published values for the GaAs(100) surface[13,17]. In curve-fitting the data, an approach similar to that detailed by Ranke and co-workers[17] was adopted.

Table 6.1. Fitting parameters for the Ga *3d* and As *3d* core-level spectra for the GaAs(100) decapped surface. All parameters expressed in eV.

	Ga *3d*	As *3d*
Spin-orbit split	0.46	0.7
Branching ratio	0.65	0.65
Gaussian width	0.55	0.55
Lorentzian width	0.14	0.14
Surface core-level shift	0.35	0.4
Excess As binding-energy shift	...	0.6

This includes using the minimum number of component peaks to obtain an acceptable fit and having confidence in the deconvolution process for peaks separated by more than half the FWHM.

Figures 6.4(a) and 6.5(a) show the normalised Ga and As *3d* core-level spectra of a clean Ga-rich surface. The As/Ga ratio derived from the total intensities of the As and Ga peaks was 0.9. Both the Ga and As *3d* core-levels are represented by a bulk and surface core-level-shifted (SCLS) component, shifted by 0.35 and 0.40 eV, respectively, in the range of the values previously reported for this As-capped surface[12]. The spin-orbit split of the core-levels into $3d_{5/2}$ and $3d_{3/2}$ levels, the latter level at higher binding-energy, can be clearly seen. The Ga *3d* spin-orbit split can not be as well resolved due to instrumental resolution.

Figures 6.4(b) and 6.5(b) illustrate the result of exposing this Ga-rich surface to molecular sulphur. A broad chemically shifted feature appears on the higher binding-energy side of the Ga *3d* core-level. An even more pronounced broadening is seen on the same side of the As *3d*. While it proved possible to fit the broadening on the Ga *3d* peak with one chemically shifted component shifted by 0.7 eV to higher binding-energy, it was found necessary to fit the high binding-energy feature on the As *3d* with two components shifted by 0.5 and 1.4 eV, respectively, from the As *3d* bulk peak. Justification for these two chemically shifted components can be made based on the change induced in the profile of the As core-level upon annealing the surface at 150 °C as shown in Figures 6.4(c) and 6.5(c). This results in the complete attenuation of the 1.4 eV As chemically shifted component leaving a single chemically shifted component at 0.5 eV, which is unaltered by the annealing cycle. This would suggest that sulphur bonds to the As surface atoms in two configurations, possibly to the bonding of one and two sulphur atoms, respectively. Estimates of the sulphur coverage from the magnitude of the chemically shifted components on both core-levels indicate that the GaAs surface is terminated by a chemically bonded sulphur monolayer. This adsorption process contrasts with the disruptive nature of oxide formation which has been seen to lead to an increase in the density of surface states.

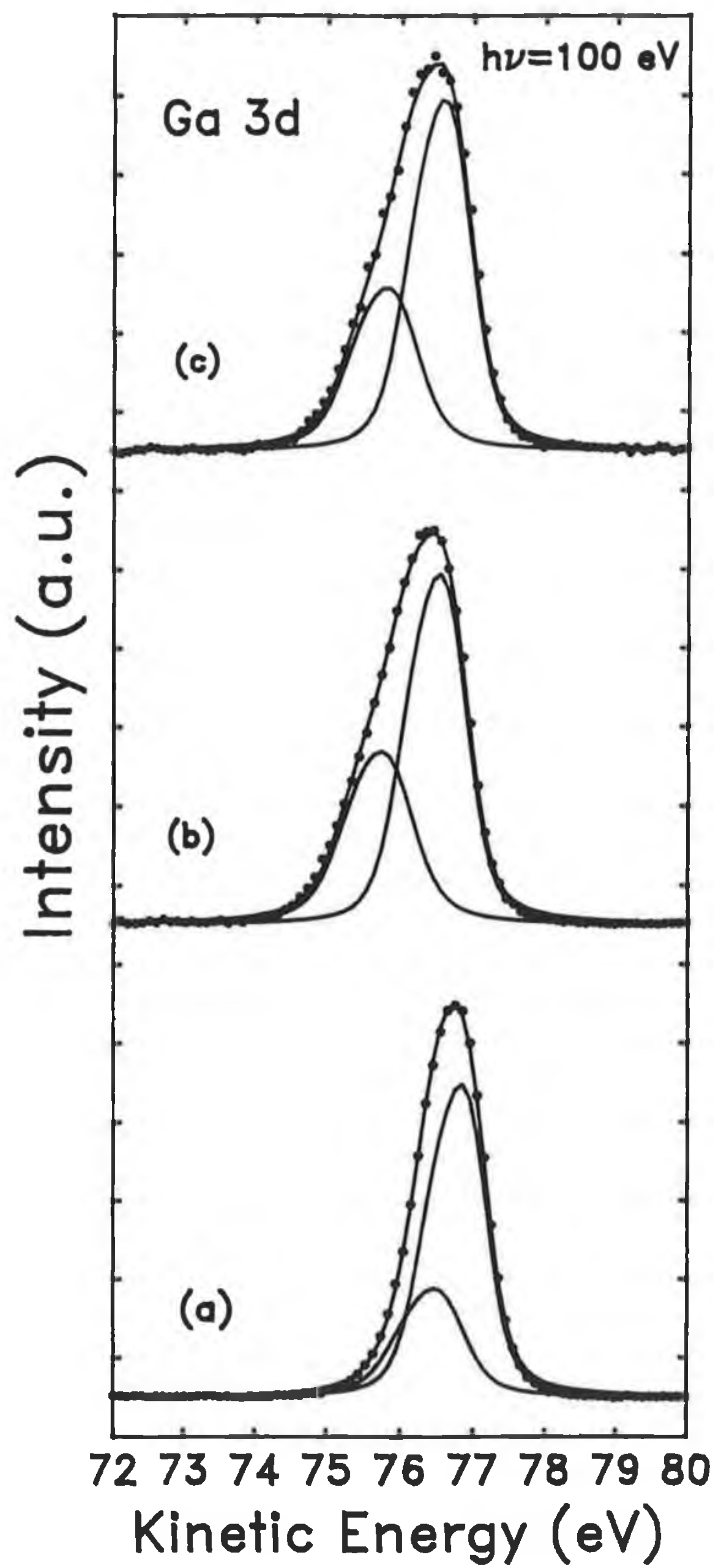

Figure 6.4. Deconvolution of the Ga *3d* SXPS spectra for Ga-rich surface (As/Ga 0.9), hv=100 eV: (a) clean surface , (b) sulphur-covered surface and (c) after annealling at 150 °C.

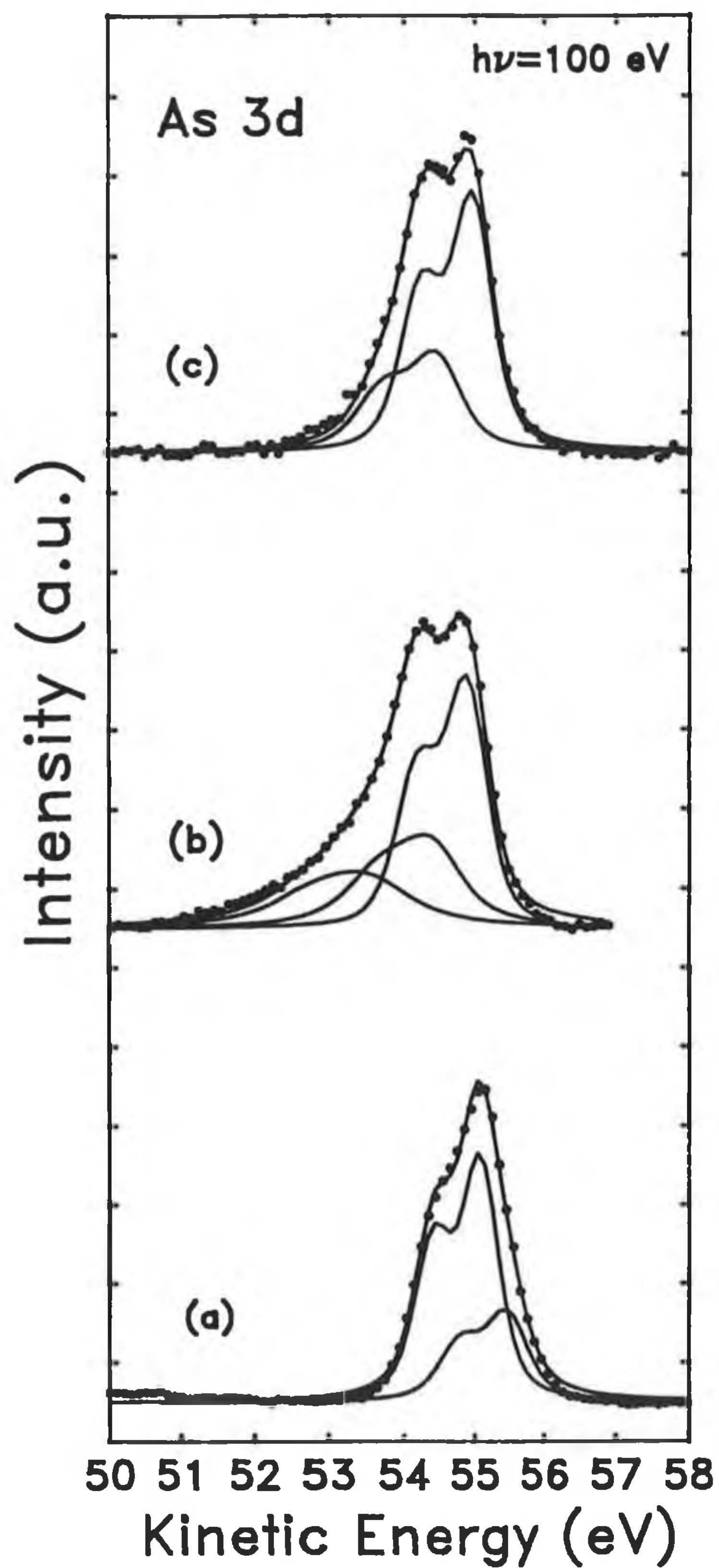

Figure 6.5. Deconvolution of the As *3d* SXPS spectra for a Ga-rich surface (As/Ga 0.9), hν= 100eV: (a) clean surface, (b) sulphur-covered surface and (c) after annealing at 150 °C.

Figures 6.6(a) and 6.7(a) show the normalised Ga and As *3d* core-level spectra of a clean As-rich surface (As/Ga ratio 1.2) produced as a result of the decapping procedure. The Ga *3d* core-level was fitted with the same parameters as on the Ga-rich surface, the only difference being the reduced intensity of the SCLS component. Similar variations in the magnitude of the SCLS component have been previously observed and attributed to the presence of an excess arsenic component on the surface[17,19]. For the As *3d*, two components together with the bulk component are necessary to produce a good fit, as has been previously reported[13]. The peak shifted by 0.6 eV to the higher binding-energy side of the bulk peak represents excess or elemental As on the surface. This binding-energy shift is comparable with the previously reported values in the range 0.5-0.7 eV, for an arsenic adatom bonded to an As surface atom[17,18]. The SCLS component is shifted by 0.4 eV to the lower binding-energy side of the bulk peak.

Figures 6.6(b) and 6.7(b) illustrate the spectra for the sulphur-covered surface, with the analysis of the Ga *3d* core-level again indicating a single chemically shifted component shifted by 0.75 eV to higher binding-energy from the bulk peak. Within experimental error, this is the same chemical shift as on the Ga-rich surface. For the As *3d* core-level, the presence of the excess arsenic chemically shifted component on the same side of the bulk peak as the chemical shift induced by the sulphur makes it difficult to resolve the correct chemical shift. By assuming that the adsorbed sulphur bonds to this surface in the same configuration as on the Ga-rich surface, the broad chemically shifted shoulder on the As *3d* peak can be fitted with two component peaks at 0.5 and 1.35 eV, respectively. The magnitude of the chemically shifted components indicate that more sulphur is bonded to the As than to the Ga which reflects the predominance of As in the topmost atomic layer for this surface. No evidence of a substantive oxide presence was detected from AES studies.

6.4 Discussion

The results of the I-V and DLTS studies indicate that the H_2S passivation of the etched GaAs surface has the effect of maintaining the surface with the post-etched characteristics. This has been established from the similarities between the electrical characteristics of the passivated sample and those of the etched surface which was immediately metallized. The etching process removes the surface oxide and the

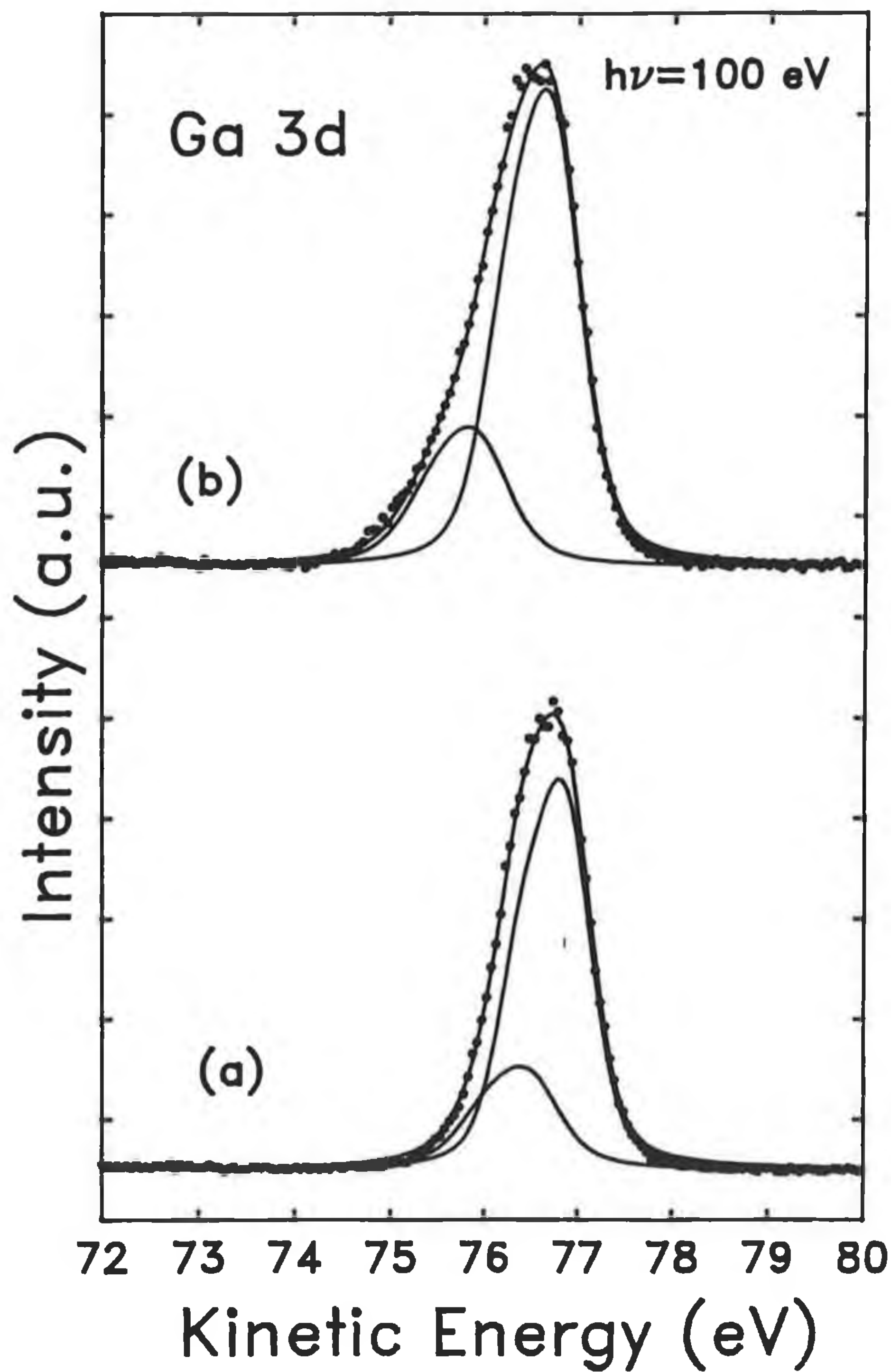

Figure 6.6. Deconvolution of the Ga *3d* SXPS spectra for a As-rich surface (As/Ga 1.2) hν=100 eV: (a) the clean surface, (b) the sulphur-covered surface.

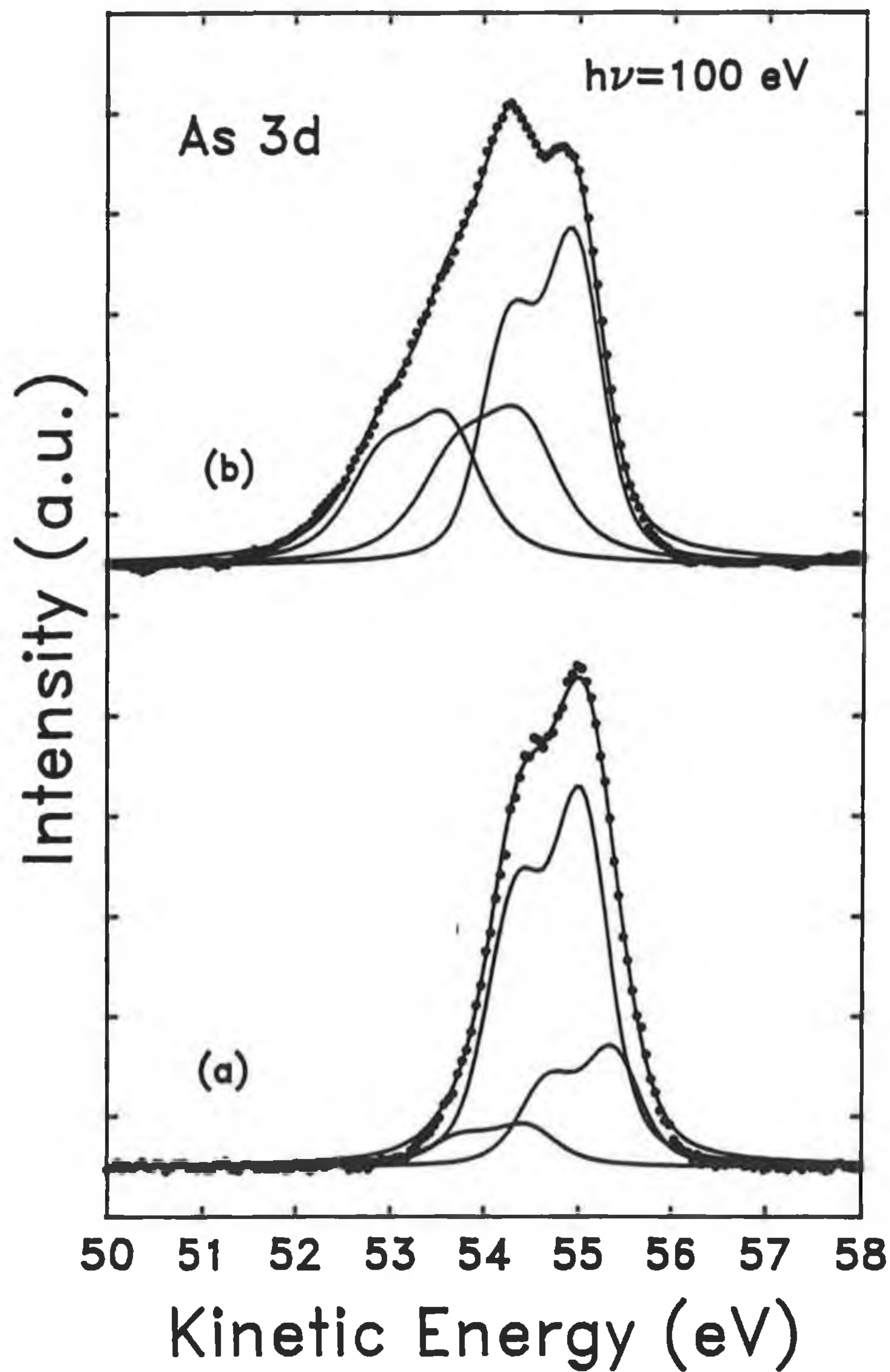

Figure 6.7. Deconvolution of the As *3d* SXPS spectra for a As-rich surface (As/Ga 1.2) taken at 100 eV photon energy: (a) the clean surface, (b) the sulphur-covered surface.

subsequent passivation or the immediate metallization of the etched surface limits the regrowth of a surface oxide, thereby giving rise to the near-ideal electrical characteristics observed. Even for the passivated sample which was subjected to prolonged exposure to atmospheric conditions, the electrical measurements indicate that the Ga and As surface atoms had remained predominantly unoxidised. This contrasts markedly with the air-exposed samples where a significant deterioration in the electrical characteristics of the surface was detected, even over a timescale of 1h.

In an attempt to correlate the effects of H_2S passivation as observed from I-V and DLTS studies, Hughes *et al*[20] carried out PL measurements on GaAs samples which were cut from the same wafer and prepared by exactly the same methods, with the exception of metallization, as those for the electrical studies discussed above. Luminescence was excited using a continuous-wave Ar ion laser operating on all lines and analysed using a Spex 1 m spectrometer. Figure 6.8(a) illustrates the PL spectrum of the untreated sample. The strong near-band edge emission in the 1.45-1.5 eV region have been attributed to unresolved donor-to-acceptor transitions[21] whereas the broad bands observed at 0.9-1.4 eV are related to donor-vacancy complexes[22]. The PL spectrum of the H_2S passivated sample, shown in Figure 6.8(b), shows a dramatic reduction in the intensity of the donor-vacancy bands relative to the near-band-edge emissions. It has been suggested that this is caused by a modification of the donor-vacancy defect and/or an increase in the number of donor species contributing to the near-band-edge luminescence, both of which are consistent with a reduction in interface state density. Thus, the PL spectra can be interpreted in terms of H_2S surface passivation of the etched surface when compared with the unpassivated surface.

Some insight into the effectiveness of H_2S passivation has been given in a paper by Kawanishi *et al*[23], who prepared clean MBE GaAs wafers which were initially passivated with H_2S *in situ* and subsequently exposed to oxygen at atmospheric pressure. By carrying out desorption studies at temperatures of 520 °C which were monitored by Reflection High Energy Electron Diffraction (RHEED) and AES, they observed the complete desorption of oxygen in the form of oxidised sulphur. Moreover, the GaAs surface was still sulphur-terminated after oxygen desorption.

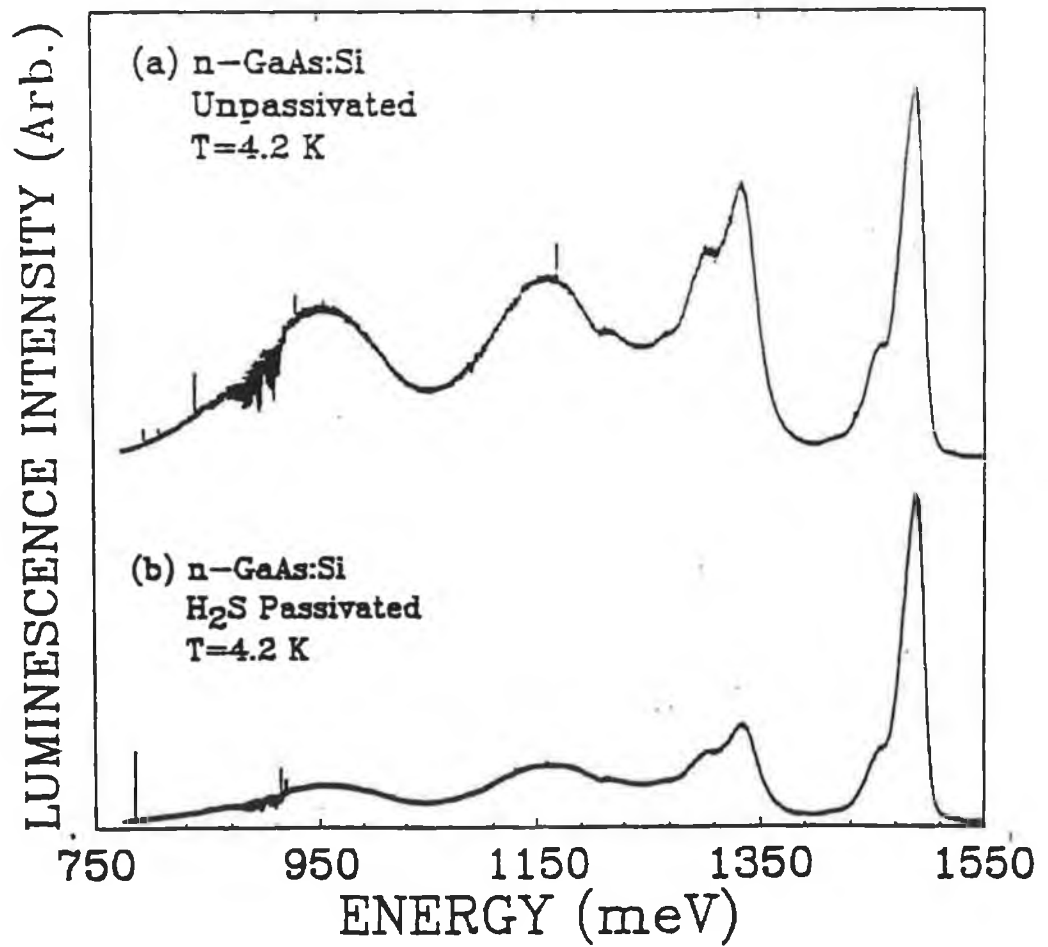

Figure 6.8. PL spectra of (a) unpassivated and (b) H_2S-passivated GaAs(100) surface. Near-band-edge emission is observed in the 1.45-1.5 eV region. The broad bands from 0.9 to 1.4 eV are due to donor-vacancy complexes.

They concluded that the passivating effect of H_2S lies in the fact that the sulphur atoms prevent oxygen from intruding deeply into the bulk GaAs.

Significantly varying results were obtained from DLTS studies of GaAs surfaces depending on the precise procedure which followed immediately after etching and prior to H_2S exposure. The longer that an etched surface is exposed to air prior to H_2S treatment, the less effective the passivating treatment. These results would support the proposal by Spindt and Spicer[24] that the sulphurization is effective in passivating the surface owing to its ability to inhibit the growth of surface oxides. The deterioration in the electrical characteristics of the passivated surface which underwent prolonged air exposure is also consistent with this proposal. It would be difficult to envisage a process involving the exposure of a surface to the extent that no subsequent oxidation would occur, bearing in mind the larger heats of formation of oxides compared with sulphides[24]. These findings are also supported by reports by Shin and co-workers[11] that the uptake of sulphur on the GaAs(100) surface varies depending on the extent to which the surface is oxidised prior to H_2S exposure. They have also suggested that there is a kinetic barrier to sulphur; therefore the degree of sulphur uptake on a particular surface depends on whether there is sufficient energy to surmount this barrier. Kuhr *et al*[25,26] also investigated H_2S adsorption on GaAs. They found that the amount of H_2S adsorption critically depended on the order and composition of the GaAs surface. Indeed, the results of the SXPS studies reflect that the critical factor in determining the form of the interaction between molecular sulphur and the GaAs surface is the As/Ga surface ratio. These findings are in broad agreement with another more recent work by Shin and co-workers[27] for the treatment of chemically etched GaAs(100) surfaces with both the inorganic sulphides and H_2S.

Variations in intensity of the chemically shifted components on both the Ga and As *3d* core-levels can be attributed to changes in the surface composition. When the intensities of the chemically shifted components are small, it is necessary to rely on the accuracy of the deconvolution process to determine the magnitude of the chemical shifts. Therefore, changes in the surface component can make it difficult to unambiguously determine the precise chemical shifts. On the Ga-rich surface, it has been found necessary to fit the chemically shifted As component with two peaks

while the Ga chemically shifted component can be accommodated by a single peak fit. This may be interpreted in terms of sulphur bonding to the As surface atoms in more than one configuration. The annealing experiment would support this distinction, since the component shifted by 1.4 eV disappears completely while the component shifted by 0.5 eV is unattenuated. There is no evidence from the Ga core-level to suggest a similar bonding configuration, since the chemically shifted component can be satisfactorily fitted with a single peak shifted by 0.7-0.75 eV on both surfaces investigated and no significant change is observed on annealing. This, however, could be due to the small magnitude of the chemically shifted Ga components and the associated difficulty in resolving individual components by the deconvolution process. In addition, the presence of the SCLS and the chemical shift on the same side of the Ga *3d* core-level further complicates the fitting procedure. The difficulty in resolving the chemically shifted Ga component becomes more acute as the surface becomes increasingly arsenic rich and this can lead to a greater uncertainty in determining the magnitude of the chemical shift.

The problems associated with curve-fitting the chemical shifts on a surface with an excess arsenic component present have also been encountered by Ranke *et al*[17] in their investigation of the interaction of H_2S with a variety of GaAs surfaces. The As *3d* core-level has been fitted with two chemically shifted components similar in binding energy to the Ga-rich surface, but of significantly greater intensity. While it would also be feasible to curve-fit this chemically shifted component with one broad peak shifted by 1.0 eV from the bulk As peak, it seems justifiable to use a two-peak fit based on the results obtained for the Ga-rich surface. It is obvious from the intensity of the excess arsenic component that there is less than one monolayer coverage present on this surface. It can be reasonably assumed that increasing the magnitude of this component would result in an increase in the intensity of the Ga chemically shifted component. Therefore, it is possible to see how relatively small alterations in the surface composition can affect the measurement of the chemical shifts. This observation may go some way towards explaining the larger chemical shifts previously reported for the As *3d*[9,10,27] and the difficulty in detecting the presence of a Ga chemically shifted component for some surface preparations[28]. Two alternative explanation for the larger chemical shifts reported by other workers could be as follows. The first may lie in Shin and co-workers' kinetic barrier proposal in

that for all the reports of photoemission studies of sulphur passivation, the sulphur was activated, whether by heating the solution, as in the case of NH_4S_x[9], activation by a hot filament, as in the case of H_2S[10] or annealing the GaAs substrate during H_2S adsorption[27]. A summary of the chemical shifts obtained in these works, as well as the data obtained in this study, is presented in Table 6.2. In all cases, the kinetic barrier is the dissociation of either the H_2S or the NH_4S_x molecule, which, it is believed, is overcome by activation of the sulphur. By comparison, molecular sulphur deposition takes place at room temperature. It appears, therefore, that the higher the activation energy, the larger the measured chemical shift. The second explanation for the larger chemical shifts could lie in the fact that all of the passivation treatments listed in Table 6.2 were performed on wet chemically prepared GaAs surfaces. Thus, one cannot be sure of the surface composition prior to sulphur treatment. On the other hand, UHV-cleaned surfaces were used in this study, thereby providing a means of pre-characterising the surface before exposure to sulphur atoms.

Table 6.2. Summary of chemical shifts from different methods of sulphur passivation.

Work	Method	Chemical Shifts	
		As *3d*	Ga *3d*
Sugahara[9]	sample immersed in NH_4S_x at 60 °C	1.7	≈2.0
Tiedge[10]	H_2S activated by hot filament	0.6	1.5-2.0
Shin[27]	H_2S; substrate annealed at 160 °C	1.0	...
	200 °C	1.6	...
This work	molecular sulphur deposition at r.t.	0.5, 1.4	≈0.7

The core-level studies also indicate that the S-As bond forms more readily than the S-Ga bond. This can be deduced from the larger chemically shifted component on the As than on the Ga *3d* core level evident from the data in Table 6.3. Even on the Ga-rich sample, the ratio of the chemical shifted component intensity I_{cs} to the bulk peak intensity I_b on the As at 1.0 is significantly larger than the corresponding ratio for Ga (0.6). However, when this sulphur saturated surface is heated to 150 °C, the As-S chemically shifted component at 1.4 eV completely disappears and this ratio becomes comparable for both core-levels (As:0.48; Ga:0.53).

The preferential attenuation of the higher binding-energy chemically shifted component indicates a distinction between the thermodynamic stability of the two

Table 6.3. As/Ga ratios for the clean surface, compared with the ratios of the chemically shifted components I_{cs} to bulk peak components I_b, for the two surfaces.

As/Ga ratio on clean surface	Core-level	I_{cs}/I_b	I_{cs}/I_b after anneal
0.9	As *3d*	1.0	0.48
	Ga *3d*	0.6	0.53
1.2	As *3d*	1.3	...
	Ga *3d*	0.3	...

chemically shifted As components. The 1.4 eV chemically shifted component may correspond to a more volatile sulphide which is more easily desorbed at a relatively low annealing temperature. The attenuation of As-S chemically shifted components following low-temperature annealing has also been observed for the inorganic sulphide-treated GaAs surfaces by several other groups[4,27,29].

Estimates of the sulphur coverage from the magnitude of the chemically shifted components of both the Ga and As *3d* core-levels following annealing would suggest that the surface is terminated by a sulphur monolayer. In comparison to previous synchrotron radiation studies of wet chemically prepared surfaces treated with inorganic sulphides[29,30], the intensities of the chemically shifted components from spectra of these samples are smaller. The intensities in this work are, however, consistent with a monolayer coverage when the surface sensitivity of the synchrotron source is considered[31]. In addition, while the magnitudes of the chemical shifts fall within the range of the reported values[17,27,29], a larger chemical shift for the sulphur bonded to Ga than to As surface atoms on the annealed surface is observed. These results imply that S atoms easily form As-S bonds at room temperature, although As-S bonds are thermodynamically less stable than the Ga-S bonds. This is further evidence of the importance of accurately characterising the composition of the topmost atomic layer prior to sulphur deposition. These changes in composition, which can be clearly detected by using a synchrotron radiation source, appear to dictate the form of the bonding interaction between molecular sulphur and the GaAs surface.

6.4. Summary

It has been found in these studies that the exposure of freshly etched GaAs(100) surfaces to H_2S leads to the chemical stabilisation of the surface to the extent that it retains the as-etched electrical characteristics in air. This can be contrasted with the the rapid deterioration of the electrical characteristics of air-exposed untreated surfaces. The effectiveness of the passivation has been found to depend on the degree to which the surface has been exposed to air prior to H_2S treatment. Significant differences in the adsorption characteristics of sulphur on the clean GaAs(100) surface have been observed which can be attributed to subtle changes in the surface composition. The core-level studies would suggest that a critical factor in determining this adsorption is the composition of the topmost atomic layer. Both the intensity of the chemically shifted components and the magnitude of the chemical shifts can be related to the As/Ga surface composition. In terms of an activation energy the smaller magnitude of the As chemical shifted components may also be a result of the method of sulphur deposition. Although sulphur is found to adsorb more readily on the As surface atoms, this can be substantially accounted for by considering the two distinct chemically shifted components on the As core-level, one which is thermally unstable at 150 °C. Finally, the interaction of molecular sulphur with the GaAs(100) surface results in the adsorption of approximately one monolayer of sulphur.

References

[1] Sandroff C.J., Nottenburg R.N., Bischoff J.C. and Bhat R., Appl. Phys. Lett. **51** (1987) 33.

[3] Oigawa H., Fan J.-F., Nannichi N., Sugahara H. and Oshima M., Jpn. J. Appl. Phys. **30** (1991) L322.

[4] Oigawa H., Fan J.-F., Nannichi N., Ando K., Saiki K. and Koma A., Jpn. J. Appl. Phys. **28** (1989) L340.

[5] Liu D., Zhang T., LaRue R.A., Harris Jr. J.S. and Sigmon T.W., Appl. Phys. Lett. **53** (1988) 1059

[6] Carpenter M.S., Mellock M.R. Cowans B.A. Dardas Z. and Delgass N., J. Vac. Sci. Technol. B **7** (1989) 845.

[7] Samaras J.E. and Darling R.B., J. Appl. Phys. **72** (1992) 168.

[8] Fan J. Oigawa H. Nannichi N., Jpn. J. Appl. Phys. **27** (1988) L2125.

[9] Sugahara H., Oshima M., Oigawa H., Shigekawa H. and Nannichi Y., J. Appl. Phys. **69** (1991) 4349.

[10] Tiedje T., Colbow K.M., Rogers D., Fu Z. and Eberhardt W., J. Vac. Sci. Technol. b **7** (1989) 837.

[11] Shin J., Geib K.M., Wilmsen C.W. and Liliental-Weber Z., J. Vac. Sci. Technol. A **8** (1990) 1894.

[12] The As-capped GaAs wafers were kindly donated by Dr. D. Woolf, from the University of Wales, Cardiff.

[13] LeLay G., Mao D., Kahn A., Hwu Y. and Margaritondo G., Phys. Rev. B, **43** (1991) 14301.

[14] Drathen P., Ranke W. and Jacobi K. Surf. Sci. **77** (1978) L162.

[15] Mao D., Kahn A., LeLay G., Marsi M., Hwu Y., Margaritondo G., Santos M., Shayegan M., Florez L.T. and Harbison J.P., J. Vac. Sci. Technol. B. **9** (1991) 2083.

[16] The curve fitting software was developed by A.C. Caffolla, Dublin City University.

[17] Ranke W., Finster J. and Kuhr H.J., Surf. Sci. **187** (1987) 112.

[18] Van der Veen J.F., Smit L., Larsen P.K. and Neave J.H., Physica B **117** (1983) 822.

[19] Katnani A.D., Sang H.W., Chiaraida P. and Bauer R.S., J. Vac. Sci. Technol. B **3** (1985) 608.

[20] Hughes G., Roberts L., Henry M.O., McGuigan K., O'Connor G.M., Anderson F.G., Morgan G.P. and Glynn T., Materials Science and Engineering **B9** (1991) 37.

[21] Van der Ven, J., Hartman W.J.A.M. and Giling L.J., J. Appl. Phys. **60** (1986) 3735.

[22] Williams E.W., Phys. Rev. **167** (1968) 922.

[23] Kawanishi H., Sugimoto Y. and Akita K., J. Appl. Phys. **70** (1991) 805.

[24] Spindt C.J. and Spicer W.E., Appl. Phys. Lett. **55** (1989) 1653.

[25] Kuhr H.J., Ranke W. and Finster J., Surf. Sci. **192** (1986) 171.

[26] Ranke W., Kuhr H.J. and Finster J. Surf. Sci. **192** (1987) 81.

[27] Shin J., Geib K.M. and Wilmsen C.W., J. Vac. Sci. Technol. B **9** (1991) 2337.

[28] Sandroff C.J., Hegde M.S., Farrow L.A. Chang C.C. and Harbison J.P., J. Vac. Sci. Technol. B **7** (1989) 841.

[29] Spindt C.J., Liu D., Miyano K., Meissner P.L., Chiang T.T., Kendelwicz T., Lindau I. and Spicer W.E., Appl. Phys. Lett. **55** (1989) 861.

[30] Takakuwa Y., Niwano M., Fujita S., Takeda Y. and Miyamoto M., Appl. Phys. Lett. **58** (1991) 1635.

[31] Schnell R.D., Rieger D., Bogen A., Wandelt K. and Steinmann W., Solid State Commun. **53** (1985) 205.

Chapter 7 Photoemission Studies of the Deposition of Titanium on Oxidised GaAs(100) Surfaces

7.1. Introduction

Thin oxide layers are of significant technological importance for practical device applications. Examples of such layers have been reported for silicon, aluminium, chromium and titanium evaporated on oxidised GaAs substrates[1-5]. Titanium-based metallisations are freqently used to form Schottky contacts in the fabrication of high-speed GaAs field-effect transistors (FETs). There have been several previous photoemission studies of the interaction of titanium with both the clean and oxidised GaAs surface. Particular interest has focused on the thermal stability of Ti-GaAs interfaces. Studies by Ludeke and Landgren[6] and Ruckman *et al*[7] of the reactive interaction of Ti with the clean GaAs surface have shown evidence of extensive interdiffusion across the metal-semiconductor interface resulting in the formation of a highly non-abrupt interface. The non-abrupt nature of the contact makes it difficult to distinguish the critical factors which determine Schottky barrier behaviour. Previous photoemission studies of the deposition of Ti on the oxidised GaAs surface[4,5] have demonstrated the ability of Ti to completely reduce the native oxides even up to a thickness of 10 Å. It has been seen in Chapter 5 that the presence of these oxides has been linked to poor electrical characteristics of devices fabricated on these surfaces. Conseqently, their incorporation into the metal overlayer could provide an effective means of removing them from the interface. Ti can form a range of metal oxides from TiO to TiO_2 depending on the Ti/O stoichiometry. In the investigation of the interaction of Ti with a heavily oxidised GaAs surface Li *et al*[5] reported the formation of a TiO_2 overlayer when there was sufficient oxygen for reaction. They also observed a significant degree of out-diffusion of substrate elements into the metal film with evidence of As being detected in the Ti overlayer 40 Å from the interface. In this chapter, a synchrotron radiation photoemission study of the reduction of the native oxides of GaAs by Ti deposition to form TiO_x overlayers ($1 \geq x \leq 2$) is presented. The high resolution offered by the synchrotron source enables the precise mechanism of oxide reduction to be investigated in detail, providing information on the sequence of oxide reduction and the evolution of the TiO_x-GaAs interface. Two experiments involving two different initial sample preparations were carried out. In a preliminary experiment, GaAs surfaces were

prepared by the $H_2SO_4/H_2O_2/H_2O$ etch procedure outlined in Chapter 4, section 4.2.2. The brief exposure to air in transferring samples to UHV ensured that a thin native oxide layer formed on these GaAs surfaces[8]. Indeed, such an etch procedure is known to provide a passivating surface-oxide layer on GaAs substrates prior to MBE growth[9]. SXPS studies of the reduction of this oxide by deposition of Ti indicate that the Ga and As oxides are completely reduced to form a TiO_x ($x \approx 2$) like overlayer. Moreover, there is evidence to suggest that, with subsequent Ti deposition, the stoichiometry undergoes a transition by which the TiO_x ($x \approx 2$) overlayer is further reduced to TiO_x ($x \approx 1$). Based on the results of this first experiment, and in an attempt to investigate the precise mechanism of oxide formation and reduction, a second experiment was performed in which clean GaAs(100) surfaces were prepared by the thermal desorption of a protective As cap as outlined in the Chapter 4, section 4.3.2. These samples were then subjected to controlled oxidation, allowing the surface coverages to be limited to approximately one monolayer. This would suggest that as the titanium coverage approaches one monolayer, the stoichiometry would favour the formation of a TiO_x ($x \approx 1$) like overlayer at the interface. Since TiO_x ($x \approx 1$) is a metallic transition metal oxide, its formation on the semiconductor surface could provide a method of removing the thin native oxide and replacing it with a metal contact. As the thickness of the Ti metal overlayer is further increased, the contact would become increasingly metal rich, the important point being that the interfacial oxide has been removed. Of further importance is that the thin native oxide layer could act as a buffer layer and in doing so, could prevent the condensation energy of the Ti atoms from being released into the GaAs substrate, thereby suppressing interface disruption. Indeed, the results of this study would suggest that for a GaAs surface covered by approximately one monolayer of oxygen, the surface oxides are completely reduced by an ultra-thin metal overlayer and the subsequent metal-semiconductor interface formed is extremely abrupt.

The layout of this chapter is as follows. The results of investigations into titanium deposition on oxidised chemically etched and As-decapped GaAs(100) surfaces will be presented in sections 7.2 and 7.3, respectively. A discussion of the experimental studies is given in section 7.4 together with the related works of other researchers. A summary of the chapter is given in section 7.5.

7.2 Ti Deposition on Chemically Etched and Oxidised GaAs(100)

GaAs (100) samples (n =5x10^{16} cm^{-3}), similar to those used to obtain the results in Chapters 5 and 6, were chemically etched as outlined in section 4.2.2. Following the etching procedure, samples were exposed to normal laboratory air for periods up to 15 minutes before being transferred to UHV. The extremely low Ti deposition rates (0.01 Å per second) enabled the oxide reduction and overlayer formation to be studied in detail by SXPS. The photon energy chosen for all experiments was 100 eV. This provided maximum surface sensitivity with near identical escape depths for the photemitted Ga and As *3d* electrons as well as allowing the Ti *3p* and *3d* core levels to be probed. The overall instrumental resolution at hν=100 eV was 0.45 eV, however it was possible to reproducibly determine the binding energy of a core level to less than 0.1 eV.

Figure 7.1 illustrates a typical process of the reduction of Ga and As native oxides by Ti deposition at room temperature. The figure shows photoemission spectra of (i), the As and Ga *3d* core levels of the chemically etched and oxidised surface, followed by various steps of the reduction process, shown in (ii)-(vi). The chemically shifted compents due to the As and Ga oxides, located on the high binding-energy side of the As and Ga *3d* levels can easily be seen in (i). It is clear from the relative heights of the As and Ga chemicaly shifted components that the surface is Ga-oxide rich. This was generally the case for all chemically etched and oxidised surfaces investigated in these studies, irrespective of the times of exposure to atmosphere and can be expected since it is widely known that the substrate GaAs can react with the As-oxide to form Ga-oxide and elemental As[10]. Following the deposition of 0.25 Å of Ti, there is clear evidence of a dramatic reduction in the intensities of both the As and Ga chemically shifted components. Indeed, at a coverage of only 0.75 Å, which corresponds to approximately half a monolayer of Ti atoms (1ML = 1.4 Å Ti), the As chemically shifted component is completely reduced, signifying the total removal of As oxides from the GaAs substrate. It takes a further 4.25 Å of Ti to completely reduce the Ga-oxide signal, indicating that the surface was originally Ga-oxide rich. Two separate peaks corresponding to the Ti *3p* and *3d* levels at 60 and 95 eV, respectively, can readily be discerned at a

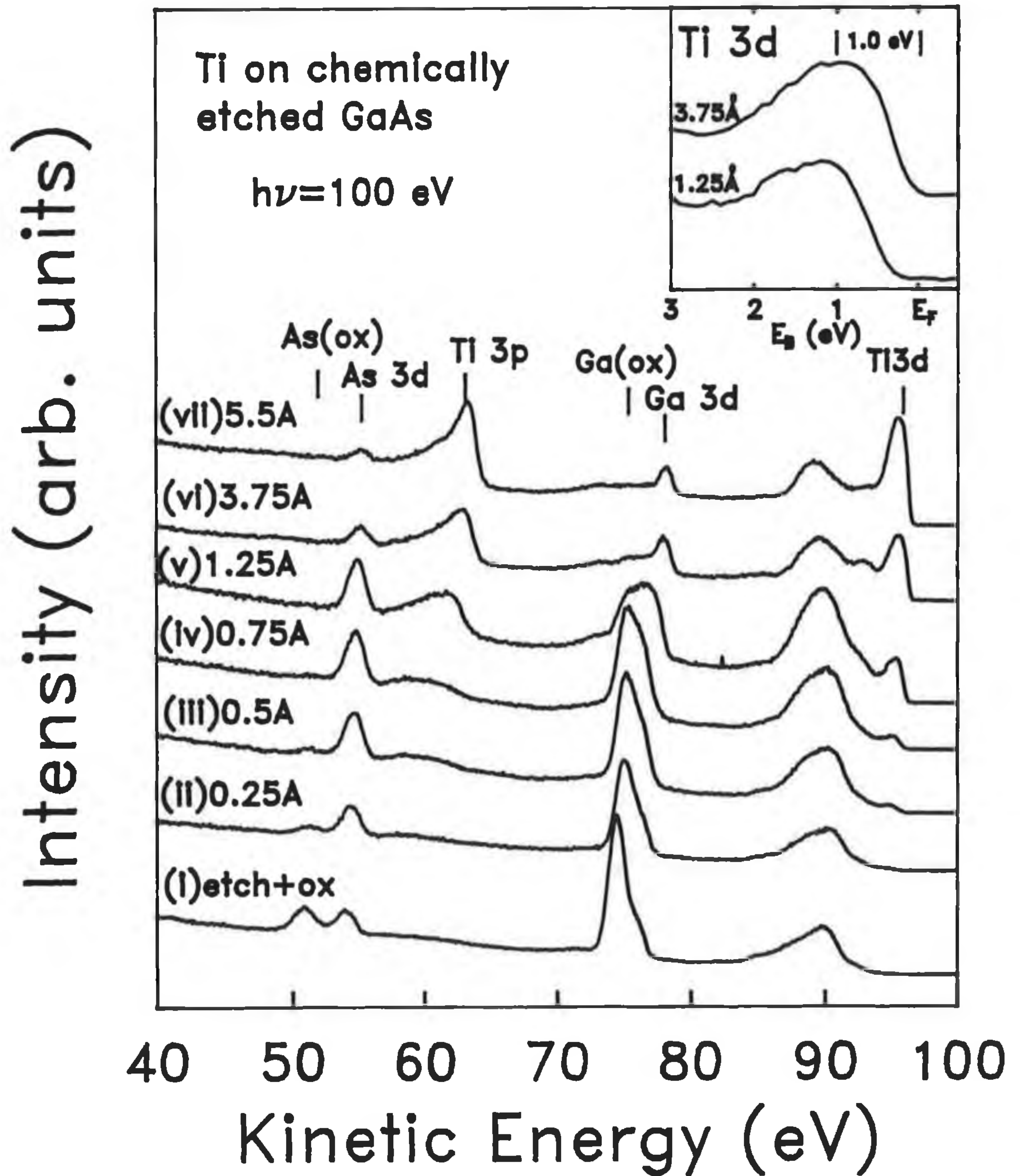

Figure 7.1. SXPS of (i) etched and oxidised surface and (ii)-(vii) various Ti coverages. Inset shows VB spectra for 1.25 and 3.75 Å coverages showing Ti 3d level.

coverage of 0.5 Å. These peaks grow rapidly with increasing Ti deposition and dominate the spectra at a Ti coverage of 5.5 Å.

The results of this experiment lead to the speculation that the As and Ga oxides are initially reduced by the Ti to form a TiO_x (x=2) overlayer. However, with subsequent depositions, this TiO_2-like overlayer is further reduced to TiO_x (x=1). Evidence for this proposal is provided for by the valence band spectra shown in the inset of figure 7.1, which shows the Ti *3d* level for coverages of 1.25 and 3.75 Å. There have several photoemission studies which show that TiO_2 is characterised by a Ti *3d* defect state which lies approximately 1.0 eV below the Fermi-level[11-15]. This feature, representing Ti *3d* ionisation, can be seen in the figure. It is caused by the creation of oxygen vacancies in TiO_2 and corresponds to a reduction of the Ti atoms, nominally to Ti^{3+}. As more Ti is deposited, the TiO_2-like overlayer is further reduced to TiO_x (x=1), i.e. Ti^{3+} is reduced to Ti^{2+}. This reduction is evidenced by the high density of states at E_f, characteristic of TiO[16,17]. This apparent shift of the Fermi-level is seen in the inset for the 3.75 Å coverage. No such shifts were detected for the As or Ga *3d* core-levels.

It would appear therefore that TiO_2 will form when there sufficient oxygen for reaction, in agreement with the proposal by Li *et al*, mentioned earlier. However, the results indicate that TiO_2 is unstable in the presence of Ti and so it is reduced to TiO. This leads to the further suggestion that limiting native oxide formation to monolayer coverages would result in the formation of a TiO-like overlayer. This suggestion formed the basis of the next experiment.

7.3 Ti Deposition on As-Decapped and Oxidised GaAs(100)

Arsenic capped GaAs epilayers (n=$5x10^{16}$ cm^{-3}) similar to those used for the studies presented in Chapter 6 were used for this experiment. The As cap was thermally desorbed at 350 °C in UHV in various annealing stages to produce a clean surface. A recent analysis of clean GaAs surfaces prepared in this way indicated that the Fermi level for n-type material is consistently found at 0.7 eV above the valence band maximum, regardless of surface As composition[18]. Oxidation of the GaAs surfaces was achieved by exposing the clean surface to air for ten minutes. This resulted in the formation of an oxide overlayer approximately one monolayer thick.

Figures 7.2(i) and 7.3(i) show the photoelectron spectra of the clean GaAs (100) decapped surface for the Ga and As *3d* core-levels, respectively. All spectra were curve-fitted using the same procedure as that described in Chapter 6 section 6.2. An As/Ga surface composition of 0.9 for this surface was determined from the relative intensities of these two peaks indicating that the clean surface was Ga rich. Both the Ga and As core-levels are represented by a bulk and surface core-level shifted (SCLS) component consistent with previous studies of the decapped surface[19,20]. Figure 7.2(ii) shows the resulting Ga 3d spectrum after exposing the surface to air for ten minutes. Two chemically shifted oxide components, 0.45 eV and 1.0 eV on the high binding energy side of the Ga *3d* bulk level can be resolved. The As *3d* spectrum of the oxidised surface, shown in figure 7.3(ii) also displays two chemically shifted components, displaced by 0.8 eV and 3.1 eV to higher binding energy. These binding energy shifts are consistent with those reported by Landgren *et al*[21] for the oxidation of the GaAs (110) surface. The intensity ratio of the chemically shifted oxide components to the bulk peak at 0.22 and 0.55 for As and Ga *3d* respectively, reflects the fact that the surface is Ga rich and confirms that the surface oxide coverage approximates to one monolayer. Figure 7.2(iii)-(vi) show the results of Ti deposition on the profile of the Ga *3d* core-level. A reduction in the magnitude of the 1.0 eV chemically shifted component can be detected for a Ti coverage as low as 0.1 Å and this peak is completely attenuated by a 0.25 Å coverage. The disappearance of the 0.45 eV shifted oxide component at a coverage just in excess of 1 Å is accompanied by the appearance and growth of a chemically shifted component displaced by 0.6 eV to lower binding energy. By a Ti coverage of 3.0 Å, this chemically shifted component becomes dominant and shifts to even higher kinetic energy, suggesting the presence of either metallic Ga (ΔE=0.9 eV) or a Ga-Ti alloy[7].

From the spectra presented in Figure 7.3(iii)-(vi) it is evident that both of the As chemically shifted oxide components are completely attenuated by a metal coverage of 0.25 Å. Higher coverages show the appearance and growth of a component which is shifted by approximately 0.5 eV to the low BE side of the As *3d* bulk level, suggesting the formation of a Ti-As complex. The kinetic energy of this component does not change with further depositions of Ti, suggesting that it is in a stable bonding configuration. The stability of the Ti-As bond over that of the Ti-Ga is

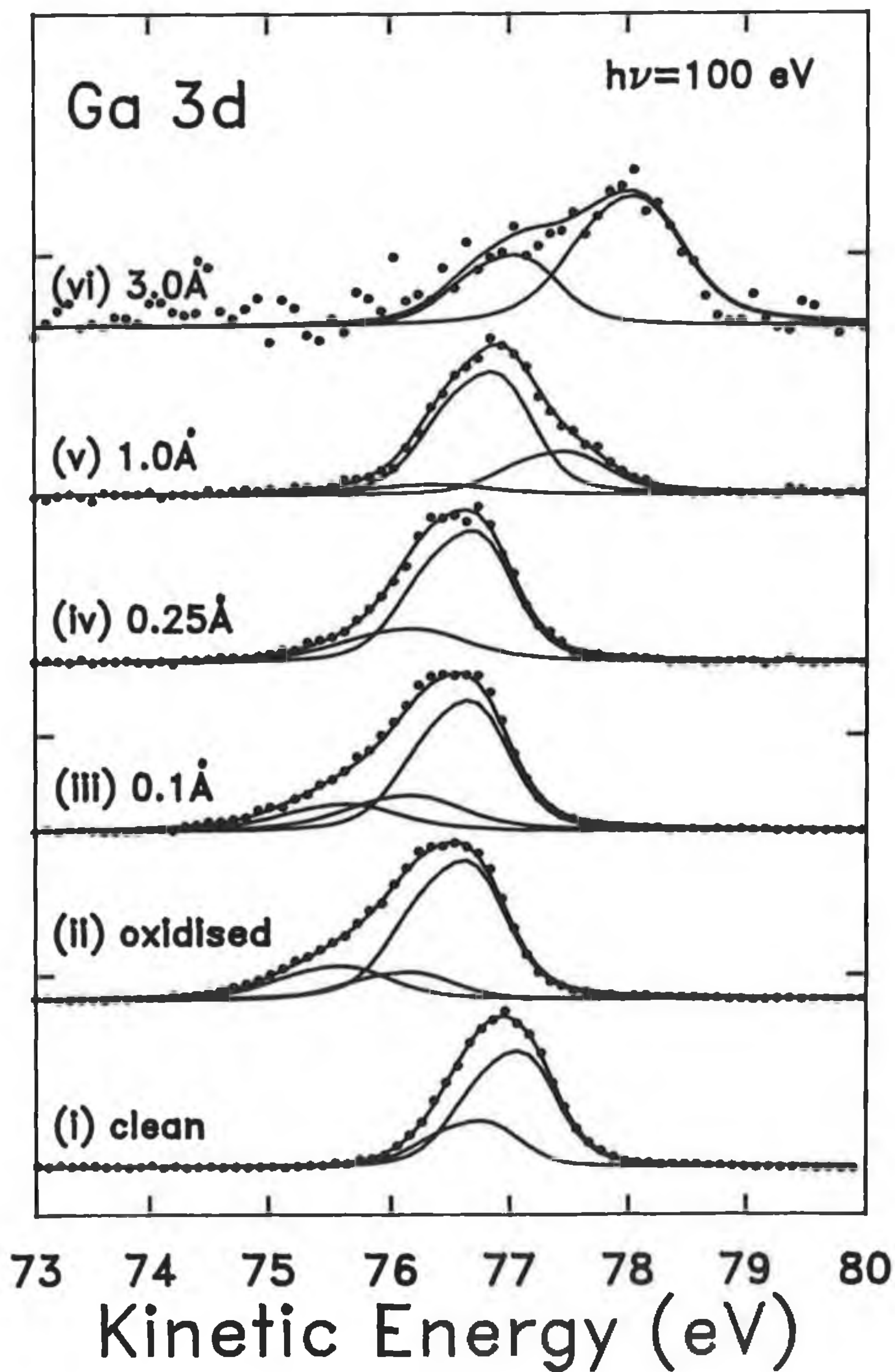

Figure 7.2. Deconvolution of the Ga 3d photoemission spectra for (i) the clean surface, (ii) the oxidised surface and (iii)-(vi) for various Ti coverages.

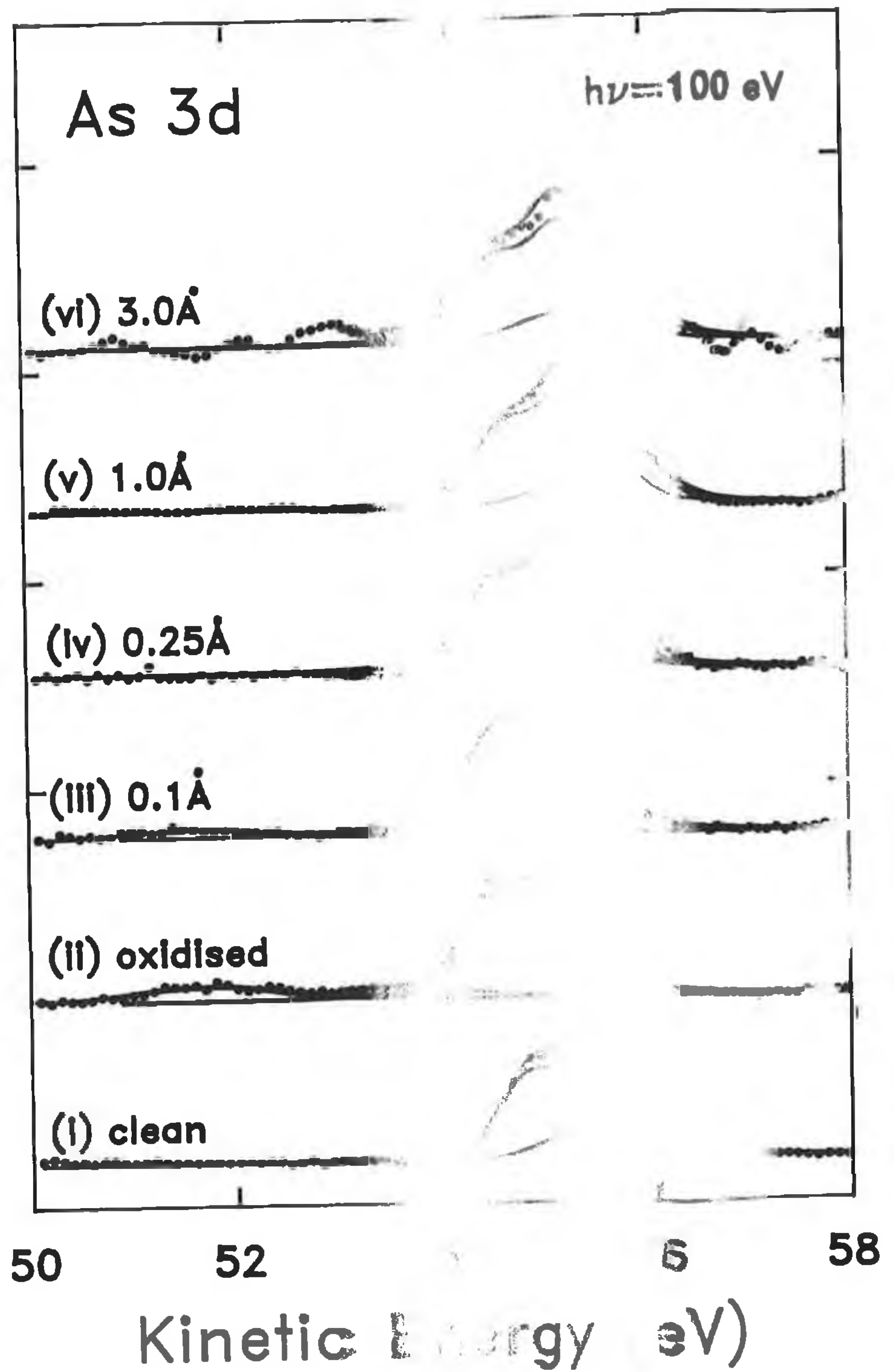

Figure 7.3. Deconvolution of the As 3d photoemiss[illegible] [illegible]ra for (i) the clean surface, (ii) the oxidised surface and (iii)-(vi) for various Ti coverage.

further supported by the larger value of enthalpy of Ti-As (-23.6 kcal/mol) as opposed to Ti-Ga (-12.2 kcal/mol) while for GaAs, the enthalpy of formation is -36.8 kcal/mol[22]. The more rapid attenuation of the chemically shifted As oxide components reflects the fact that the oxidised surface is Ga rich and displays a larger initial intensity of the Ga oxide peaks. This is also consistent with the larger magnitude of the Ti-Ga chemically shifted component compared with the Ti-As component evident from the spectra for the 3 Å Ti coverage.

7.4 Discussion

These results would suggest that the oxides on both the Ga and As surface atoms are attenuated simultaneously, with the higher oxidation states being reduced first. The Ti coverage required to completely reduce the surface oxides (approximately 1 Å is consistent with the estimate of surface oxide coverage of one monolayer since the thickness of one monolayer of Ti is 1.4 Å. The simultaneous reduction of As and Ga oxides from the studies on chemically etched and oxidised surfaces have shown that the reduction of thicker oxides on GaAs requires the deposition of greater thicknesses of Ti. It should be noted, for the purpose of clarification, that the intensities of each of the fitted spectra in figures 7.2 and 7.3 i.e. Ga and As bulk and chemically shifted components, were normalised to the total core-level signal. In fact, the results of Ti deposition were such that the intensity of the Ga and As 3d peaks were attenuated to approximately 7% of the oxidised surface intensity for a Ti coverage of 3 Å which approximates to a two monolayer coverage (monolayer ≈ 1.4 Å). Such rapid attenuation for surface sensitive conditions, leads to the conclusion that the effective electron escape depth through the Ti overlayer is of the order of 1 Å. A plot of the attenuation of the As and Ga 3d core-level signals as a function of Ti coverage is shown in figure 7.4. The dotted line corresponds to Beer's law function for layer by layer growth i.e.:

$$I/I_0 = e^{-n\lambda/d} \qquad (7.1)$$

where I/I_0 is the intensity normalised to that of the oxidised surface, n is the number of metal layers, each of thickness d and λ is the escape depth. It can be seen from the figure that the attenuation of both core-level signals, consisting of both bulk and chemically shifted components, follows Beer's law assuming an escape depth of 1 Å. This extremely short escape depth is similar to that determined by Ludeke *et al*[23]

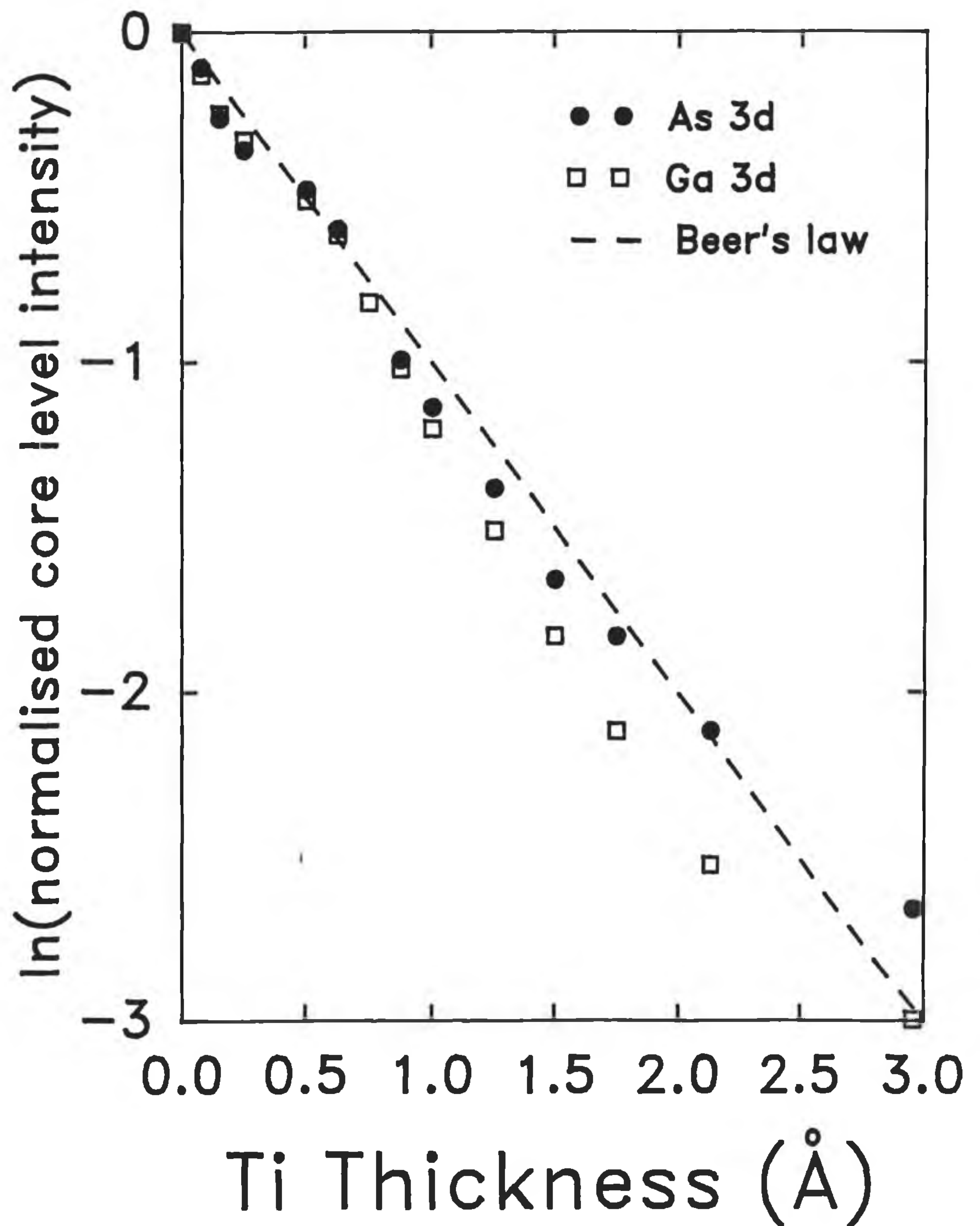

Figure 7.4. Ga 3d and As 3d attenuation curves as a function of Ti coverage. Dashed line indicates calculated attenuation of core-level intensity from Beer's Law for mean free path of 1 Å.

for the GaAs substrate peaks in the deposition of Ti on the atomically clean GaAs (110) surface. They also reported a mean free path of approximately 2 Å within the Ti overlayer. This would suggest that for the coverages investigated, there is no appreciable out-diffusion of either As or Ga into the Ti overlayer and therefore the interface formed is extremely abrupt extending no more that two or three atomic layers perpendicular to the interface. This is in sharp contrast with the extent of the interdiffusion observed in previous studies of the clean Ti-GaAs interface where there was evidence of substrate element out-diffusion in excess of 100 Å into the Ti overlayer[7]. It is also substantially different from the behaviour observed by Li *et al*[5] for the Ti deposition on a heavily oxidised GaAs surface where significant out-diffusion of As into the metal overlayer was evident above a coverage of 40 Å. It has been well established that the heavy oxidation of the GaAs surface leads to a significant degree of surface disruption extending over several atomic layers into the semiconductor[8]. This region contains stoichiometric oxide compounds such as As_2O_3, As_2O_5 and Ga_2O_3. The deposition of a highly reactive metal like Ti would be expected to result in the reduction of these oxides and consequently the release of substantial amounts of both Ga and As into the growing metal overlayer.

For the studies carried out on As-decapped samples, the photoemission data indicates that the oxidation process is confined to the surface atoms and does not extend into the semiconductor bulk. This leads to the proposal that the first layer of Ti reacts with the surface oxides to form a stable TiO_x (x=1) interfacial layer. Because the oxidation is confined to the surface, this interaction results in the release of less than a monolayer of GaAs surface atoms into the Ti overlayer. The formation of the TiO_x interfacial layer appears to inhibit further chemical interactions between the titanium and the GaAs substrate thereby making the metal-semiconductor interface substantially more abrupt than that observed for the clean Ti-GaAs interface. This thin metallic oxide appears to act as a buffer layer between the semiconductor surface and the metal having the effect of creating an extremely abrupt interface. Therefore the presence of this thin surface oxide may well provide a mechanism of limiting the extent of interdiffusion across the interface by reacting with the deposited titanium to form a stable interfacial compound. Figure 7.5 shows the valance band spectra taken of an As-decapped and oxidised sample at various stages during the evolution of the Ti overlayer. The valance band spectrum for the oxidised GaAs surface shows

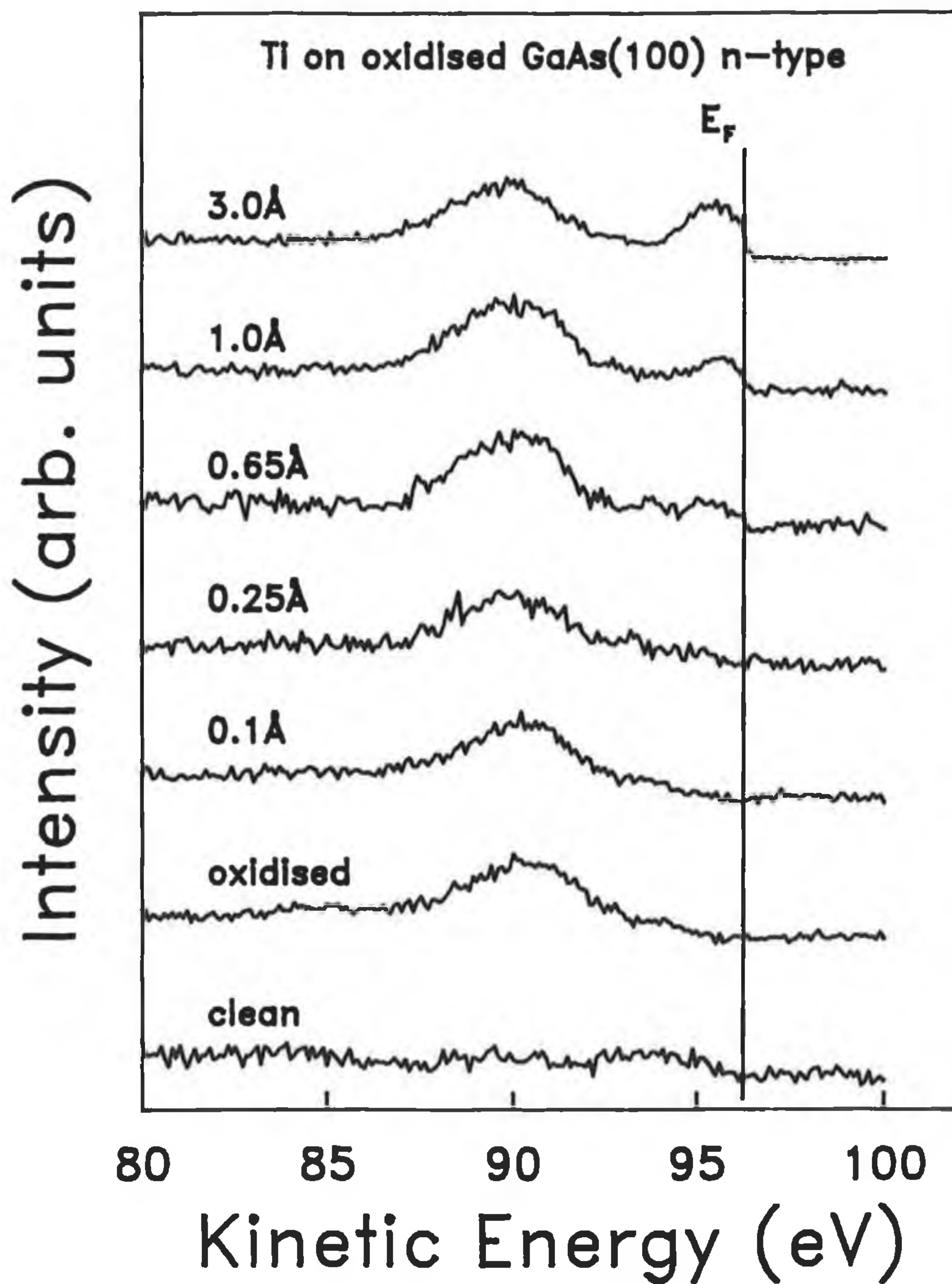

Figure 7.5. Valence band photoemission spectra of (i) the clean GaAs surface, (ii) the oxidised surface and (iii)-(vi) for Ti coverages as indicated in Å.

the oxygen 2p level, the centre of which is located at approximately 5 eV below the VBM and the Ti *3d* level. For a coverage as low as 0.6 Å there is evidence of Fermi edge emission. Since this metal coverage is less than one monolayer it cannot be attributed to a complete metallic overlayer. Nor from results of the rate of substrate peak attenuation, can it be attributed to island growth of the metallic overlayer. It would appear that it is due to the formation of a TiO_x (x=1) metallic layer incorporating the surface oxides. Further evidence for this assignment comes from the valence band spectra at coverages of 1 Å and 3 Å which are comparable to spectra of the band structure of TiO reported by Henrich *et al*[11]. The formation of a substantive TiO_2 layer at the surface can be discounted because the valence band spectrum of this compound has a very low density of states at the Fermi-level as shown above. The possibility of oxygen being incorporated into the overlayer from the vacuum environment can also be discounted since the absolute intensity of the O *2p* indicates that no subsequent oxidation takes place. In conculsion, a procedure has been demonstrated by which the reduction of a thin native oxide on GaAs and and its incorporation into a Ti metal overlayer produces an abrupt metal-semiconductor interface.

7.5 Summary

The deposition of thin Ti overlayers on the oxidised GaAs (100) surface has been shown to result in the complete reduction of the native oxides. The formation of a TiO_2-like compound appears to form when there is sufficent amounts of oxygen. However, further Ti deposition reduces this to a TiO-like compound.

When the oxide coverage is limited to approximately 1 monolayer, a TiO_x-GaAs (x=1) interface appears to form. No appreciable interdiffusion across this interface is observed and Ti deposition approximates to a layer by layer growth mode as confirmed by Beer's law. Valence band spectra taken at submonolayer Ti coverages confirm that this interfacial oxide formed is metallic in character and has a composition which approximates to TiO_x where $x \approx 1$.

References

[1] Jimenez I., Palomares F.J., Avila J., Cuberes M.T., Soria F., Sacedon J.L. and Horn K., (in press).

[2] Cuberes M.T. and Sacedon J.L., Appl. Phys. Lett. **57** (1990) 2794

[3] Seo J.M., Chen Y. and Weaver J.H., J. Appl. Phys. **70** (1991) 4336.

[4] Kowalczyk S.P., Waldrop J.R. and Grant R.W., J. Vac. Sci. Technol. **19** (1981) 611.

[5] Li Y.Z., Aastuen D.W.J., Seo J.M., Ayyala U.S. and Weaver J.H., Surf. Sci. **254** (1991) 201.

[6] Ludeke R. and Landgren G., Phys. Rev. B **33** (1986) 5526.

[7] Ruckman M.W., del Giudice M., Joyce J.J. and Weaver J.H., Phys. Rev. B **33** (1986) 2191.

[8] Wilmsen C.W. in Gallium Arsenide Technology, Chap. 8 (Editor in chief D.K.Ferry)
(Howard James and Company 1988) 359.

[9] Massies J. and Contour J.P., J. Appl. Phys. **58** (1985) 806.

[10] Thurmond C.D., Schwartz G.P., Kammlot G.W. and Schwartz B., J. Electronchem. Soc. **127** (1980) 1366.

[11] Henrich V.E., Dresselhaus G. and Zeiger H.J., Phys. Rev. Lett. **36** (1976) 1335.

[12] Egdell R.G., Eriksen S. and Flavell W.R., Solid State Commun. **60** (1986) 835.

[13] Muryn C.A., Hardman P.J., Crouch J.J., Raiker G.N., Thornton G. and Law D.S.-L., Surf. Sci. **251/252** (1991) 747.

[14] Prabhakaran K., Purdie D., Casanova R., Muryn C.A., Hardman P.J., Wincott P.L. and Thornton G., Phys. Rev. B. **45** (1992) 6969.

[15] Thornton G., Vacuum, **43** (1992) 1133.

[16] Wertheim G.K. and Buchanan D.N.E., Phys. Rev. B. **17** (1978) 2780.

[17] Henrich V., Zeiger H.J. and Reed T.B., Phys. Rev. B. **17** (1978) 4121.

[18] Le Lay G., Mao M., Kahn A., Hwu Y. and Margaritondo G., Phys. Rev. B, **43** (1991) 14301.

[19] Roberts L and Hughes G 1992 J. Vac. Sci Technol. A, **10** (1992) 1862.

[20] Mao D., Kahn A., Le Lay G., Marsi M., Hwu Y., Margaritondo G., Santos M.,

Shayegan M., Florez L.T. and Harbison J.P., J. Vac. Sci. Technol. B **9** (1991) 2083.10

[21] Landgren G., Ludeke R., Jugnet Y., Morar J.F. and Himpsel F.J., J. Vac. Sci. Technol.
B **2** (1984) 351.

[22] Miedema A.R., de Boar F.R. and Boom R., CALPHAD 1 (1977) 4

[23] Ludeke R. and Landgren G., Phys. Rev. B. **33** (1986) 5526.

Chapter 8 Conclusions and Future Work

8.1 Summary of Work

Schottky barrier formation and behaviour has been studied as a function of semiconductor surface preparation in an attempt to control the electronic properties at the metal-GaAs(100) interface. A range of experimental techniques have been use to characterise the interactions of metals with both clean, oxidised and sulphur passivated GaAs surfaces. Investigations into the formation of Schottky contacts with both unoxidised and oxidised GaAs(100) surfaces revealed that a correlation exists between the magnitude of the ideality parameter as determined by I-V measurements and the presence of interface states as detected by DLTS. The high density of interface states, (of the order 10^{11}-10^{13} $eV^{-1}cm^{-2}$), as measured by DLTS, are a direct result of the defects produced by the oxidation of GaAs surfaces prior to metal deposition.

The high density of states induced by oxidation encouraged the need to passivate GaAs surfaces. It has been found that the exposure of newly etched GaAs surfaces to H_2S leads to the chemical stabilisation of the surfaces in that it retains the as-etched electrical characteristics in air, in contrast with the rapid deterioration of the electrical characteristics of air-exposed untreated surfaces. The effectiveness of the sulphur passivation is found to depend on the degree to which the surface has been exposed to air prior to H_2S treatment.

Surface sensitive synchrotron photoemission studies of the adsorption of molecular sulphur on clean GaAs(100) surfaces indicate that the composition of the topmost atomic layer plays a vital role in determining the adsorption characteristics. The results also imply that sulphur atoms easily form As-S bonds at room temperature, although As-S bonds are thermodynamically less stable than Ga-S bonds. It is found that sulphur adsorption on clean GaAs(100) surfaces saturates at a coverage of approximately one monolayer.

The deposition of thin Ti overlayers on the oxidised GaAs(100) surfaces have been shown to result in the complete reduction of the native oxides. For the case of chemically etched and oxidised GaAs surfaces, the formation of a TiO_x (x=2)

compound appears to form when there is sufficent amounts of oxygen. However, further Ti deposition reduces this to a TiO_x (x=1) compound. When the oxide coverage is limited to approximately 1 monolayer, a TiO_x-GaAs (x=1) overlayer appears to form. These studies suggest that the interface formed in this way is extremely abrupt with no significant interdiffusion across being detected by the photoemission studies.

8.2. Suggestions for Future Work

During the course of this work, some areas where further investigations could offer a better understanding of the electronic properties of metal-GaAs(100) interfaces became apparent. It would be interesting to perform photoemission studies of molecular sulphur adsorption characteristics as function of substrate sample temperature. This could be carried out for both As-decapped and chemically etched GaAs surfaces. For the case of As-capped samples, it would be possible to prepare surfaces which either As- or Ga-rich and thereby study the adsorption characteristics of these surfaces. In the case of chemically etched samples, the experiments could provide a means of heat cleaning while simultaneously passivating the surface. There is also some doubt as to the precise LEED reconstructions of the As-decapped surface. It would useful to determine these both before and after sulphur passivation. The theroetical work carried out by Ohno *et al* (Chapter 2 section 2.4) on sulphur passivation of GaAs(100) surfaces could provide the basis for valence band photoemission studies of the interaction of molecular sulphur with GaAs surfaces. This could provide experimental evidence on the preferred adsorption sites for sulphur on GaAs surfaces.

One problem encountered when performing photoemission studies of the As-capped GaAs samples was that because of their doping concentration, (N_D-N_A=5x10^{16} cm^{-3}), the effect surface photovoltage (SPV) had to be taken into account. SPV due to electron-hole pair separation and can result in the flattening of the energy bands in the semiconductor when illuminated with light. It is particularly pronounced in moderately doped semiconductors, such as those used in these studies, and has a worse effect at lower sample temperatures. Consequently, investigations into Fermi-level movement during these studies was somewhat restricted. This problem, of course could be overcome by using higher doped (N_D-N_A≥5x10^{18} cm^{-3}) samples.

The electrochemical sulphur cell used in these studies provided a novel means of controlling the flux when depositing molecular sulphur on GaAs substrates. This same cell design is capable of generating a molecular beam of selenium. The logical, and planned extension to these studies is to look at the heterovalent exchange reactions between the group V and group VI element which occur when a III-V semiconductor surface is exposed to a group VI element at elevated temperatures. This would lead to a study of the heteroepitaxial growth of III-V semiconductors on III-V semiconductor substrates. A detailed understanding of the exchange reaction between the group VI and group V elements would then become the basis of an *in situ* UHV investigation of the interfaces which form during the early stages of MBE growth of II-VI heterostructures on III-V substrate materials.

Appendix A List of refereed publications pertaining to this work

An Investigation of Metal/GaAs(100) Interfaces by Deep Level Transient Spectroscopy
Roberts L. and Hughes G.
Applied Surface Science **50** (1991) 424-427

An Investigation of the Passivating Effects of Hydrogen Sulphide on the GaAs(100) Surface
Hughes G., Roberts L., Henry M.O., McGuigan K., O'Connor G.M., Anderson F.G., Morgan G.P. and Glynn T.
Materials Science and Engineering **B9** (1991) 37-41

A Vacuum Ultraviolet Photeleectron Spectroscopy Study of the Interaction of Molecular Sulphur with the GaAs(100) Surface
Roberts L., Hughes G., Fennema B. and Carbery M.
J. Vac. Sci. Technol. B. Vol. **10** (1992) 1862

A Synchrotron Radiation Photoemission Study of the Deposition of Titanium on the Oxidised GaAs(100) Surface.
Roberts L., Hughes G., Fennema B. and Carbery M.
Semicon. Sci. Technol. 8 (1993) 647